

DDC FILE COPY  
AD A0 65885

**LEVEL**

12

ARI-RR-139

INITIATION PHENOMENA IN PULSED  
CHEMICAL LASERS

by

James P. Moran  
R. Bruce Doak



Prepared for

NAVAL RESEARCH LABORATORY  
Monitored by Dr. S. K. Searles/5540  
4555 Overlook Avenue, S. W.  
Washington, D. C. 20375

Under Contracts

N00173-77-C-0222  
and  
N00173-78-C-0188

DISTRIBUTION STATEMENT A  
Approved for public release  
Distribution Unlimited

Sponsored by

NAVAL SEA SYSTEMS COMMAND  
and  
NAVAL MATERIALS COMMAND

Prepared by

AERODYNE RESEARCH, INC.  
Bedford Research Park, Crosby Drive  
Bedford, MA 01730

October 1978



UNCLASSIFIED

SECURITY CLASSIFICATION OF THIS PAGE (When Data Entered)

Abstract (Continued)

of  $C_2F_3$  (1750Å to 2400Å) and 13% of its energy in the absorption band of  $F_2$  (2400Å to 3400Å). Theoretical modeling of flash lamp radiation indicates that short lamp pulses appropriate to pulsed chemical lasers would show equal or better radiation distribution of lamp electrical energy in these absorption bands. The flash lamp was used in photolysis studies which show that absorption of radiation by  $C_2F_3$  results in dissociation with efficiency of order unity. Photolytic production of F-atoms could not be determined in the present UV attenuation studies due to the occurrence of a strongly absorbing unidentified photolysis product or products. ←

Cavity illumination modeling of repetitively pulsed chemical lasers points to severe penalties in electrical efficiency and gas mass utilization if spatial uniformity of photolytic initiation is to be better than ±5%. One might eliminate the penalties by spatial tailoring of trace addition of  $C_2F_3$  to laser gas mixtures. For example, with the above measured distribution of lamp radiated energy in the absorption bands of  $C_2F_3$  and  $F_2$ , a local addition of 11%  $C_2F_3$  in relation to  $F_2$  may double the local production of F-atoms at fixed illumination.

S/N 0102- LF-014-6601

UNCLASSIFIED

SECURITY CLASSIFICATION OF THIS PAGE (When Data Entered)

TABLE OF CONTENTS

<u>Section</u>	<u>Page</u>
	ACKNOWLEDGMENTS . . . . . vii
1	INTRODUCTION . . . . . 1-1
2	LASER INITIATION ENHANCEMENT OF $ClF_3$ ADDITION . . . . . 2-1
3	FLASH LAMP MODELING . . . . . 3-1
	3.1 Lamp Explosion Limit . . . . . 3-1
	3.2 Argon Flash Lamp Modeling . . . . . 3-3
4	MODELING OF THE INFLUENCE OF $ClF_3$ ON LASER PERFORMANCE . . . . . 4-1
5	PREVIOUS ATOMIC FLUORINE CONCENTRATION MEASUREMENTS . . . . . 5-1
6	FLASH LAMP SPECTRAL RADIATION MEASUREMENTS . . . . . 6-1
	6.1 Calibration and Data Processing . . . . . 6-5
	6.2 Spectral Measurements . . . . . 6-10
7	STUDIES OF PHOTOLYSIS OF $ClF_3$ . . . . . 7-1
	7.1 System Operation and Analysis . . . . . 7-1
	7.2 Measurements of Photolysis of $ClF_3$ . . . . . 7-15
8	SUMMARY . . . . . 8-1
9	REFERENCES . . . . . 9-1

ACCESSION for

NTIS  White Section

DDC  Dark Section

UNANNOUNCED

JUSTIFICATION

*After on file*

BY

DISTRIBUTION AVAILABILITY CODE

Dist. AVAIL. and/or SPECIAL

*AI*

78 12 18

## LIST OF ILLUSTRATIONS

<u>Figure</u>		<u>Page</u>
1	UV Absorption Spectra of $F_2$ , $C\ell F_3$ , and $C\ell F$ Taken From Reference (7) . . . . .	1-2
2	Weighted Absorption Spectrum for a Mixture of 98% $F_2$ Plus 2% $C\ell F_3$ . . . . .	2-2
3	Cavity Cross Section Geometry for Illumination Modeling . . . . .	2-3
4	Normalized Cavity Illumination Contours . . . . .	2-5
5	Case B . . . . .	2-6
6	Nonuniformity in Cavity Illumination with Extended Lamps . . . . .	2-7
7	Lamp Energy Demand for Extended Lamp Planes . . . . .	2-9
8	Case C . . . . .	2-10
9	Spatially Tailored $C\ell F_3$ Addition . . . . .	2-12
10	Loading (Joules per inch) at Which Linear (Quartz Envelope) Flashtubes Explode (From EG&G Data Sheet F1002C-2) . . . . .	3-2
11	Lamp Radiation Modeling in the Optically Thick Limit . . . . .	3-7
12	Lamp Spectral Energy Efficiencies at Two Wavelengths as Functions of Argon Fill Pressure . . . . .	3-14
13	Lamp Spectral Energy Efficiencies at Two Wavelengths as Functions of Capacitor Voltage . . . . .	3-15
14	Lamp Spectral Energy Distributions at Two Wavelengths as Functions of Capacitor Voltage . . . . .	3-16
15	Lamp Radiation Modeling in the Optically Thick Limit . . . . .	3-18
16	Comparison of Lamp Spectral Energy Efficiencies of a Short Pulse Lamp for Two Operating Conditions . . . . .	3-24
17	Apparatus for Measurements of Atomic Fluorine Concentration . . . . .	5-2
18	Absolute Variation in Absorption Cross Section of Molecular Fluorine With Temperature Increase Above 300°K by: (a) 210°K; (b) 360°K; (c) 500°K; (d) 690°K . . . . .	5-6
19	Lamp Electrode With Gas Supply and Wall Mounting Fittings . . . . .	6-2
20	Photolysis Cell End Plugs With Fittings . . . . .	6-3
21	Lamp Spectral Energy Measurements Schematic . . . . .	6-4

List of Illustrations (Continued)

<u>Figure</u>		<u>Page</u>
22	Transmission Spectra of Eight UV Filters, See Table 6-1 for Filter Specifications . . . . .	6-6
23	Total Spread In Response of Five UV Spectral Data Channels Using Each of Eight Narrow Band UV Filters . . . . .	6-7
24	Spectral Response of Silicon Diode/Amplifier Elements in the Flash Lamp Spectral Energy Measurements Array . . . . .	6-8
25	Comparison of Lamp Spectral Energy Efficiencies of a Flash Lamp at Two Periods in Its Lifetime . . . . .	6-11
26	Comparison of Measured Lamp Spectral Energy Efficiencies With Theory . . . . .	6-13
27	System Schematic for UV Attenuation Studies . . . . .	7-2
28	Attenuation Channel (6) Detector Signals Through Eight Narrow Band UV Filter With and Without Corning Glass No. 7740 Inserted . . . . .	7-4
29	Ratio of Wall to Lamp Detector Signal Versus Spectral Reflectivity (Eq. (7-3)) . . . . .	7-8
30	Measured Ratios of Wall to Lamp Detector Signals $L_w/L$ , and Calculated Wall Spectral Reflectivities $r_w$ . . . . .	7-12
31	Attenuation at $3210\text{\AA}$ by $C\ell F_3$ at Partial Pressures of 30.4, 15.2, and 7.6 torr with Flash Photolysis . . . . .	7-16
32	Attenuation at $2400\text{\AA}$ by $C\ell F_3$ at Partial Pressures of 7.6 and 3.8 torr with Flash Photolysis . . . . .	7-19
33	Histories of $C\ell F_3$ Attenuations at $2400\text{\AA}$ and $3210\text{\AA}$ During Exposure to the Arc Lamp Attenuation Probe Beam . . . . .	7-21
34	Attenuation at $2400\text{\AA}$ by $C\ell F_3$ at Partial Pressures of 0.76 and 0.95 torr with Flash Photolysis . . . . .	7-23

## ACKNOWLEDGMENTS

The author gratefully acknowledges the advice and program direction offered by the program monitor, Dr. S.K. Searles of the Naval Research Laboratory. Work was sponsored by the Naval Sea Systems Command and Naval Materials Command.

## 1. INTRODUCTION

A renewed interest in the details of photolytic initiation of pulsed HF/DF chemical lasers has developed recently. This interest stems from a broadened base of laser performance data obtained from the PHOCL-50 single pulse system developed at Boeing Aerospace Co.<sup>(1)</sup> Pulse energy measurements were performed with this system for a variety of chemical compositions and flash lamp operating conditions. These results were compared with previous measurements in a much smaller device by Chen, et al.<sup>(2)</sup> on the basis of a theoretically derived correlation parameter,<sup>(3,4)</sup>  $p_{F_2} (p_F/p_{F_2})^{1/2}$ , where  $p$  refers to the partial pressure of the indicated species after flash lamp initiation. This comparison shows that the outcoupled energy, per unit cavity volume, in the large scale PHOCL-50 system, is of order 0.50 to 0.60 time that of the smaller device. This difference raises doubts regarding the validity of predicting the performance of large scale systems from small scale experiments and scaling relations. A variety of explanations may be offered for this difference; one of which may be to suspect the accuracy of the stated initiation level,  $p_F$ , since it cannot presently be measured directly. Photolytic dissociation of  $F_2$  in laser gas mixtures is deduced in both Refs. (1) and (2) by the rate of progress of the resultant chain reaction, as determined by the rate of consumption of  $F_2$ . However, differences in details of the measurement techniques, as discussed below, might lead to differences in inferred initiation levels.

The current Aerodyne program is mainly concerned with enhancement of photolytic initiation (i.e., F-atom production), in pulsed HF/DF chemical lasers. It was proposed that the addition of trace amounts of an interhalogen compound,  $ClF_3$ , might substantially increase the production of F-atoms under practical flash lamp operating conditions by the overall reaction  $ClF_3 + h\nu \rightarrow ClF + 2F$ . This would occur most favorably over the UV absorption band,  $1800\text{\AA} < \lambda > 2400\text{\AA}$ , which is not an effective region for the photodissociation of  $F_2$ . Since  $ClF_3$  has a peak absorption cross section which is approximately 50 times larger than that of  $F_2$ , as shown in Figure 1, concentrations of only a few percent  $ClF_3$  in relation to  $F_2$  should be sufficient to achieve this end.

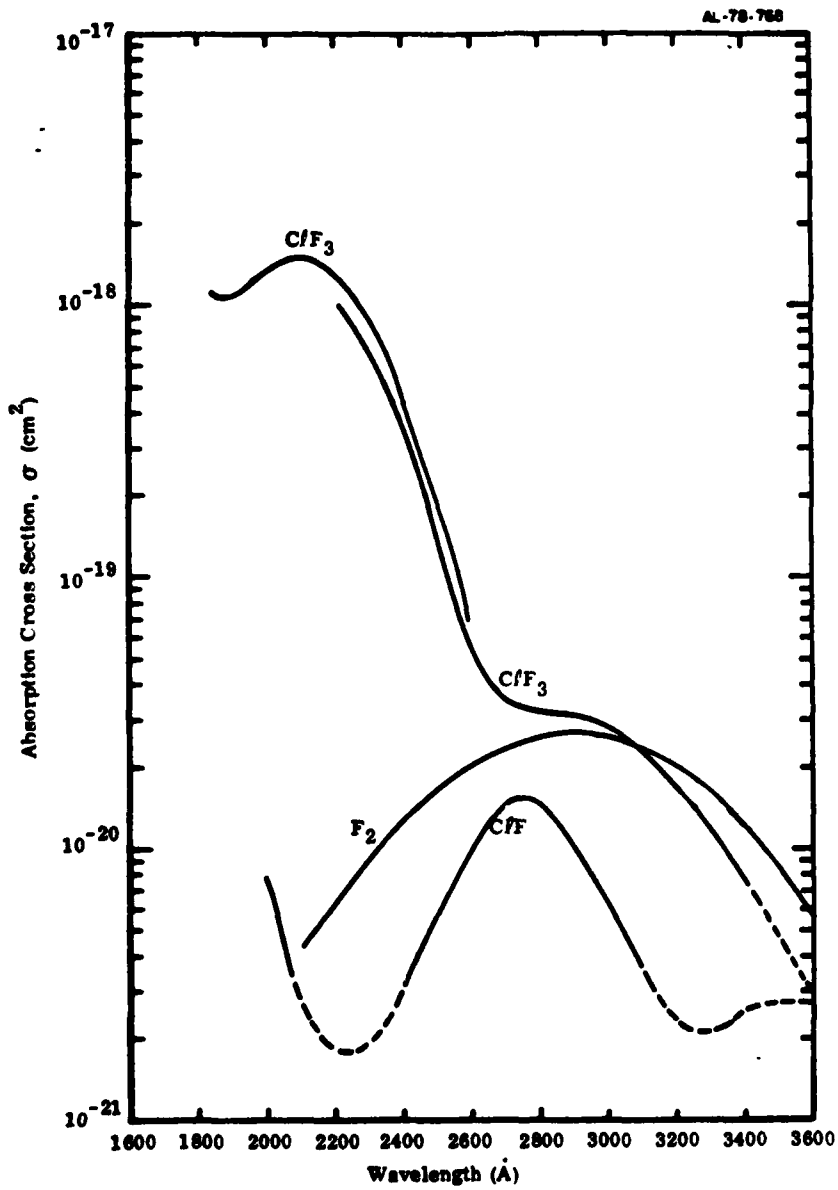


Figure 1. UV Absorption Spectra of  $\text{F}_2$ ,  $\text{CF}_3$ , and  $\text{CF}$  Taken From Reference (7)

The elements of the experimental program were planned to be: (1) construction, operation, and UV spectral analysis of a flash lamp to demonstrate substantial radiant energy in the photolysis band of  $C\ell F_3$ ; (2) demonstration and utilization of an F-atom measurements technique as described by Schlossberg<sup>(5)</sup> which is based upon the predicted absorption line of F-atoms at approximately  $404 \text{ cm}^{-1}$ ; (3) observation of the photolytic depletion of  $C\ell F_3$  and the resultant production of F-atoms using the above technique. This report discusses experimental results which pertain to items (1) and (3) above. It was determined during the course of the work that item (2) was too ambitious an undertaking for this contract; this is in light of the fact that the technique is new and not yet fully demonstrated by other investigators. The program was refocused to demonstrate the photolytic dissociation of  $C\ell F_3$  by measurements of variation in UV attenuation and to determine the UV spectral energy content of the flash lamps. It is still desirable, however, to pursue the future development of an F-atom measurements technique for the direct determination of initiation level in pulsed HF/DF lasers.

Spatial uniformity of laser initiation is a major consideration for efficient delivery of laser radiation to a distant target. An overall variation of initiation level of less than  $\pm 5\%$  is felt necessary to achieve program objectives. In the present program, Aerodyne has developed a code to evaluate uniformity of cavity illumination (hence laser initiation), by flash lamps in geometrical configurations which are representative of repetitively pulsed chemical lasers. This code was applied to assess the trade-off between system electrical efficiency and spatial uniformity of initiation. The resulting study points to the possibility of a very favorable trade-off if  $C\ell F_3$  is added as a trace species in a spatially tailored manner. Concentrations of  $C\ell F_3$  would be increased in cavity regions of low lamp illumination to achieve uniformity in laser initiation by the enhanced F-atom production due to  $C\ell F_3$  photolysis.

Analytical studies of flash lamp performance were carried out to aid in design of the experiment and to allow a plausible extrapolation of results to pulsed laser systems with short lamp pulses. The RESALE<sup>(6)</sup> laser performance code was used to assess the overall influence of  $C\ell F_3$  addition to HF laser performance. The code predicts no significant degradation in performance resulting from the inclusion of  $C\ell F_3$  at concentrations consistent with the above stated objectives.

## 2. LASER INITIATION ENHANCEMENT BY $\text{C}\ell\text{F}_3$ ADDITION

The photolytic absorption cross sections of  $\text{C}\ell\text{F}_3$  and  $\text{F}_2$  are given in Ref. (7) and here in Figure 1. One sees the absorption peak for  $\text{C}\ell\text{F}_3$  in relation to  $\text{F}_2$  is approximately 50 times larger and occurs at substantially shorter wavelength. In a gas mixture containing  $\text{C}\ell\text{F}_3$  and  $\text{F}_2$  in the proportion 1:50, the weighted absorption cross section for  $\text{C}\ell\text{F}_3 + \text{F}_2$  is shown in Figure 2. If photon absorption by  $\text{C}\ell\text{F}_3$  results in the products  $\text{C}\ell\text{F} + 2\text{F}$ , then the production of F-atom in this gas mixture by a flash lamp with uniform energy distribution over the band of Figure 2, would be approximately 66% higher than that in a mixture with  $\text{C}\ell\text{F}_3$  omitted. This illustrates the potential for dramatic increases in lamp energy utilization for HF/DF laser initiation and the attendant increases in overall electrical efficiency. Realization of these gains rests upon the conditions that significant lamp radiation occurs in the absorption band of  $\text{C}\ell\text{F}_3$  and that F-atoms are produced by this absorption. Measurements are discussed later which address these conditions. Broader implications of initiation enhancement by  $\text{C}\ell\text{F}_3$  addition are discussed next with relation to spatial uniformity.

Theoretical cavity illumination studies were conducted, using the variable geometry shown in Figure 3. The model is two dimensional; however, lamp and wall contributions to illumination and cavity gas attenuation are properly treated in the direction parallel to the cavity optical axis. Consequently, Figure 3 and the associated analysis approximates a laser cavity section normal to the optical axis midway between distant cavity optical elements. Two sides of the section are assigned variable, independent reflectivities and represent flow entry and exit planes in a repetitively pulsed device. Top and bottom sides are dedicated to flash lamps banks, as shown, and are assigned a third, variable wall reflectivity. The broken line in Figure 3 represents the active laser cavity. All system dimensions are adjustable except those which define lamp spacing and lamp recess geometry as indicated in Figure 3. Attenuation is assumed constant throughout the active cavity and is assigned by a value of the product

$$\epsilon_{\text{ph}} = \sigma n w_2 \quad (2-1)$$

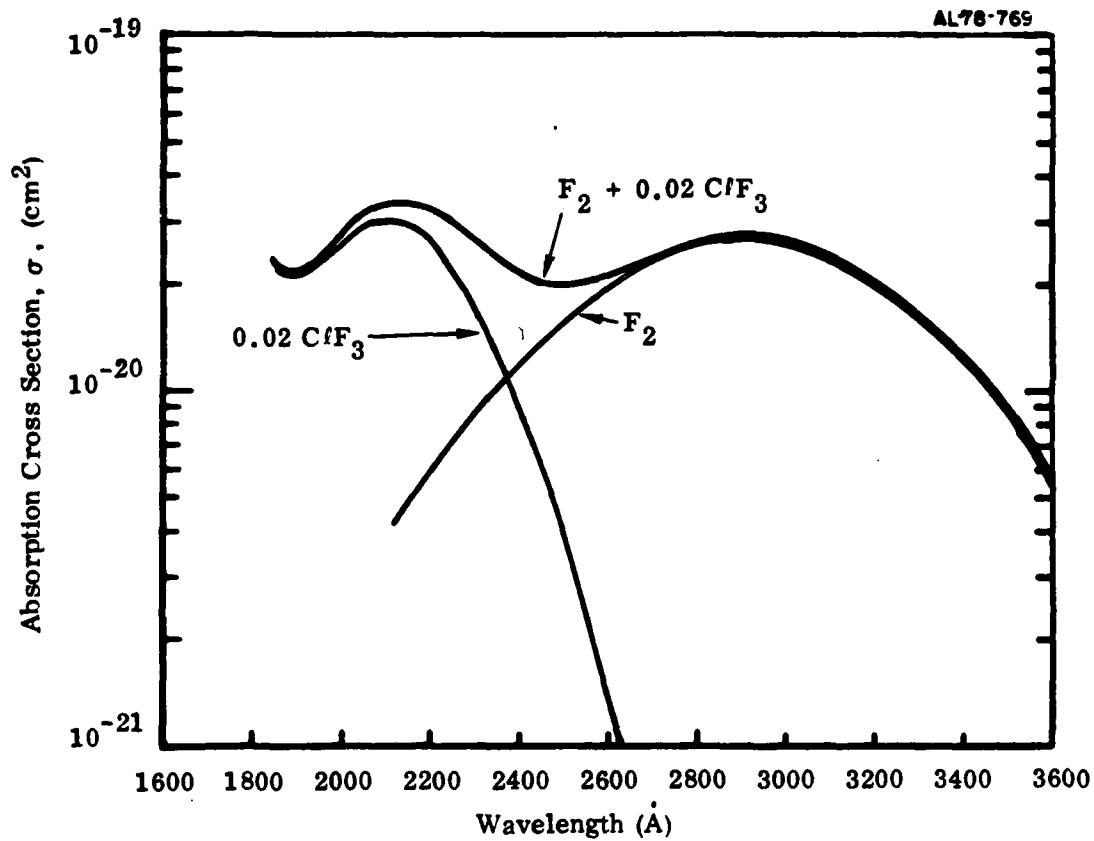


Figure 2. Weighted Absorption Spectrum for a Mixture of 98%  $\text{F}_2$  Plus 2%  $\text{ClF}_3$

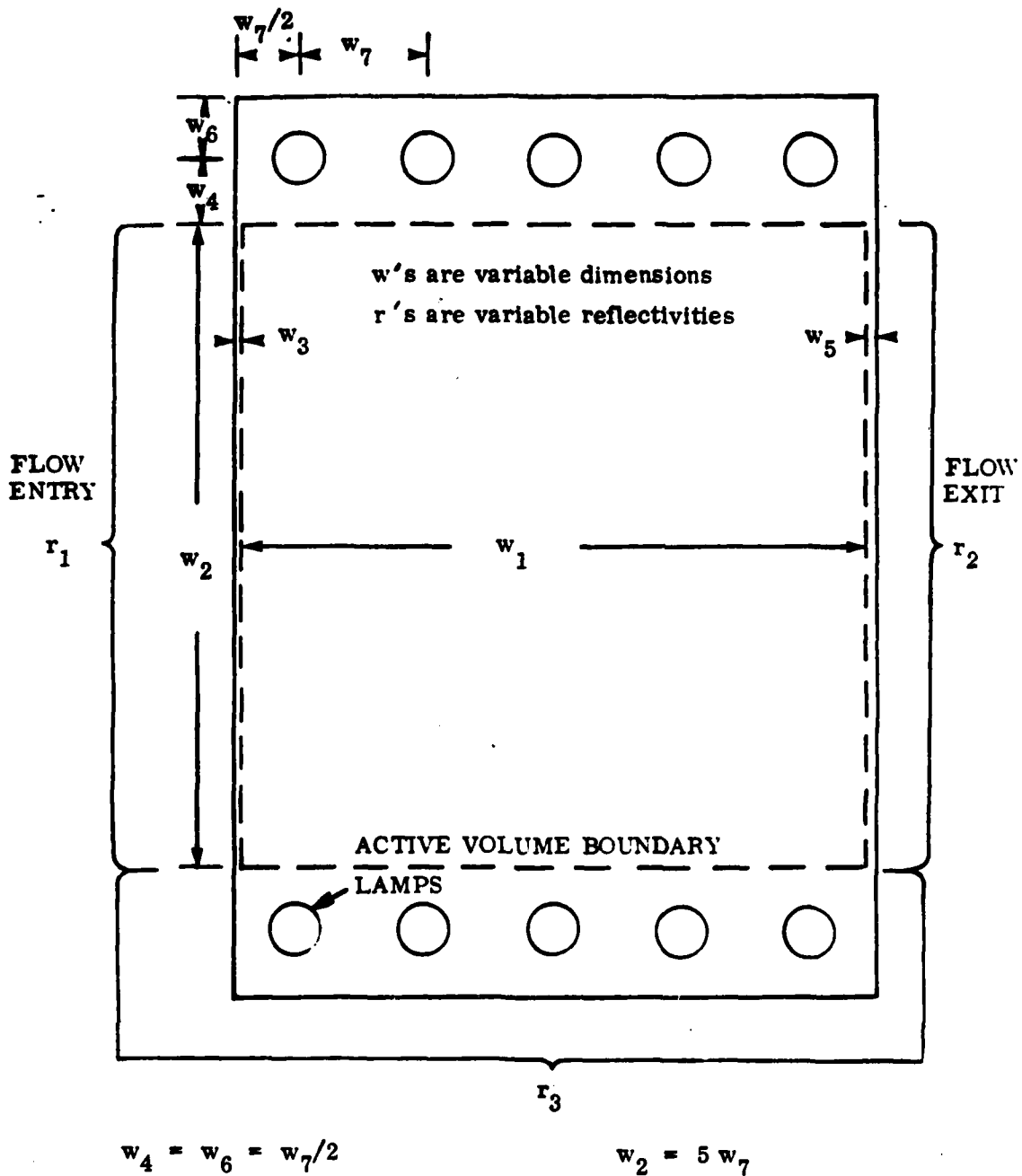


Figure 3. Cavity Cross Section Geometry for Illumination Modeling

where  $\sigma = \sigma(\lambda)$  is the gas absorption cross section at wavelength  $\lambda$ ;  $n$  is the number density of the absorbing species and  $w_2$  is the cavity height as shown in Figure 3.

This simple but flexible geometry allows fair assessment of uniformity of cavity illumination for a variety of realistic operating conditions in repetitively pulsed devices and also in a single pulse device with associated high wall reflectivity. The model is first applied to a rather idealized case of a single pulse device in which the cavity cross section is square and all walls have a reflectivity of 0.8. The solution is symmetric about the center-plane and is therefore shown only in the top half of Figure 4. Here isointensity contours, for a gas absorption,  $\epsilon_{ph} = 0.05$ , show an overall variation of  $\pm 8.5\%$ . The model is next applied to a representation of a repetitively pulsed device in the rather extreme case when flow entry and exit planes of a square cavity are assumed to be totally absorbing as a result of concessions given to entry mixing hardware and exit acoustical damping. Lamp walls are again give a reflectivity of 0.8. This solution is also symmetric about the center plane and is shown in the bottom half of Figure 4. Isointensity contours, for a gas absorption  $\epsilon_{ph} = 0.05$ , show a distressing overall variation of  $\pm 37\%$ . It is clear that measures must be taken to improve illumination or initiation uniformity in the repetitively pulsed case to insure reasonable outcoupled power, as well as good beam quality. Even the idealized single pulse example of Figure 4 may have unacceptable spatial variations in illumination.

Two geometrical exercises are next examined for the repetitively pulsed case to assess penalties in system electrical efficiency associated with improvements in illumination uniformity. In Case B, the lamp planes are extended both upstream and downstream from a square laser cavity section as shown in Figure 5. Lamp spacing is held fixed, so that the number of lamps is increased in units of four between runs, such that their total number is proportional to cavity width. The average cavity illumination intensity was held fixed between runs and the associated increase in lamp energy and improvement in illumination uniformity were obtained.

Figure 6 shows the decrease in initiation nonuniformity with increasing numbers of lamps in the extended lamps exercise for the repetitively pulsed Case B. This shows that the lamp planes must be extended to 3.4 times the laser cavity extent in

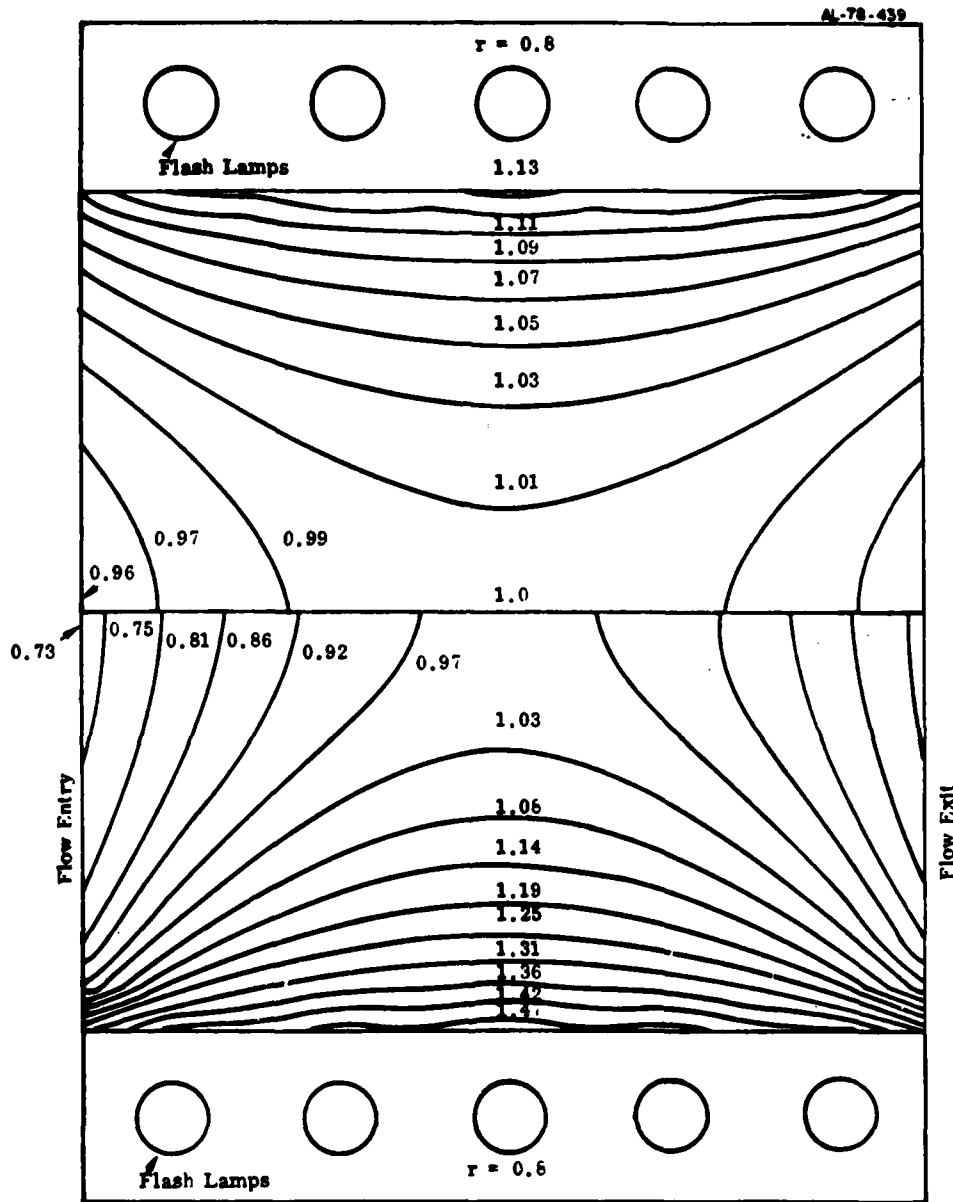
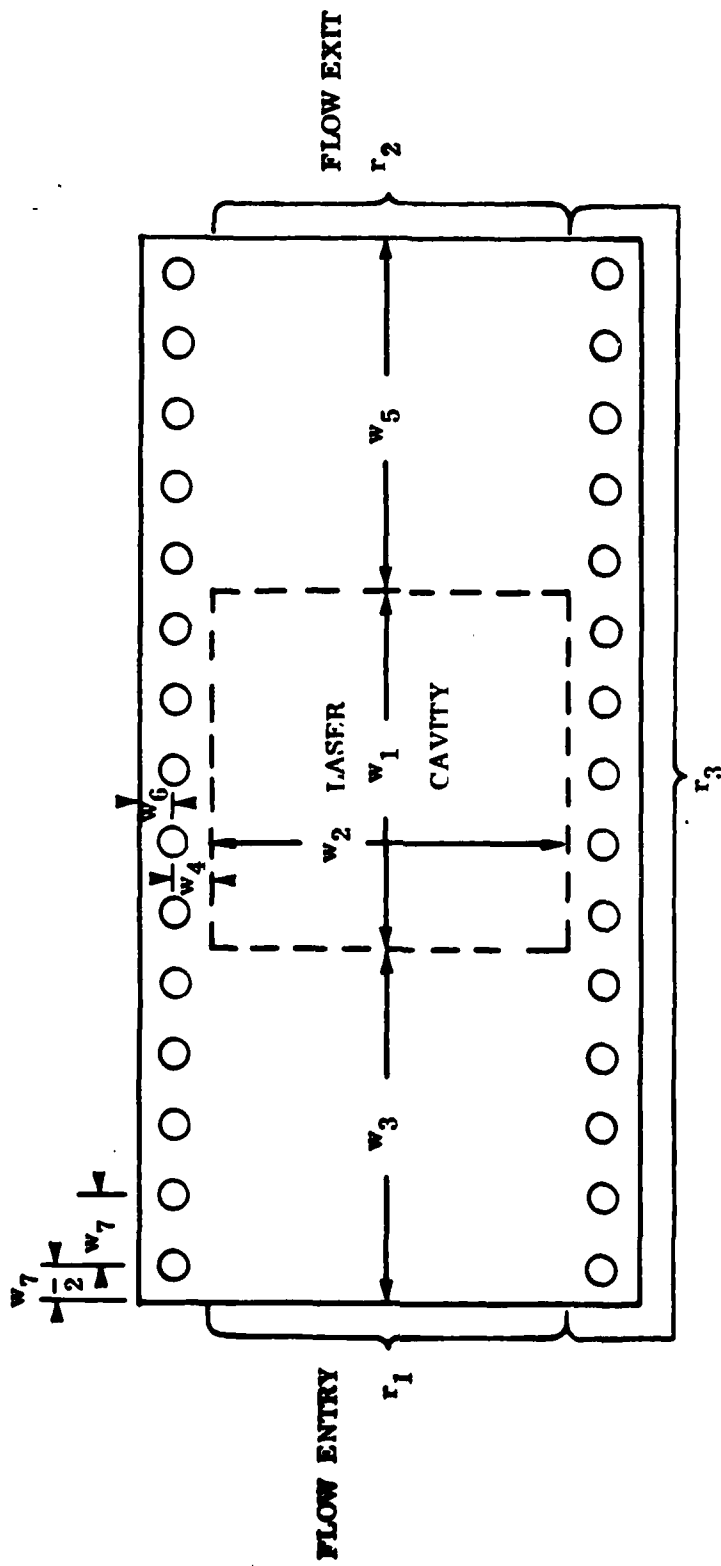


Figure 4. Normalized Cavity Illumination Contours. Top Half: Case A. All Walls Reflecting  $r = 0.8$ . Bottom Half: Flow Entry and Exit are Nonreflecting



$$w_4 = w_6 = w_7/2 \qquad r_1 = r_2 = 0.0 \qquad w_2 = 5 w_7$$

$$w_1 = w_2 \qquad w_3 = w_5 \qquad \sigma_n w_2 = 0.05$$

$$r_3 = 0.8$$

Figure 5. Case B. Extended Lamps. Flow Entry and Exit are Nonreflecting

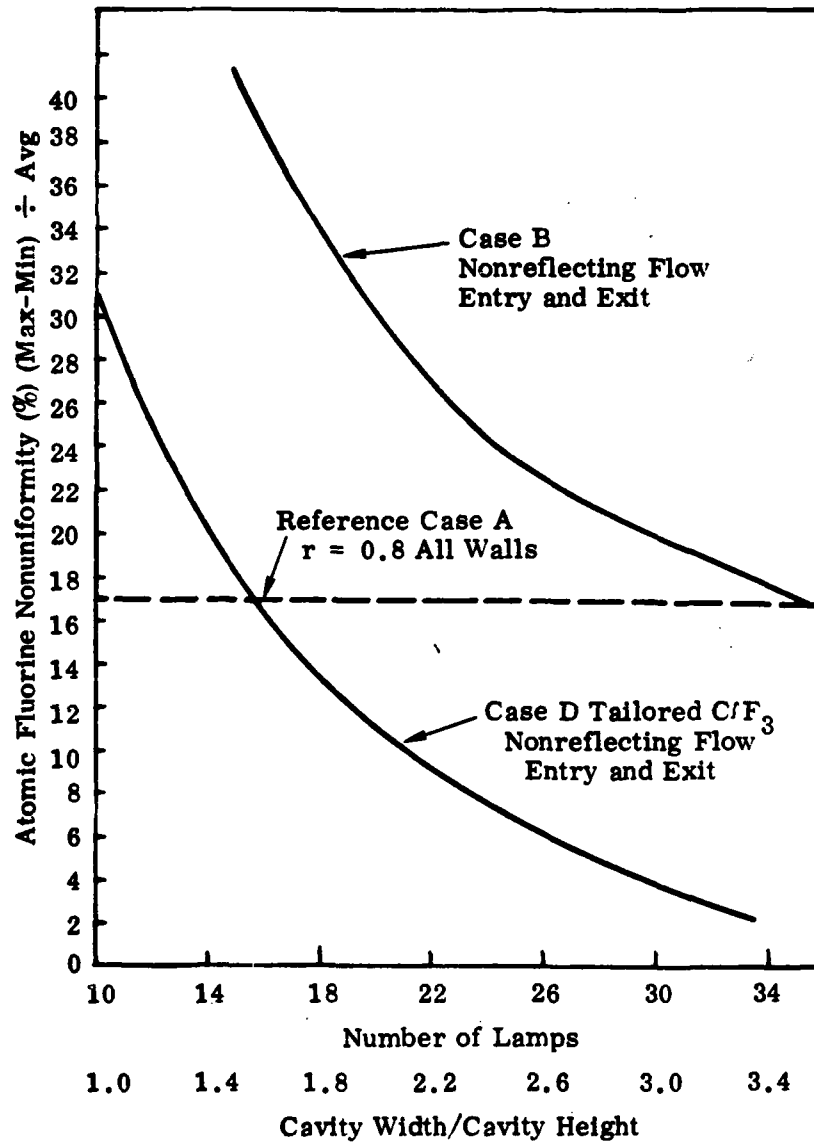


Figure 6. Nonuniformity in Cavity Illumination with Extended Lamps. With (Case D) and Without (Case B) Tailored  $C/F_3$  Addition

the flow direction to achieve a degree of cavity initiation uniformity equal to that of the single pulse Reference Case A of Figure 4. For fixed laser cavity illumination it is clear from Figure 5 that absorbing flow entry and exit planes and extended lamp planes require increased total flash lamp energy. Figure 7 shows this increase in lamp energy demand as lamp planes are extended for the repetitively pulsed Case B. Here lamp energy is normalized by that required for Reference Case A, where all walls are reflecting at  $r = 0.8$ . Comparison of Figures 6 and 7 shows that the repetitively pulsed Case B achieves the same level of initiation and degree of uniformity as Case A when the lamp planes are extended to 3.4 times the cavity width in the flow direction and the lamp electrical energy is increased by a factor of 3.6. This unattractive prospect is even less desirable if one considers the penalties in acoustical damping and gas mass utilization efficiency associated with the geometry of Figure 5. The severity of these requirements are somewhat diminished if the lamp planes are crowned rather than flat and may be significantly diminished if some degree of reflectivity is retained in the flow entry and exit planes.

All the above analysis uses a gas absorption parameter,  $\epsilon_{ph} = 0.05$ . Solutions were carried out for Case A, also, for a range of absorption  $0 \leq \epsilon_{ph} \leq 0.20$ ; the associated variation in degree of illumination nonuniformity increased with increasing gas absorption over the range  $\pm 7.8\%$  to  $\pm 11.3\%$ . A second geometrical exercise was carried out with this illumination code in which the lamp planes were withdrawn from the active laser cavity as shown in Figure 8. Average cavity intensity was held fixed between runs and the associated increase in lamp energy and improvement in illumination uniformity were obtained. It was found that the illumination uniformity was equal to that of Reference Case A when the lamp plane separation,  $(2w_4 + w_2)$ , was approximately three times the active cavity height,  $w_2$ ; the associated lamp energy required was equal to 6.9 times that for Case A. Since this lamp energy requirement is not practical, this case is not discussed further. These two exercises, extended lamps and remote lamps, are extreme geometric alterations which, when combined, would allow a great variety of configurations. One may expect that for all such combinations with nonreflecting flow entry and exit planes, the lamp energy penalty for a specified degree of illumination uniformity will not be better than that of Case B.

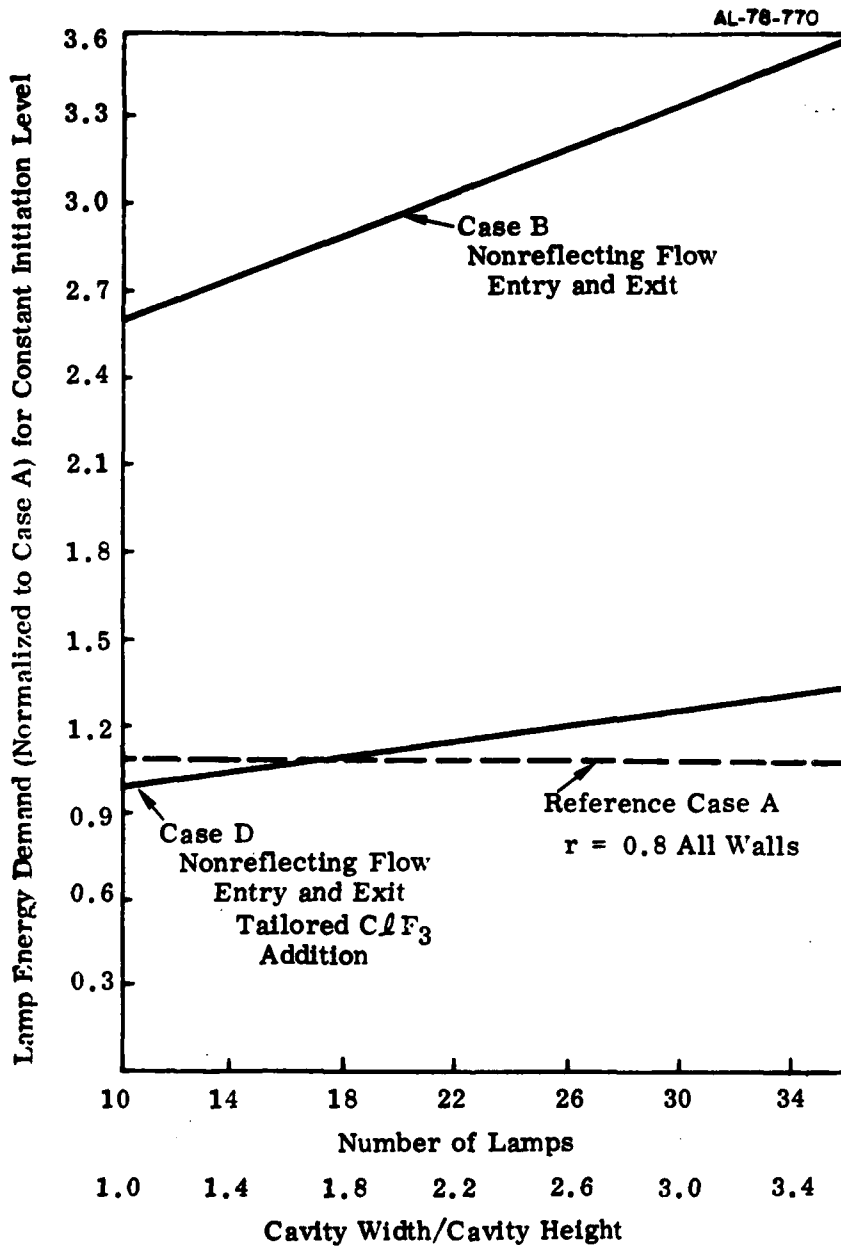
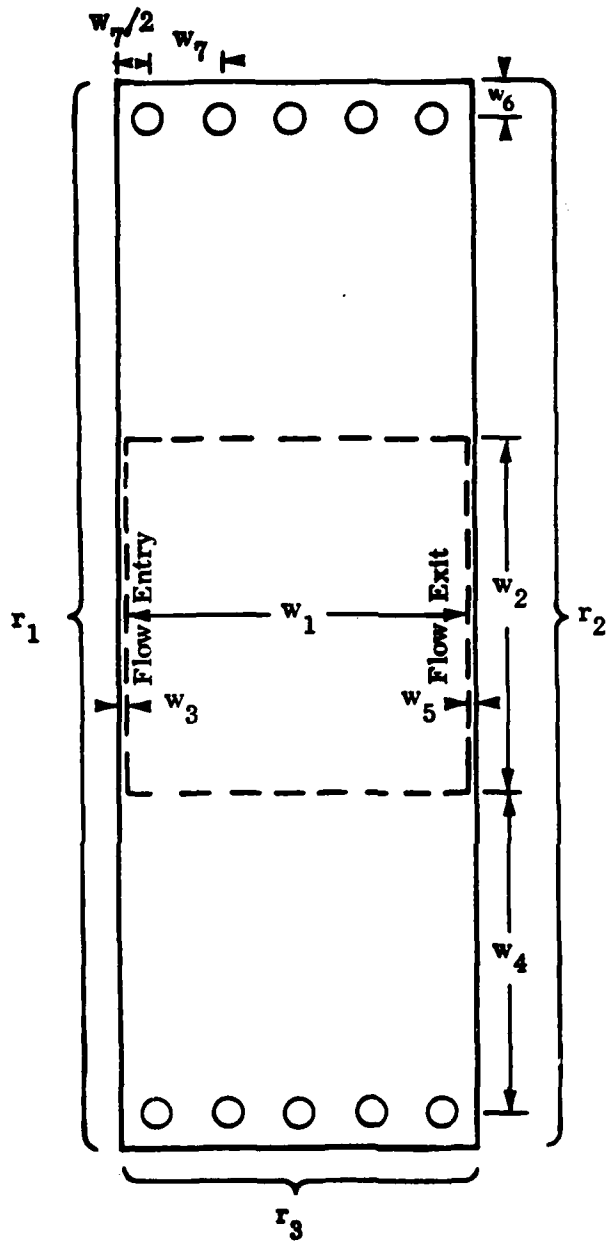


Figure 7. Lamp Energy Demand for Extended Lamp Planes



$$\begin{aligned}
 w_6 &= w_7/2 & r_1 &= r_2 = 0.0 & w_2 &= 5w_7 \\
 w_1 &= w_2 & \sigma n w_2 &= 0.05 & r_3 &= 0.8 \\
 w_3 &= w_5 = 0.0 & & & & 
 \end{aligned}$$

Figure 8. Case C. Remote Lamps. Flow Entry and Exit are Nonreflecting

The illumination contours in Figure 4 suggest that spatial uniformity in initiation may be improved considerably if F-atom production were enhanced near the cell center plane. This might be achieved by the introduction of a spatially tailored steady flow of  $C\ell F_3$ , such as shown in Figure 9. This addition of  $C\ell F_3$  to the steady flow of  $F_2 + He$  in a repetitively pulsed system, shows a spatially uniform portion of 2% in relation to  $F_2$ , plus a parabolically tailored steady flow portion with a center plane maximum of 3% in relation to  $F_2$ . The uniform portion is suggested for an overall increase in initiation level associated with the broadened UV band for F-atom production as described earlier. The spatially tailored portion is intended to increase F-atom production near the cavity center plane to offset diminished lamp illumination as shown in the lower part of Figure 4. If we assume uniform lamp radiation over the UV absorption bands of  $C\ell F_3$  and  $F_2$ , and assume photon absorption by  $C\ell F_3$  yields two F-atoms, then the concentration profile of Figure 9 yields a spatial variation in initiation level of  $\pm 15.5\%$ . For equal average levels of initiation, the example of Figure 9 has a lamp energy demand of 0.95 times that for Reference Case A. Further increases in initiation uniformity may be obtained again by extending the lamp planes in the flow direction. With tailored  $C\ell F_3$  addition and absorbing flow entry and exit planes, results of this exercise are shown as Case D in Figures 6 and 7. Figure 6 shows that initiation uniformity, with tailored  $C\ell F_3$  addition in the repetitively pulsed case, equals that of the single pulse closed cell (Reference Case A), when lamp planes are extended both upstream and downstream of the active cavity by 25%. Figure 7 shows that the associated lamp energy demand is approximately equal to that of Reference Case A for equal initiation levels. In summary, tailored  $C\ell F_3$  addition offers the possibility of achieving, in a repetitively pulsed laser with nonreflecting flow entry and exit planes, the same spatial uniformity of initiation as might be achieved in a single pulse system where all walls are efficient UV reflectors. Furthermore, this may be achieved in a practical geometry in view of acoustical and gas mass utilization requirements, and with a lamp energy demand equal to that of the single pulse system. Comparisons of Case B and D in Figures 6 and 7 point to considerable added difficulties without tailored  $C\ell F_3$  addition in repetitively pulsed devices of good beam quality, in the areas of overall electrical efficiency, interpulse acoustical damping and efficiency of gas mass utilization.



### 3. FLASH LAMP MODELING

Successful enhancement of pulsed HF/DF laser initiation by  $C\ell F_3$  addition requires efficient lamp radiation in the absorption band. Figure 1 shows that significant lamp radiation must occur over the spectral region between 1750Å and 2400Å. Although a good data base has recently been established<sup>(8)</sup> for short pulse flash lamp radiation in the absorption band of  $F_2$ , this is not the case for the absorption band of  $C\ell F_3$ . Consequently, we have developed some preliminary modeling of this phenomenon to aid in the selection of lamp operating conditions for  $C\ell F_3$  photolysis experiments, described later, and to aid in the extrapolation of these results to short lamp pulse operation appropriate to pulsed chemical lasers. This lamp modeling is not definitive, but is directed to satisfy these narrow goals. The experimental study uses argon lamp fill, hence, this modeling also is limited to argon. The modeling, in its present form, assumes optically thick blackbody radiation at all wavelengths and assumes uniform gas conditions across cylindrical flash tube radius. Approximate corrections to the assumptions are applied to the resulting solutions to provide qualitative predictions of lamp performance.

#### 3.1 Lamp Explosion Limit

Lamp explosion criteria for xenon filled tubes are provided by EG&G<sup>(9)</sup> and are shown in Figure 10. These results, which apply to critically damped lamp circuits, show a lamp energy capacity which varies as the square root of lamp pulse duration. This failure is likely due to a tube surface thermal loading which results from a combination of thermal conduction and radiation absorption. This failure would follow the scaling,

$$E_{i, \max} \sim \pi d l \tau_l^{1/2} \quad (3-1)$$

where  $E_i$  is initial capacitor energy;  $d$  is lamp inside diameter;  $l$  is tube length and  $\tau_l$  is lamp pulse duration. The EG&G failure criteria apply to long lamp pulses,

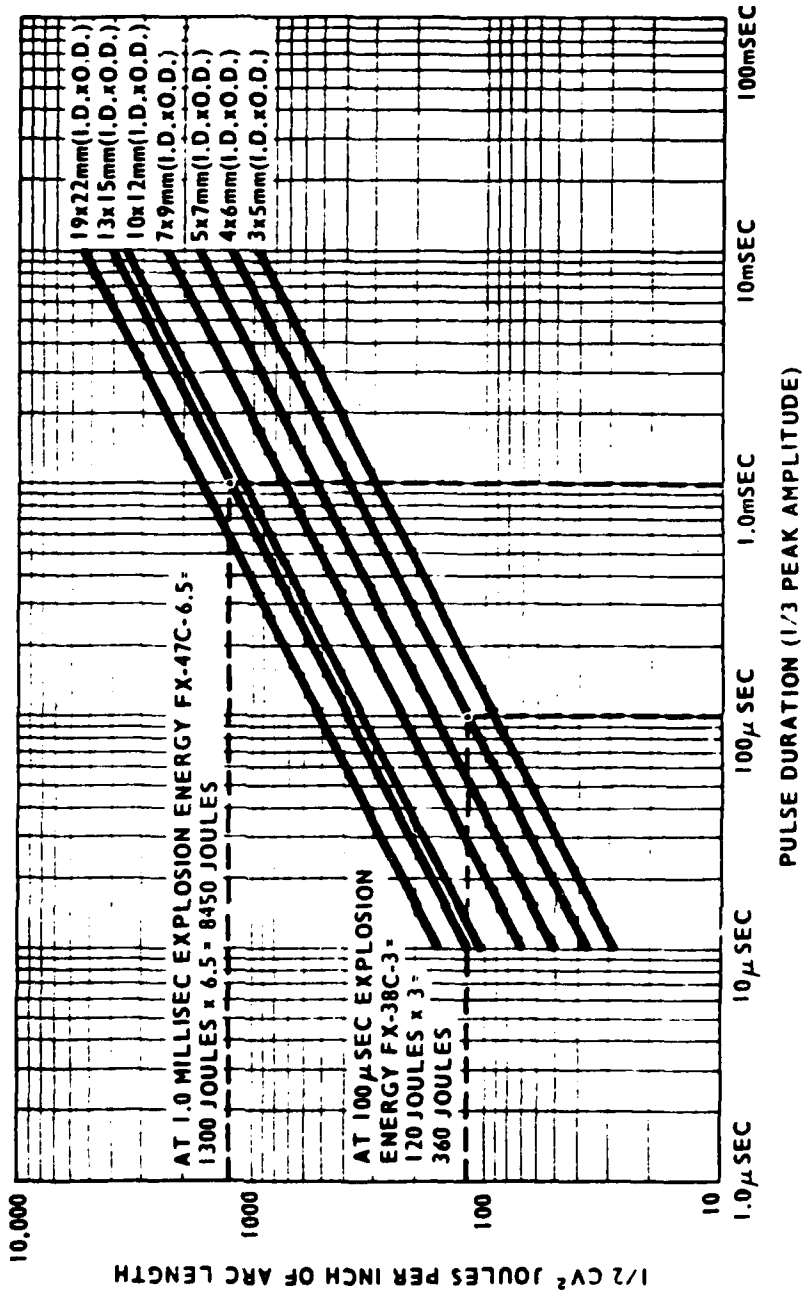


Figure 10. Loading (Joules per inch) at Which Linear (Quartz Envelope) Flashtubes Explode (From EG&G Data Sheet FI002C-2)

defined here as those whose pulse duration is controlled by the circuit characteristic time  $R_l C$ . Conversely, short lamp pulses are defined as those whose pulse duration is controlled by lamp gas radiation cooling time. Long lamp pulse duration is proportional to  $R_l C$ , where  $R_l$  is a characteristic lamp gas resistance and is relatively insensitive to varying lamp circuit parameters and gas fill pressure and thus varies primarily as  $(l d^{-2})$ . Consequently, Eq. (3-1) is replaced by:

$$\left( \frac{1}{2} C V_i^2 \right)_{\max} \sim \pi d l (R_l C)^{1/2} \sim l^{3/2} C^{1/2} \quad (3-2)$$

The coefficient in the scaling relation, Eq. (3-2), may be taken from any point in Figure 10 to yield the explosion limit equation, in MKS units.

$$\left( C^{1/2} V_i^2 \right)_{\max} = 3.5 \times 10^6 l^{3/2} \quad (3-3)$$

This relation, which applies to xenon gas fill and long lamp pulses, was used to select tube and circuit operating parameters in the present experimental study with argon lamps.

### 3.2 Argon Flash Lamp Modeling

This modeling ignores: 1) wall conduction cooling, 2) lamp circuit inductance, 3) lamp optical transparency, and 4) lamp radial property variations. Assumption 1) applies when  $(R_l C)$  and lamp radiation cooling time are short compared to wall conduction cooling time; this assumption is valid for the operating conditions of current interest. Assumption 2) applies when the induction rise time,  $\sqrt{LC}$ , is small compared to either  $(R_l C)$  or the radiation cooling time, whichever is larger. For long lamp pulses, this constraint is unrealistic for practical considerations of lamp lifetime, but it should not qualitatively alter the model predictions. For short lamp pulses, results below will show that assumption 2) is valid. Assumptions 3) and 4) are unrealistic and have been imposed for the sake of simplicity. Resulting predictions overestimate UV lamp radiation, but then are modified by approximate corrections to yield qualitative lamp performance predictions.

Lamp operation is at sufficiently high ionization levels that transport properties are controlled by charged particle collisions. Thermal conductivity is given by Mitchner and Kruger<sup>(10)</sup> in the Spitzer limit as:

$$k_{\ell} = 3.2 k^2 n_e T (m_e \nu_{ei})^{-1} \quad , \quad (3-4)$$

where  $k$  is Boltzmann's constant;  $T$  is electron temperature,  $n_e$  is electron density;  $m_e$  is electron mass, and  $\nu_{ei}$  is electron-ion collision frequency. This collision frequency is given in Ref. (10) for a singly ionized gas in MKS units as:

$$\nu_{ei} = 3.64 \times 10^{-6} n_e (\ell n \Lambda) T^{-3/2} \quad , \quad (3-5)$$

where

$$\Lambda = 1.24 \times 10^7 (T^3/n_e)^{1/2} \quad . \quad (3-6)$$

The conduction cooling time for the gas is:

$$\tau_c = \rho c_p a^2 (4k_{\ell})^{-1} \quad , \quad (3-7)$$

where  $\rho$  is gas density,  $c_p$  is gas specific heat, and  $a$  is depth of gas cooling at the tube wall in time  $\tau_c$ . This conduction cooling time, when applied to lamp operating condition below, may be shown to be substantially larger than lamp pulse duration in all cases. One such example is given below.

Argon degree of ionization is approximated as singly ionized by fitting the Saha equation to equilibrium calculation of Menard and Horton,<sup>(11)</sup> which takes the following form in MKS units,

$$\phi^2 (1 - \phi)^{-1} = 93.9 T^{3/2} p_1^{-1} \text{Exp} (-1.83 \times 10^5/T) \quad , \quad (3-8)$$

where  $p_1$  ( $n/m^2$ ) is initial lamp pressure. Argon energy density is approximated by fitting a calorically perfect gas relation to the calculations of Ref. (11) to yield, in MKS units,

$$e \text{ (J/m}^3\text{)} = 5.1 \times 10^{-3} p_1 T(1 + \phi) + 6.17 \times 10^2 p_1 \phi \quad (3-9)$$

Gas resistivity is given in Ref. (10) and here in MKS units as:

$$\rho_l \text{ (\Omega m)} = 66.2 (l n \Lambda) T^{-3/2} \quad (3-10)$$

where  $\Lambda$  is given in Eq. (3-6). The lamp circuit equation, with low inductance, takes the form,

$$\frac{dE_c}{dt} = - \frac{2E_c}{R_l C} \quad (3-11)$$

where  $E_c$  is instantaneous capacitor energy,

$$E_c = \frac{1}{2} CV^2 \quad (3-12)$$

and

$$R_l = \rho_l l \left( \frac{\pi}{4} d^2 \right)^{-1} \quad (3-13)$$

The circuit energy equation, with lamp cooling by only blackbody radiation, is:

$$\left( \frac{\pi}{4} d^2 l \right) \frac{de}{dt} = 2 \frac{E_c}{R_l C} - \sigma (\pi d l) T^4 \quad (3-14)$$

where  $\sigma$  is the Stefan-Boltzmann constant.

Solution of the above set of equations requires geometry and circuit inputs;  $d$ ,  $l$ ,  $C$ , and initial conditions for capacitor energy  $E_i$  and argon fill pressure at room temperature  $p_1$ . In addition, an initial value for either  $T_1$  or  $\phi_1$  must be

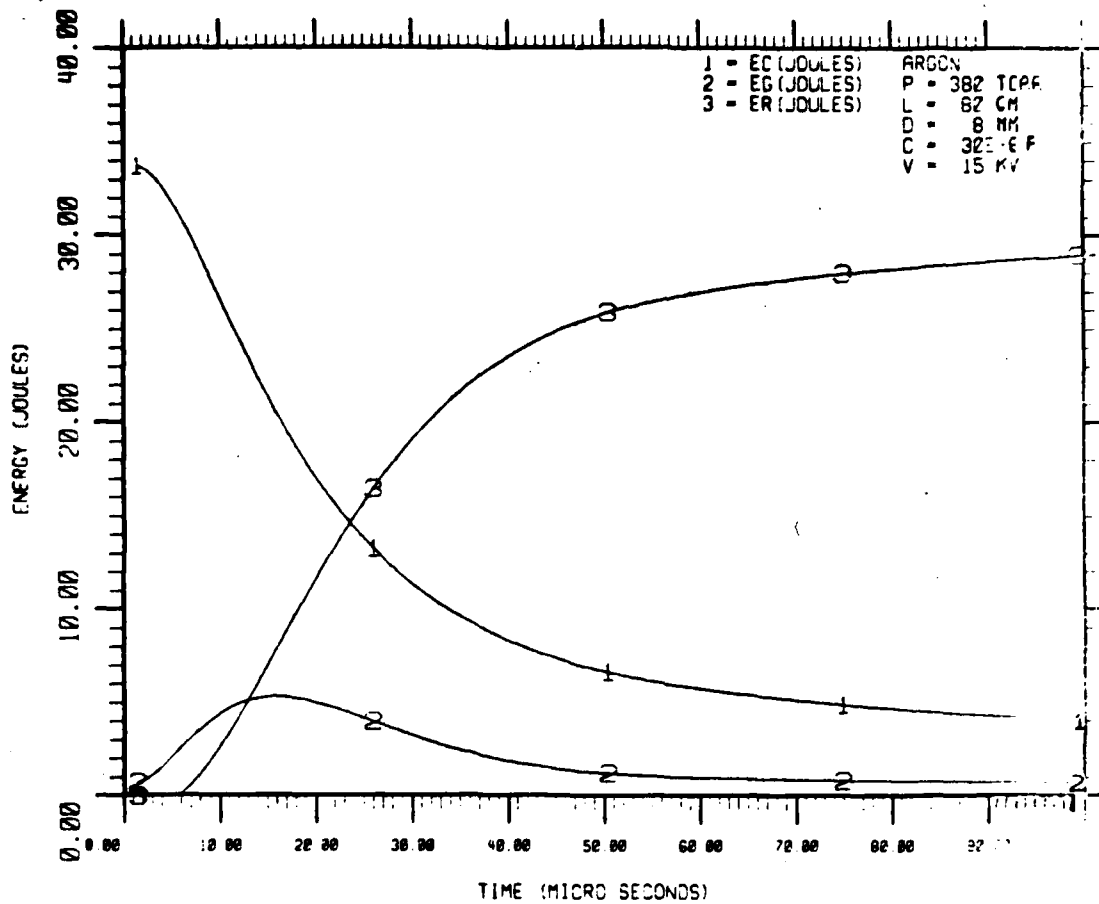
specified to approximate lamp discharge initiation. All solutions were started with the condition  $\phi_1 = 10^{-3}$ . An example is shown in Figures 11a and 11b for a tube inside diameter of 8 mm, an arc length of 80 cm, and a capacitance of 30  $\mu$ f. The explosion limit criteria of Eq. (3-3) specifies a maximum initial voltage  $V_{i_{\max}} = 21.4$  kv and an associated charging energy  $E_{i_{\max}} = 6860$  j. The example considers an energy loading of approximately half this limit,  $E_i = 3375$  j, or charging voltage,  $V_i = 15$  kv. Figure 11a shows capacitor energy  $E_c$ , gas energy  $E_g$ , and radiated energy  $E_r$  versus time. The gas never contains a significant portion of the system energy and the lamp pulse duration is controlled by the circuit characteristics time  $R_l C$ . This is representative of long lamp pulses. Figure 11b shows gas temperature  $T$ , degree of ionization  $\phi$ , lamp resistance  $R_l$ , capacitor voltage  $V$ , and radiated power  $P$  versus time. Lamp pulse duration (FWHM) is seen from Curve 5 to be 27  $\mu$ sec. The circuit characteristic time, based on the minimum value of  $R_l$  is 43  $\mu$ sec. The peak temperature is 17,000°K with a corresponding ionization level of 0.25.

The gas conduction cooling time, for an inward penetration of 1.0 mm from the tube wall, was calculated for gas properties at maximum temperature in Figure 11b. Substitution of these conditions into Eqs. (3-4) through (3-7) yields a conduction cooling time  $\tau_c = 116$   $\mu$ sec. Consequently, wall conduction cooling may be neglected compared with radiation cooling in a time frame of 27  $\mu$ sec. This statement applies to all examples considered in this report.

The time history of lamp gas temperature and the input conditions to the above analysis are sufficient to provide a spectral analysis of lamp radiation in the optically thick limit. Planck's radiation formula provides radiated power per unit lamp area per unit wavelength,

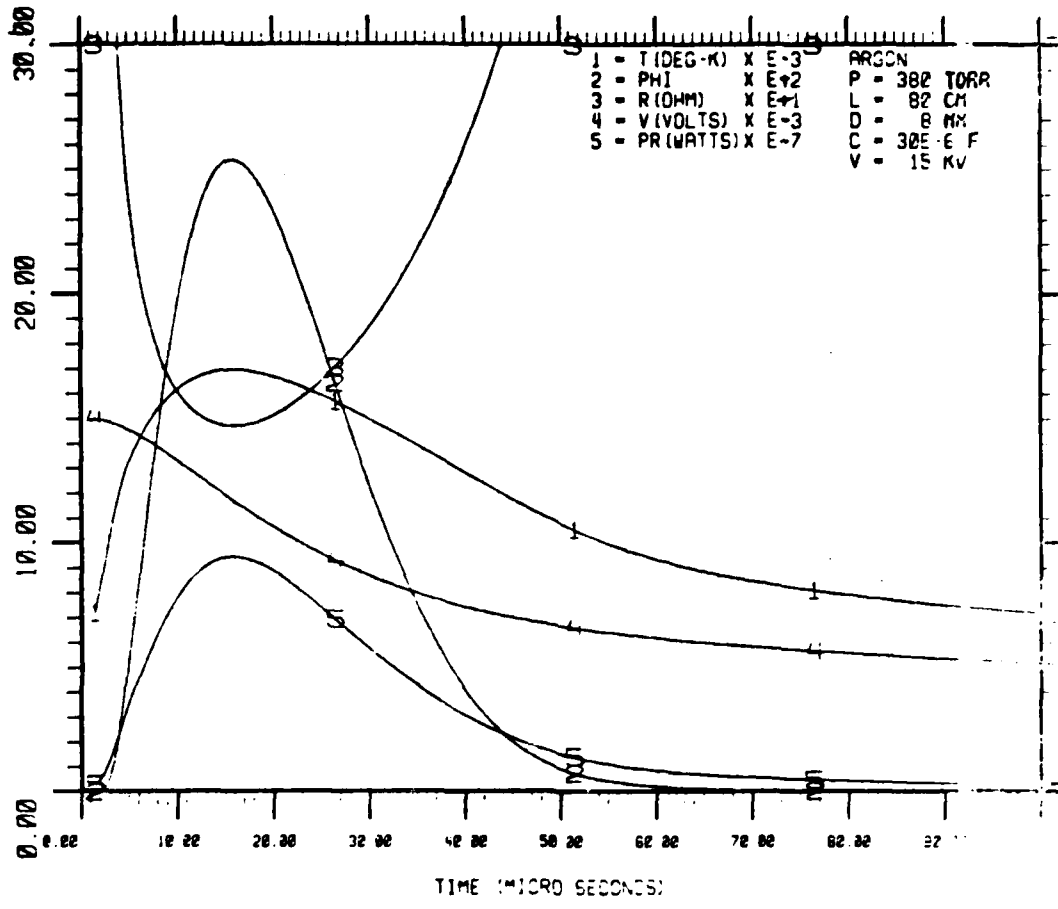
$$P_\lambda = 2\pi c^2 h \lambda^{-5} \left[ e^{\frac{hc}{\lambda kT}} - 1 \right]^{-1} \quad (3-15)$$

where  $c$  is the speed of light;  $h$  is Planck's constant; and  $\lambda$  is the wavelength of radiation. The fraction of total energy which has radiated in unit wavelength interval, at time  $t$  is given by:



11a. Flash Lamp Energy Distribution vs Time

Figure 11. Lamp Radiation Modeling in the Optically Thick Limit.  
 Long Lamp Pulse Example



11b. Flash Lamp Gas Properties vs Time

Figure 11. (Continued)

$$E_{\lambda}/E_i = \frac{\pi d \ell}{E_i} \int_0^t P_{\lambda} dt \quad (3-16)$$

Equation (3-15) is plotted in Figure 11c versus time for six values of wavelength; operating conditions are those of the previous example. The spectral energy radiation efficiency, Eq. (3-16) is shown as a function of wavelength for three values of time after initiation in Figure 11d. Figures 11c and 11d are not corrected for lamp envelope transmission.

Errors in the above analysis, which result from the assumption of optical opacity, are now assessed in terms of a gray body attenuation. It is assumed that the lamp gas is in thermal equilibrium and has spatially uniform properties. Under these conditions, the spectral attenuation coefficient for a singly ionized gas is obtained from Zel'dovich and Raizer,<sup>(12)</sup> in MKS units as:

$$\alpha_{\lambda} = 9.2 n_e^2 T^{-1/2} \omega^2 e^x \quad (3-17)$$

where

$$\omega = 2\pi c/\lambda \quad (3-18)$$

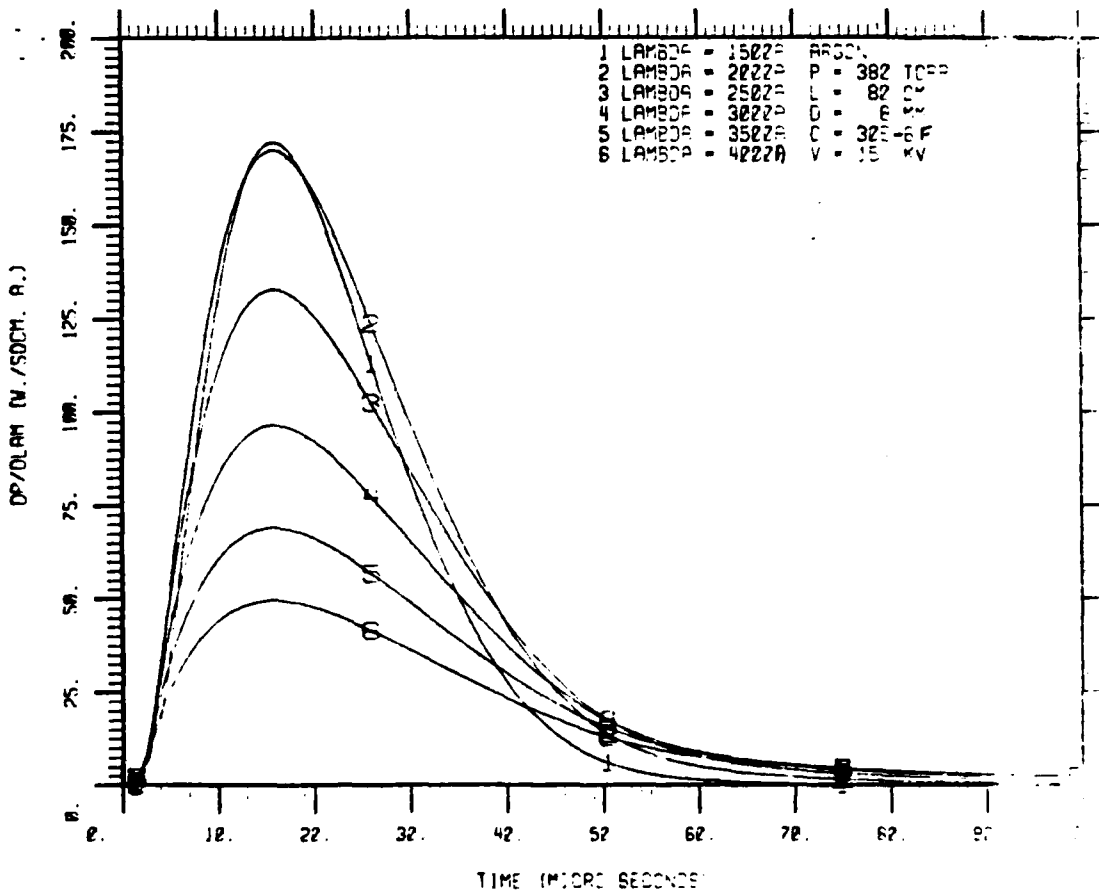
and

$$x = h\omega(2\pi kT)^{-1} = 7.65 \times 10^{-12} \omega/T \quad (3-19)$$

Radiation emitted from a uniform gas in thermal equilibrium along a path of length,  $d$ , is given as:<sup>(13)</sup>

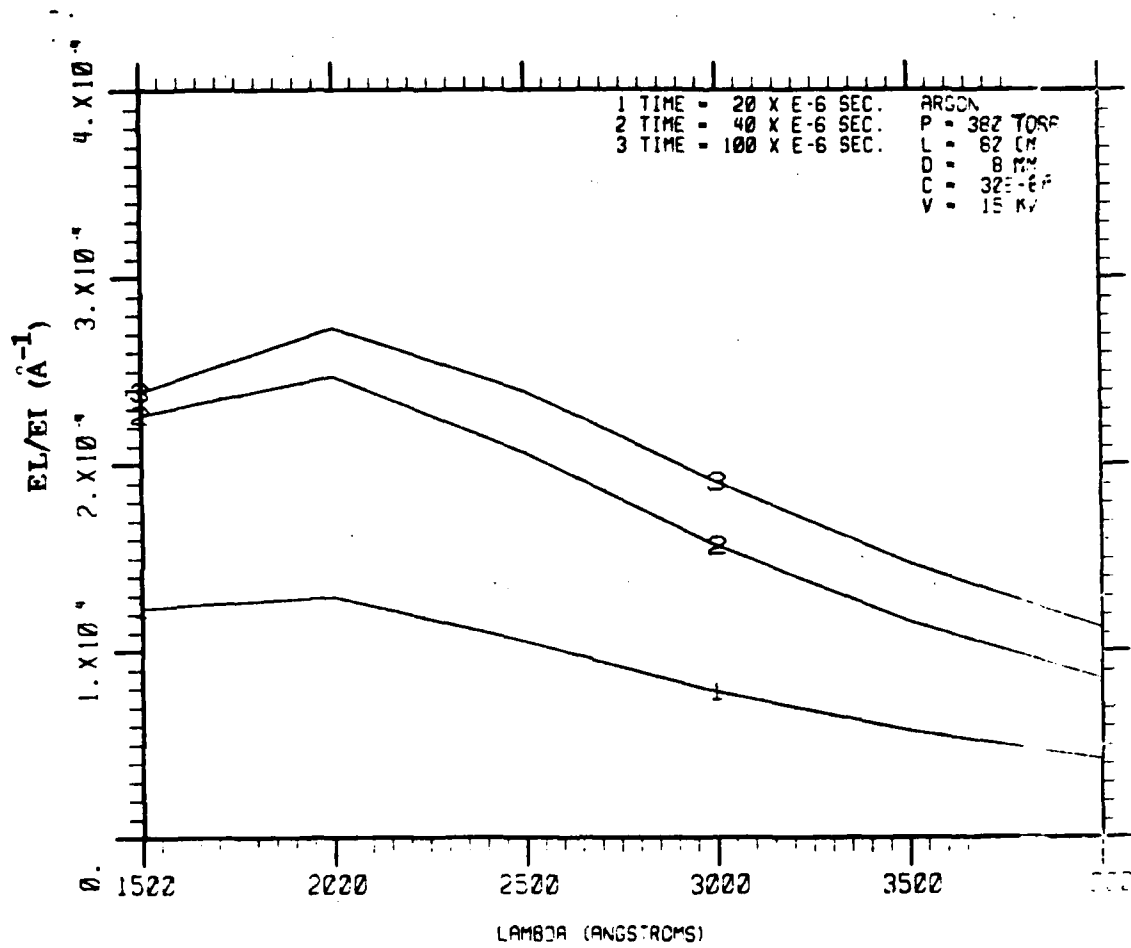
$$i_{\lambda} = i_{\lambda BB} (1 - e^{-\alpha_{\lambda} d}) \quad (3-20)$$

where  $i_{\lambda BB}$  is the radiation associated with  $d \rightarrow \infty$ , which corresponds to a black-body. Directionally averaged power radiated from unit area of a flash lamp may be



11c. Lamp Spectral Power vs Time

Figure 11. (Continued)



11d. Lamp Spectral Radiation Efficiency

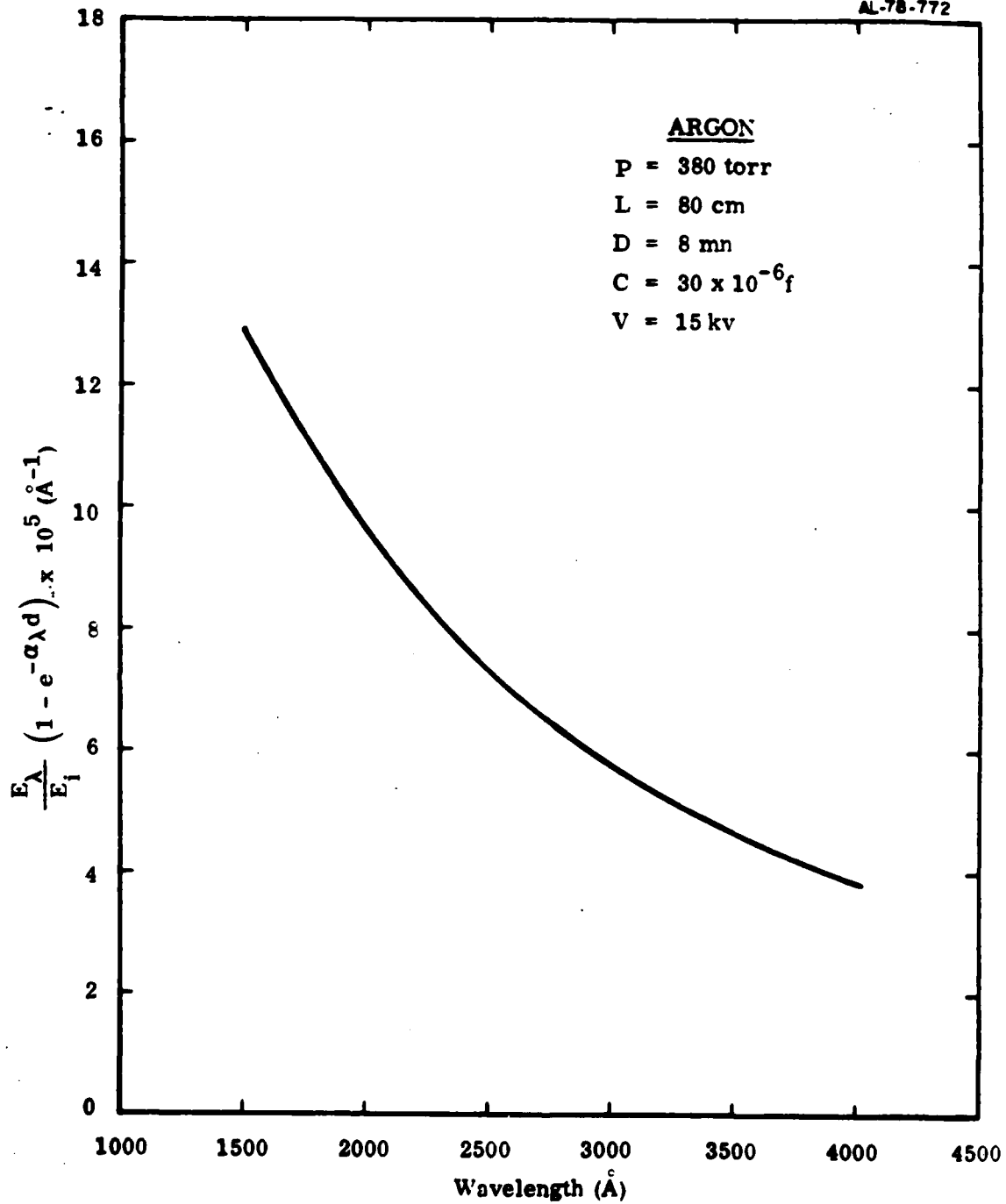
Figure 11. (Continued)

roughly approximated by multiplying Eq. (3-15) by Eq. (3-20), with  $d$  representing tube diameter. In the example of Figure 11, the spectral radiation efficiency at  $t = 100 \mu\text{sec}$  in Figure 11d was modified by the transparency correction Eq. (3-20) using lamp gas properties at peak temperature and the results are shown in Figure 11e. This shows that one may expect substantial radiation in the absorption bands of both  $\text{C}_2\text{F}_3$  and  $\text{F}_2$  for these lamp operating conditions. These are the lamp operating conditions of the photolysis study which is discussed later.

The remainder of this section addresses two questions: (1) How might varying gas fill pressure and capacitor voltage improve the spectral radiation efficiency in  $\text{C}_2\text{F}_3$  and  $\text{F}_2$  absorption bands? (2) How might these long lamp pulse results apply to short lamp pulses, which are appropriate for pulsed chemical laser applications?

A series of lamp model runs were conducted with operating conditions of Figure 11, except argon fill pressure was varied from 76 to 1520 torr. Resulting lamp spectral radiation efficiencies at  $2000\text{\AA}$  and  $3000\text{\AA}$  are presented in Figure 12 with inclusion of the transparency correction Eq. (3-20). A significant improvement in radiation efficiency is predicted for both wavelengths with increasing pressure. Radiation at  $2000\text{\AA}$  is substantially stronger than at  $3000\text{\AA}$  for all fill pressures. This prediction supports the requirement that a significant fraction of radiation occurs in the photolysis band of  $\text{C}_2\text{F}_3$  when compared to that of  $\text{F}_2$ . Potential gains in radiation efficiency with increasing pressure have attendant increases in lamp pulse duration and lamp trigger voltage.

A series of lamp model runs were conducted with operating conditions of Figure 11, except the fill pressure was 760 torr and capacitor charging voltage was varied from 10 to 25 kv. Resulting lamp spectral radiation efficiencies at  $2000\text{\AA}$  and at  $3000\text{\AA}$  are presented in Figure 13 with inclusion of the transparency correction, Eq. (3-20). Corresponding absolute lamp spectral radiation energies are presented in Figure 14. Figure 13 shows a significant increase in radiation efficiency at both wavelengths as charging voltage is increased. Absolute predictions of spectral energy content in Figure 14 show a variation of over two decades at both wavelengths for the voltage range considered. The explosion limit, Eq. (3-3), corresponds to a charging voltage of 21.4 kv, therefore, the penalty in lamp lifetime associated with this method of radiation enhancement is evident.



11e. Lamp Spectral Energy Efficiency with Optical Transparency Correction

Figure 11. (Continued)

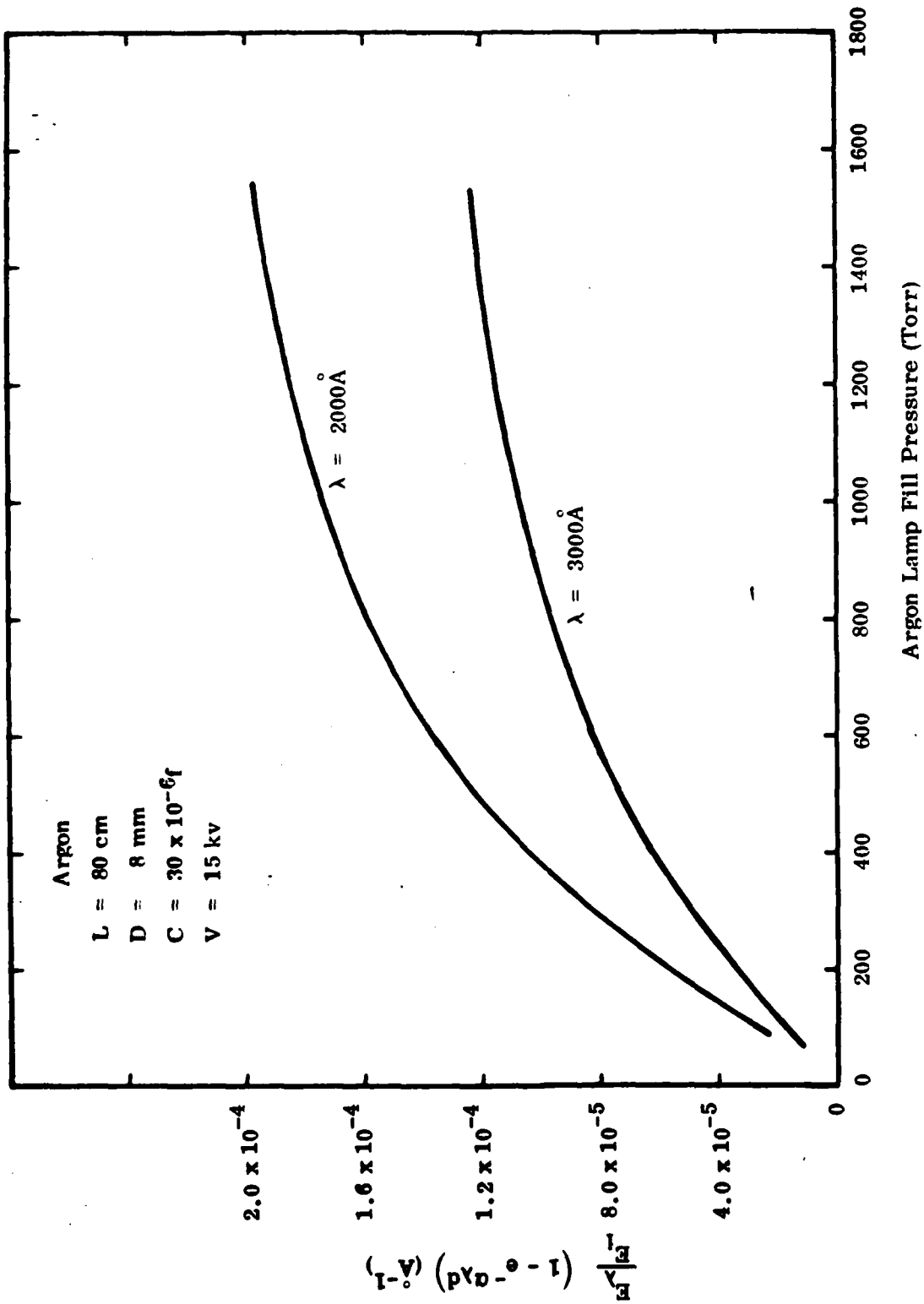


Figure 12. Lamp Spectral Energy Efficiencies at Two Wavelengths as Functions of Argon Fill Pressure

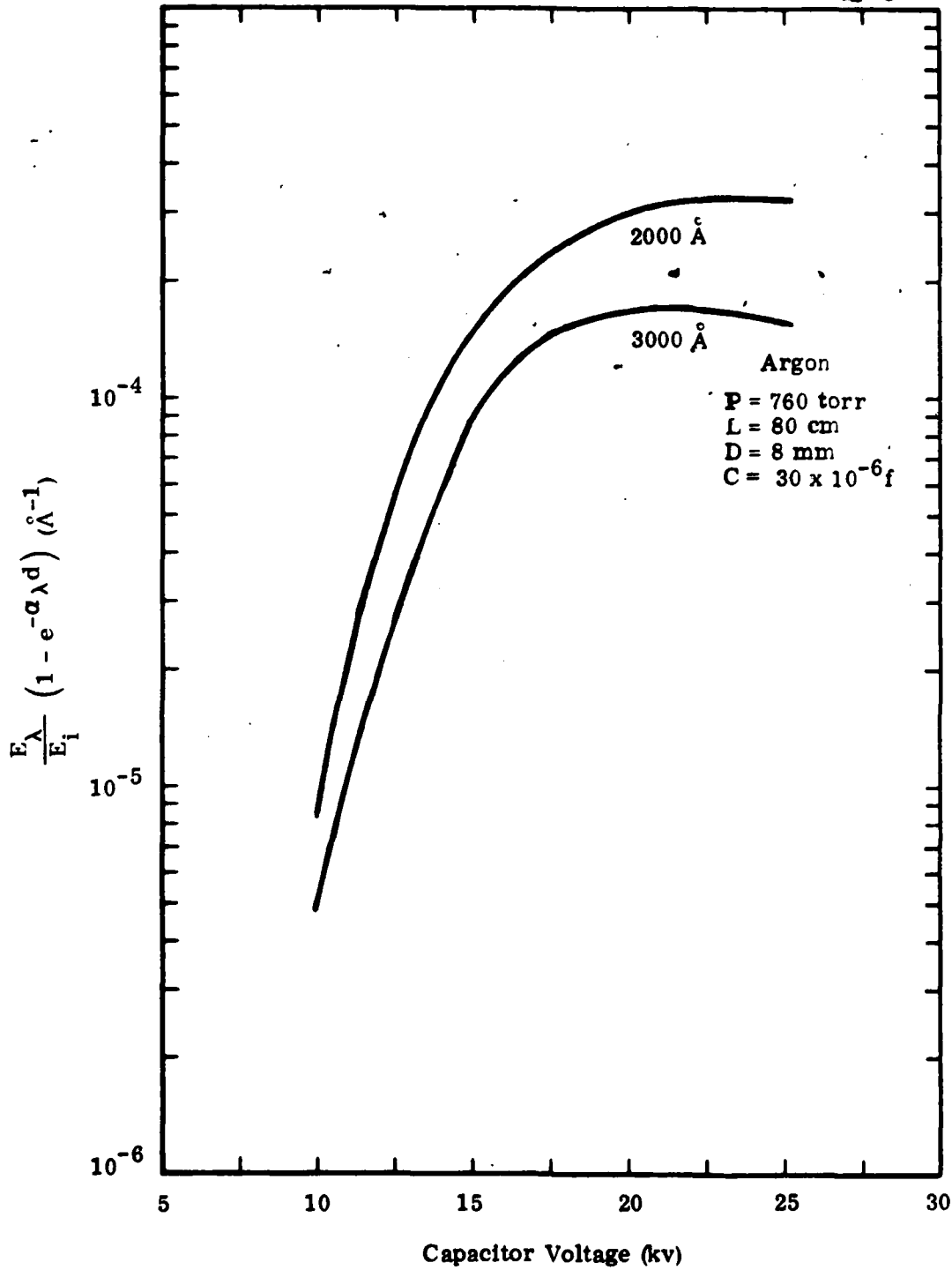


Figure 13. Lamp Spectral Energy Efficiencies at Two Wavelengths as Functions of Capacitor Voltage

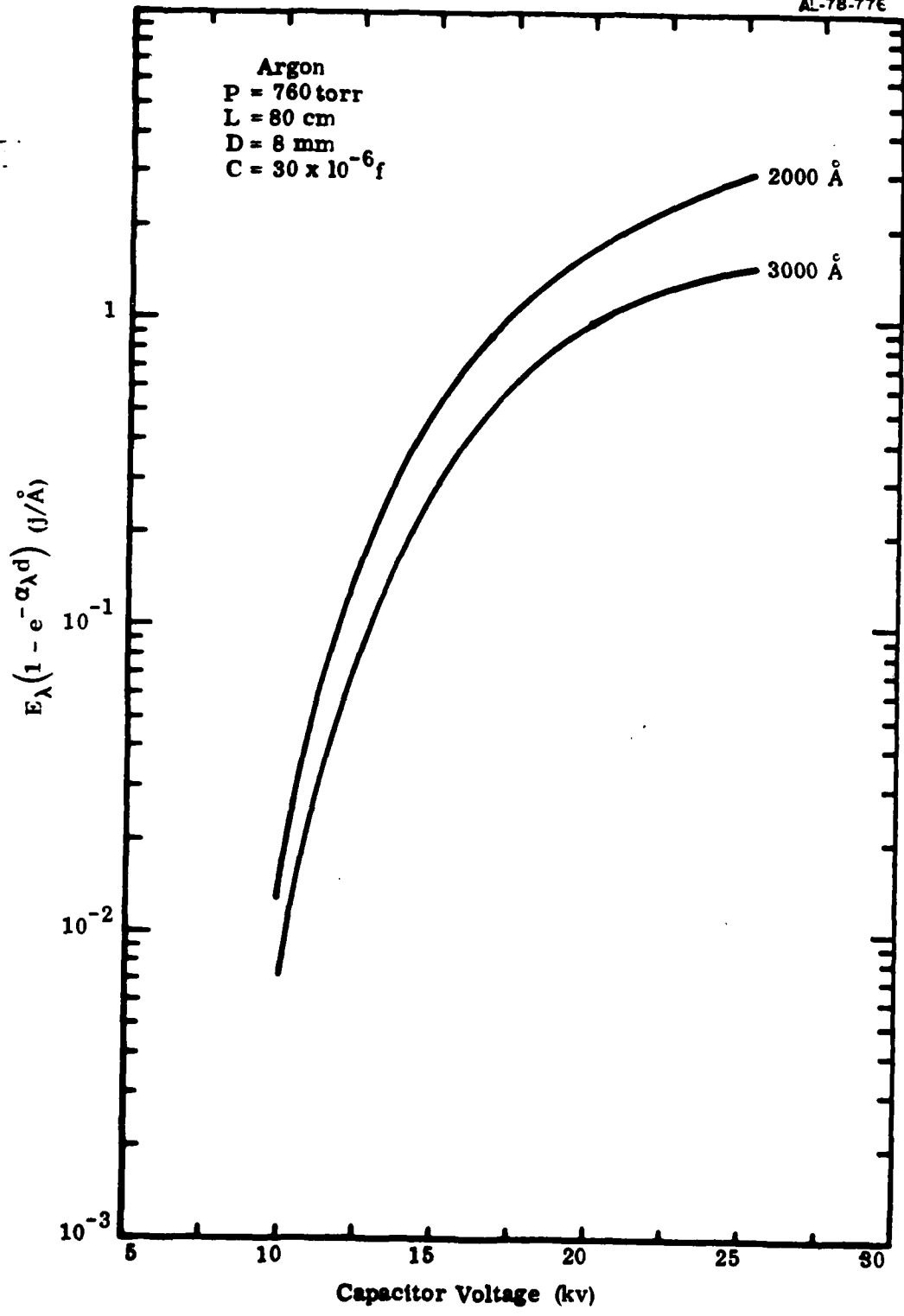
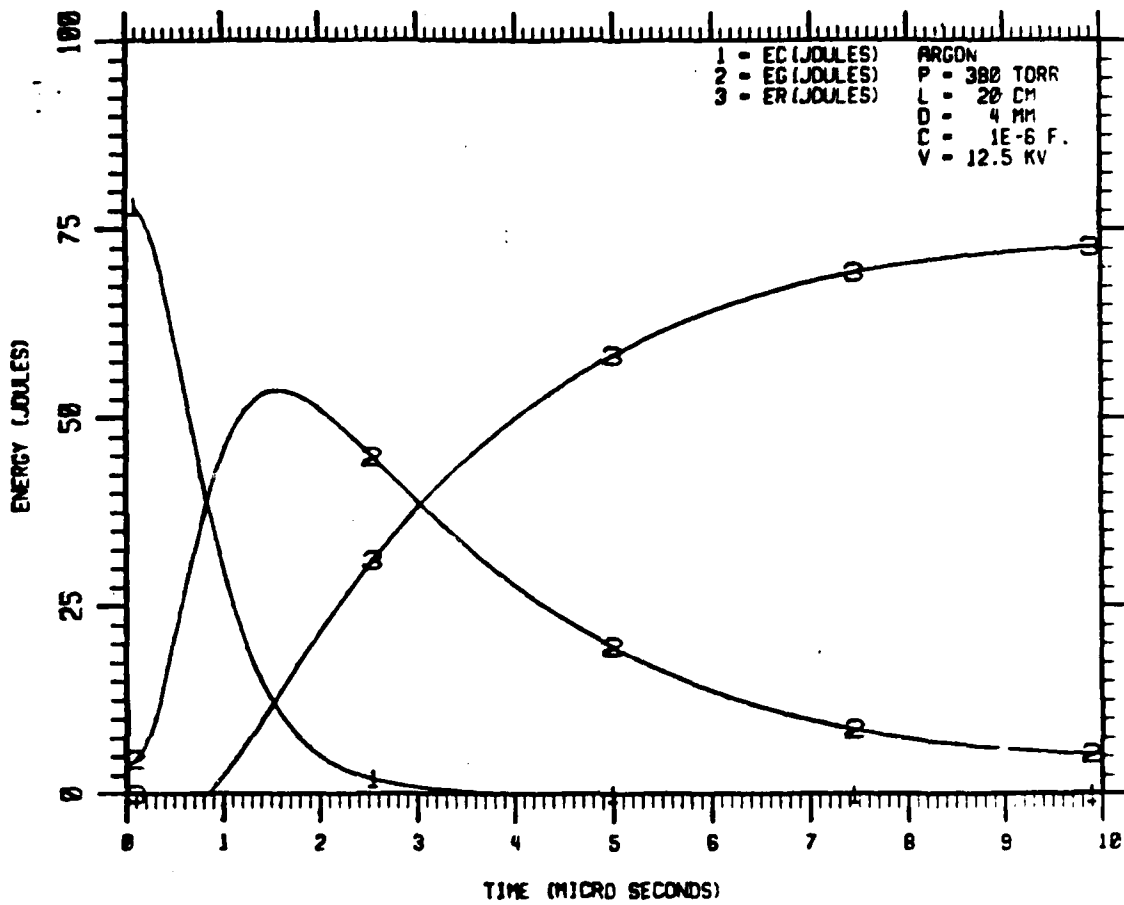


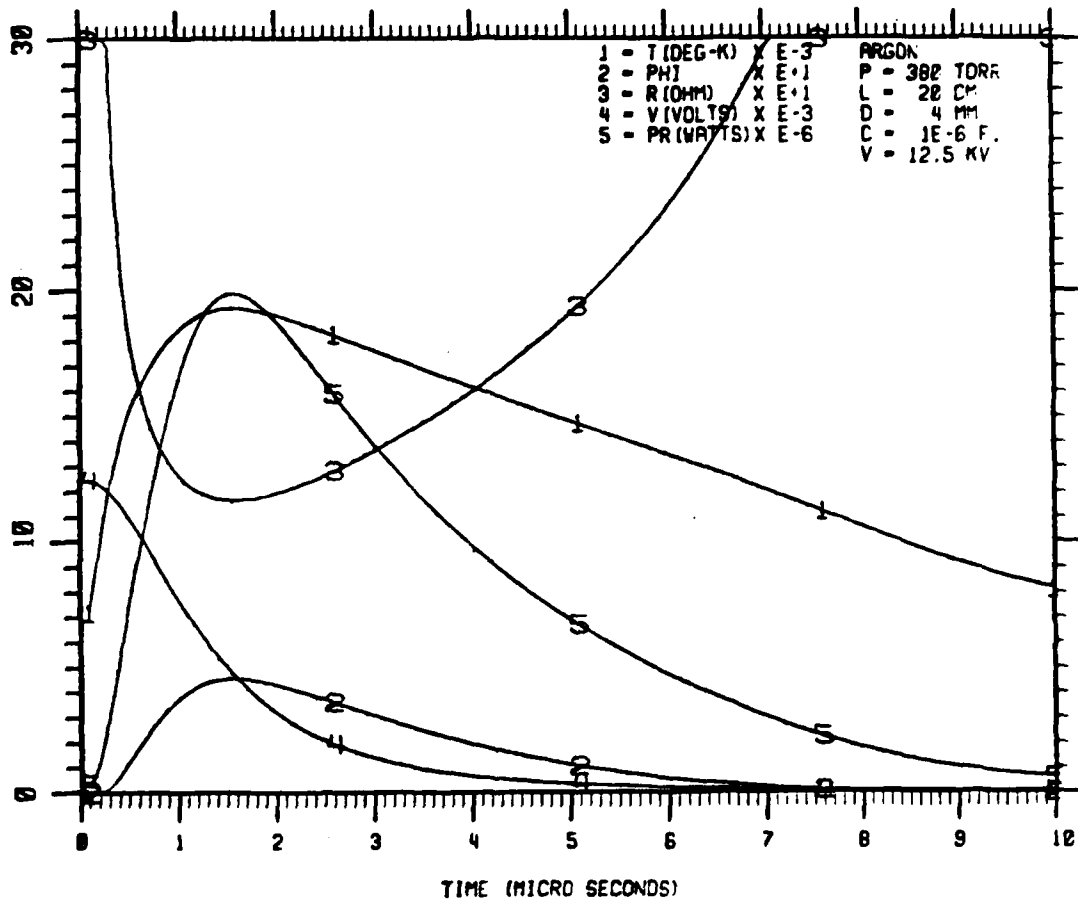
Figure 14. Lamp Spectral Energy Distributions at Two Wavelengths as Functions of Capacitor Voltage

Extensive modeling studies were conducted with the above tube and circuit conditions, which are appropriate to a long lamp pulse, since they satisfy the needs of the present  $C\ell F_3$  photolysis study. That is, large allowed lamp energies associated with long lamp pulses improve signal levels in the study of photolytic destruction of  $C\ell F_3$ . It is important, however, to establish that  $C\ell F_3$  photolysis may also be achieved in short lamp pulses which occur in pulsed chemical lasers. This, of course, requires significant lamp radiation in the  $C\ell F_3$  absorption band (see Figure 1). An example of short lamp pulse modeling results is shown in Figure 15. The example considers a tube 20 cm in length and 4 mm in diameter, a capacitance of 1.0  $\mu f$  and charging voltage of 12.5 kv, and argon fill at 0.5 atmospheres. Figure 15a shows a deposition of capacitor energy into the lamp gas and a subsequent lamp radiation cooling. Thus, the lamp pulse duration is controlled by the radiative cooling time rather than the circuit characteristic times  $R_L C$ . This feature is not present in Figure 11a; it is the basis for the present definition of a short lamp pulse. Operating conditions are, as in the long lamp pulse example, at approximately 50% of the explosion limit given by Eq. (3-3), and thus ensure reliable practical operation. Time histories of lamp gas properties are shown in Figure 15b. Plot 5 shows a lamp pulse duration (FWHM) of 3.4  $\mu sec$ , a peak temperature of 19,300 $^{\circ}K$ , a peak ionization level of 0.45 and an associated lamp resistance of 1.17 $\Omega$ . It is noted that the inductive rise time,  $\sqrt{LC}$ , must be less than 0.5  $R_L C$  if the lamp is critically damped. This requirement for laser application, in the present example, says  $\sqrt{LC} \leq 0.59 \mu sec$ . The radiation rise time in Figure 15b is 0.75  $\mu sec$ , consequently, inclusions of critically damped lamp circuit inductance would not significantly alter these results. This feature is common to all short lamp pulse studies. Lamp spectral power histories are shown in Figure 15c for six values of wavelength. Spectral energy efficiency is shown as a function of wavelength, in the optically thick limit, in Figure 15d at three times after lamp initiation. A comparison of Figures 15d and 11d shows that the spectral energy efficiencies are very similar for long and short lamp pulses when both are operated at 50% of their explosion limits. A more realistic comparison of UV spectral energy content may be obtained after applying the optical transparency correction, Eq. (3-20), to results in Figure 15d. The resulting lamp spectral energy efficiency



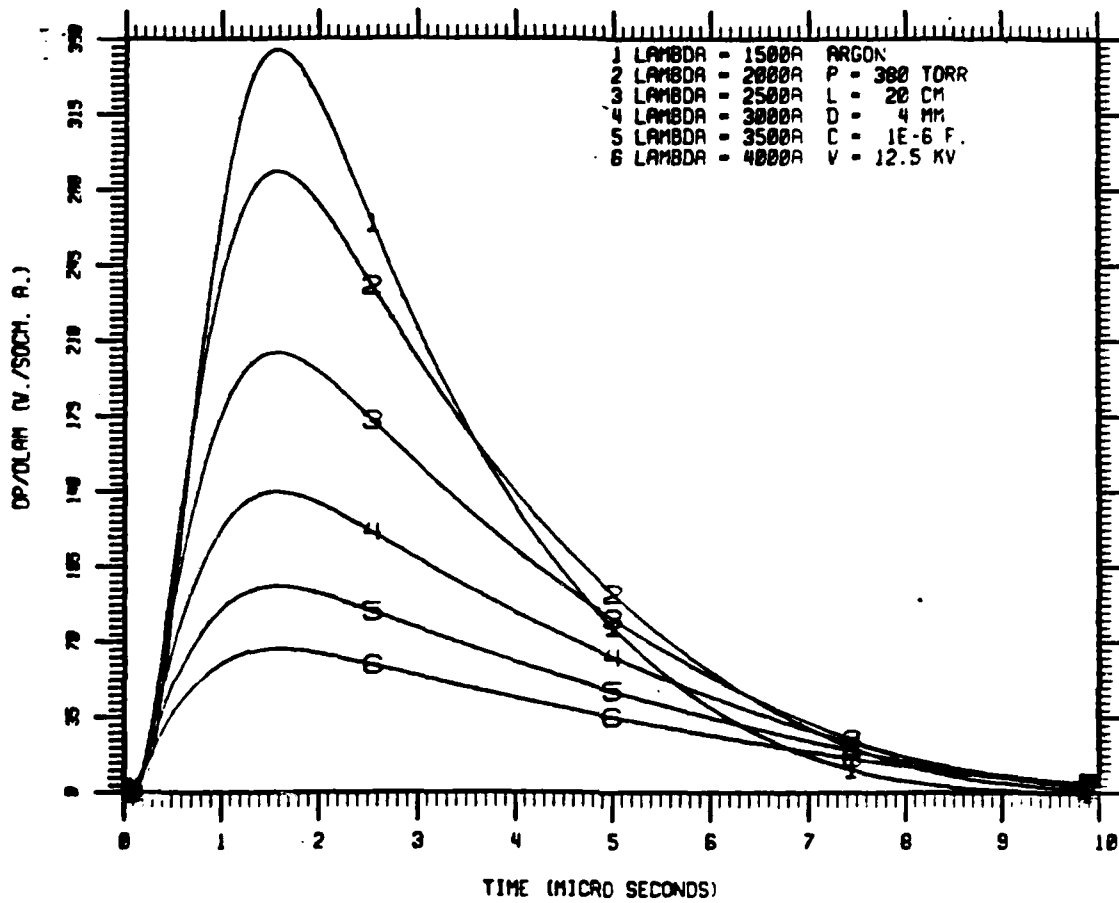
15a. Flash Lamp Energy Distribution vs Time

Figure 15. Lamp Radiation Modeling in the Optically Thick Limit.  
Short Lamp Pulse Example



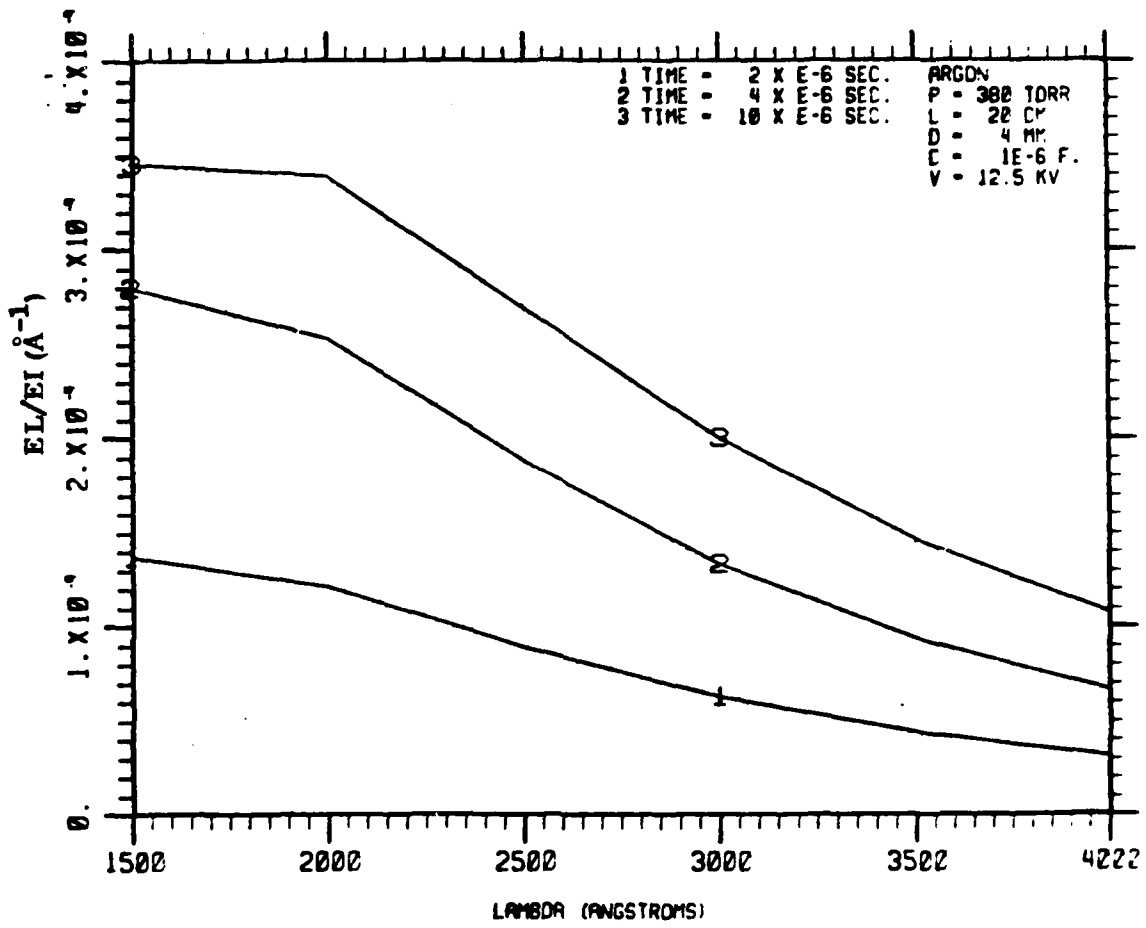
15b. Flash Lamp Gas Properties vs Time

Figure 15. (Continued)



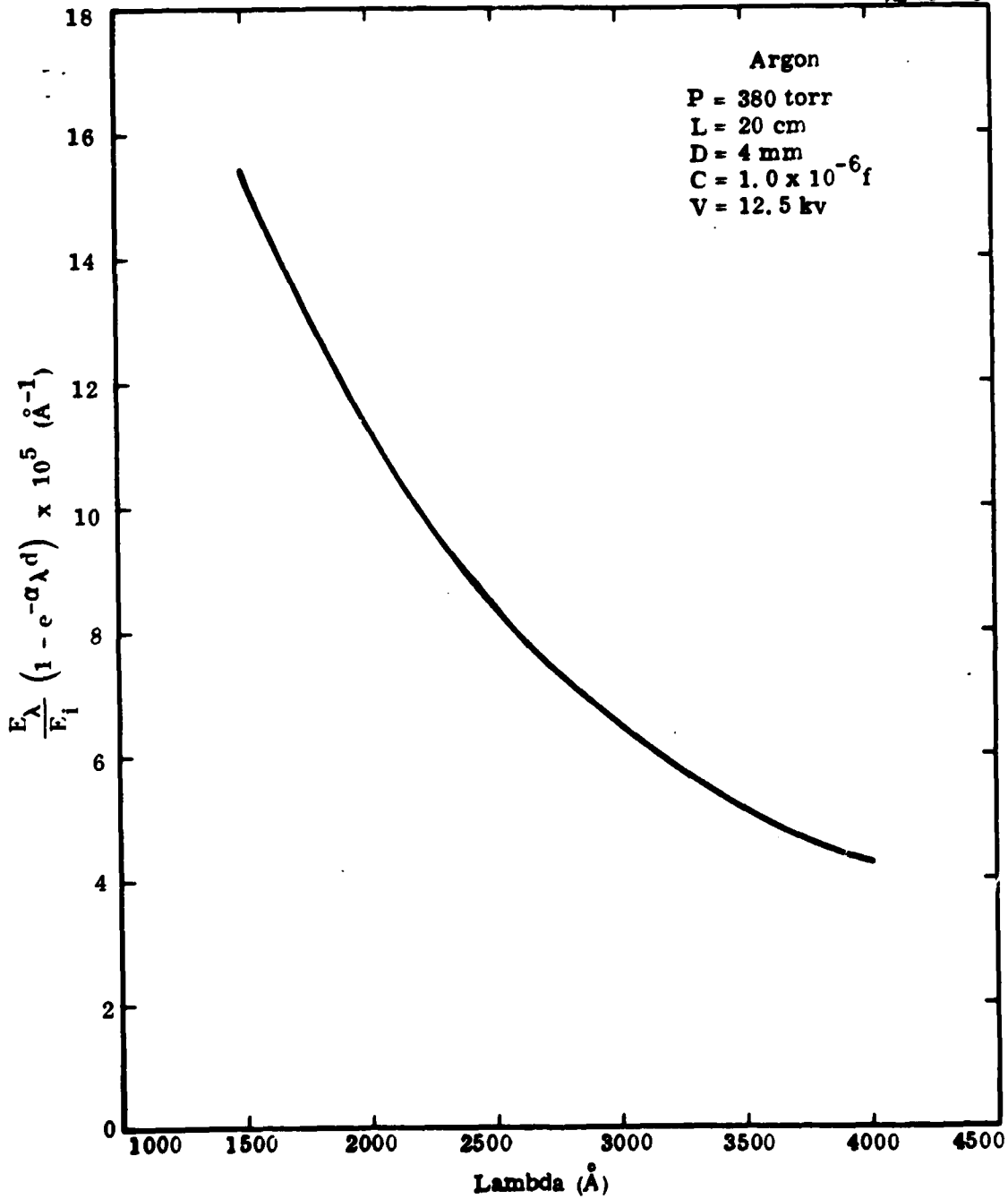
15c. Lamp Spectral Power vs Time

Figure 15. (Continued)



15d. Lamp Spectral Radiation Efficiency

Figure 15. (Continued)



15e. Lamp Spectral Energy Efficiency With Optical Transparency Correction

Figure 15. (Continued)

is shown in Figure 15e as a function of wavelength. Comparison of Figure 15e and 11e again show similar spectral energy efficiencies for short and long lamp pulses; in fact, the spectral efficiency of short pulse example is slightly higher than that of the long pulse example over the absorption bands of  $\text{C}\ell\text{F}_3$  and  $\text{F}_2$ . One concludes from this exercise, that the present experimental studies of photolytic destruction of  $\text{C}\ell\text{F}_3$ , which are discussed later, should have application in pulsed chemical lasers where lamp pulses are of order of a few microseconds.

The explosion limit criteria, Eq. (3-3), is based on long lamp pulse performance. It may underestimate the explosion limit for short lamp pulses.<sup>(8)</sup> Consequently, another short lamp pulse case is analyzed which is like that of Figure 15, except that the lamp fill pressure is 2.0 atm and the capacitor voltage is 17.5 kv. The predicted peak temperature is  $19,200^\circ\text{K}$  and the ionization level is 0.259. The lamp pulse duration (FWHM) is  $3.1 \mu\text{sec}$ . A comparison of transparency corrected spectral energy efficiencies is shown in Figure 16 for the present case and that of Figure 15. The high pressure, high voltage example shows the possibility of greatly increased spectral efficiency over absorption bands of  $\text{C}\ell\text{F}_3$  and  $\text{F}_2$  if lamp design allows operation near the limit set by Eq. (3-3). The high load case in Figure 16 corresponds to 18% radiation of initial capacitor energy in a band from  $2400\text{\AA}$  to  $3000\text{\AA}$  which is usable in  $\text{F}_2$  photolysis, and 18.5% in the band from  $1750\text{\AA}$  to  $2400\text{\AA}$  which is usable in  $\text{C}\ell\text{F}_3$  photolysis.

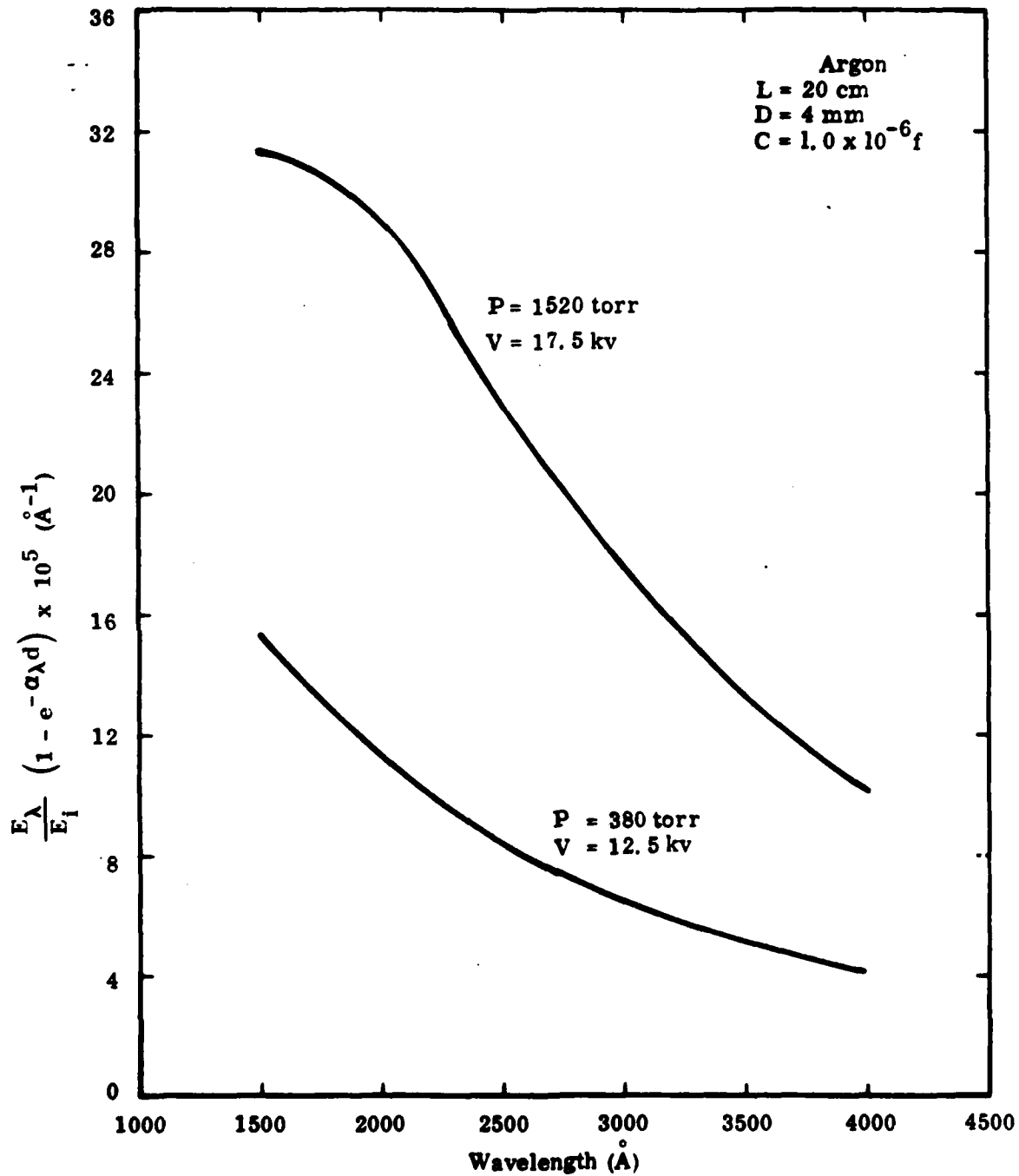
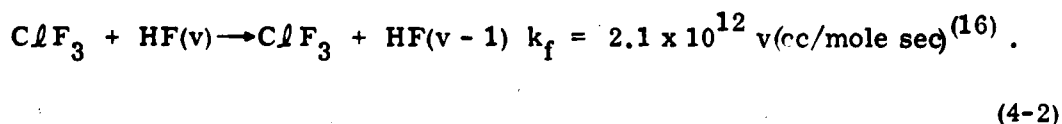
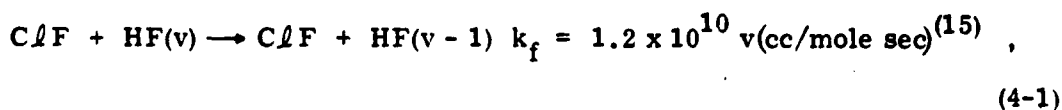


Figure 16. Comparison of Lamp Spectral Energy Efficiencies of a Short Pulse Lamp for Two Operating Conditions

#### 4. MODELING OF THE INFLUENCE OF $C\ell F_3$ ON LASER PERFORMANCE

Pulsed HF laser performance is modeled by the RESALE<sup>(6)</sup> code which was developed at Aerospace Corporation. In its present version, only single vibrational quantum transitions are allowed in HF and the code contains the recent rate coefficient compilation of Cohen and Bott<sup>(14)</sup> which is consistent with this constraint. The addition of  $C\ell F_3$  to conventional pulsed HF laser mixtures is accounted for in two respects. The expected enhancement of photoinitiation by trace addition of  $C\ell F_3$  is included in the initial F-atom concentration at the start of a run. Also, the effects of collisional deactivation of HF(v) by  $C\ell F$  and  $C\ell F_3$  are included using the rate coefficients



The above coefficients were measured only for  $HF(1) \rightarrow HF(0)$ ; the vibrational level dependence is not presently known.

As an example, consider a mixture at atmospheric pressure and room temperature with post-flash composition in mole fractions of:  $X_{H_e} = 0.80$ ,  $X_{F_2} = 9.79 \times 10^{-2}$ ,  $X_{H_2} = 9.79 \times 10^{-2}$ ,  $X_F = 10^{-3}$ ,  $X_{C\ell F} = 2 \times 10^{-4}$ ,  $X_{C\ell F_3} = 3 \times 10^{-3}$ . These proportions of  $C\ell F_3$  and  $F_2$  correspond to the average composition of the example of Figure 9. RESALE predictions of laser performance are shown in Table 4-1. The effects of collisional deactivation of HF(v) by  $C\ell F$  and  $C\ell F_3$  may be examined by considering a case without  $C\ell F_3$  addition where the laser initiation level is the same as in the above example. Practically, this would be achieved by

increased flash lamp illumination. An example is considered with composition:  $X_{He} = 0.80$ ,  $X_{F_2} = 9.95 \times 10^{-2}$ ,  $X_{H_2} = 9.95 \times 10^{-2}$ ,  $X_F = 10^{-3}$ ; results are compared with the above example in Table 4-1. This comparison shows that  $ClF_3$  addition has no noticeable effect on temporal behavior of the laser pulse or on laser pulse energy.

It is noted that pulse energy predictions in Table 4-1 are substantially higher than those observed experimentally. Pulse energy is observed to scale as  $p_{F_2} \times (p_F/p_{F_2})^{1/2}$  by McClure, et al.<sup>(1)</sup> where p is species post flash partial pressure. If this scaling is applied to the experimental results of Chen, et al.<sup>(2)</sup>, the present RESALE predictions should be scaled down by a factor of 0.38 to agree with this data. If this scaling is applied to the experimental results of McClure, et al., the present RESALE predictions should be scaled down by a factor of 0.19 to agree with the data. Even with these large differences between theory and experiment, it is felt that the theory in its present form is suitable for comparative studies, such as that considered here.

Table 4-1. RESALE Predictions of Laser Performance With and Without  $ClF_3$  Addition

	Without $ClF_3$	With $ClF_3$
Cavity Initial Pressure (torr)	760	760
Cavity Initial Temperature ( $^{\circ}K$ )	300	300
Composition (Mole Fraction x 100) He/ $F_2$ / $H_2$ /F/ $ClF_3$ / $ClF$	80/9.95/9.95/ 0.1/0/0	80/9.79/9.79/0.1/ 0.3/0.02
Saturated Gain ( $cm^{-1}$ )	$4.46 \times 10^{-3}$	$4.46 \times 10^{-3}$
Time to Peak Power ( $\mu sec$ )	1.05	1.03
Laser Pulse Duration (FWHM) ( $\mu sec$ )	0.94	0.95
Laser Pulse Energy ( $J/l$ )	308	315

## 5. PREVIOUS ATOMIC FLUORINE CONCENTRATION MEASUREMENTS

Initiation level, i.e., level of initial production of atomic fluorine, is a critical parameter in theoretical laser performance modeling and in experimental performance evaluation. Several schemes for direct determination of F-atom concentration have been reviewed and evaluated by Schlossberg.<sup>(5)</sup> The simplest of these, for application to pulsed laser cavity environments, seems to be the measurement of F-atom attenuation at  $404 \text{ cm}^{-1}$ . In the original plan, this scheme was to be implemented in the present program to measure the F-atom yield by photolysis of  $\text{ClF}_3$ . A system for implementation is shown schematically in Figure 17. A tunable diode laser source is directed through a 1.0m monochromator for single line selection. The selected line is then directed through KRS-5 windows of a photolysis cell; through an LWIR long wavelength pass filter and onto a Cu/Ge detector. The laser path contains KRS-5 optical elements on source and detector and on the photolysis cell. The remainder of the optical elements are reflective. A scanner is shown in Figure 17 which is arranged to allow a translation of the laser beam in a direction perpendicular to its axis, while this axis remains parallel to the photolysis cell axis. Expected system performance is shown in Table 5-1. The diode laser was supplied by Laser Analysts, Inc., with typical multiline power substantially in excess of  $100 \mu\text{w}$ . With indicated losses through monochromator and optics, the DC laser power to the detector was expected to be greater than  $0.67 \mu\text{w}$ . For conditions shown in Table 5-1, the laser line attenuation in an 80 cm cell would be 14% due to F-atoms formed by photolysis. With suppliers specifications of detector response and  $D^*$ , an attenuation signal of 4.94 mv, with a signal-to-noise ratio of 93, is predicted at a frequency response of 15 kHz. The measurement scheme would drive the diode laser line through a spectral range of  $0.33 \text{ cm}^{-1}$  at a cycle rate of 100 Hz, by superimposing a current sawtooth onto a DC current level in the diode laser controller. This frequency turning would drive the selected line through a distance of 1.25 mm at the exit slit of the monochromator. Consequently, an exit slit setting of 1.0 mm would chop the laser beam and provide a measure of its DC power

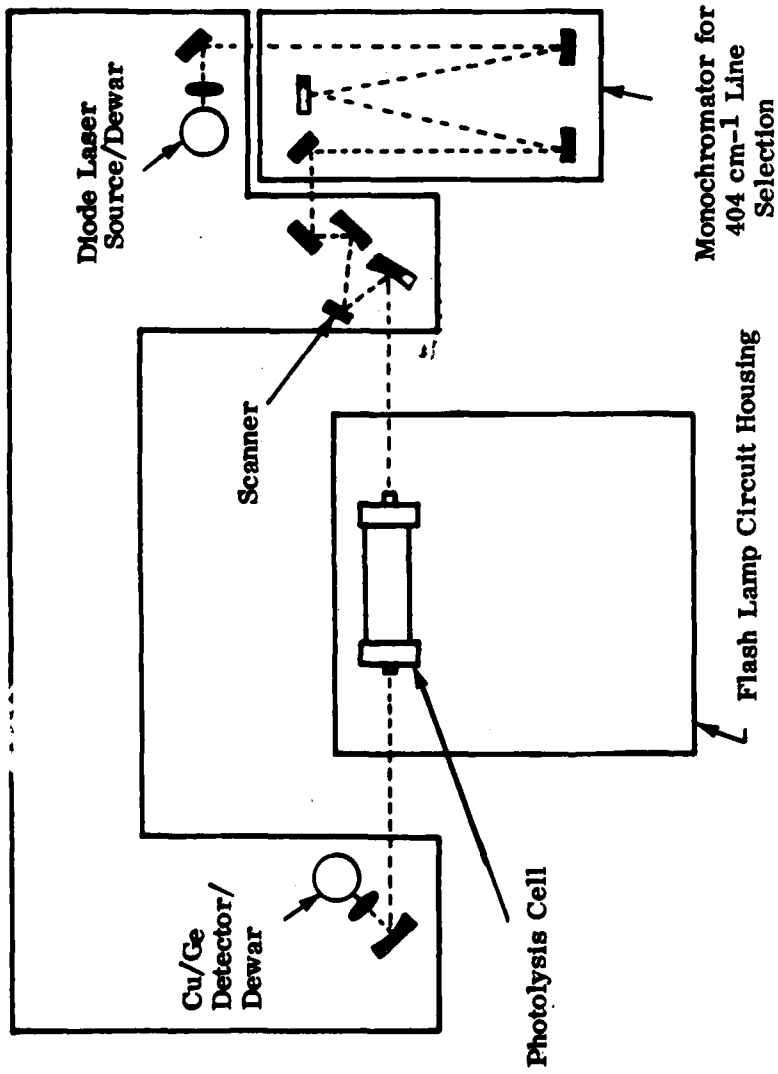


Figure 17. Apparatus for Measurements of Atomic Fluorine Concentration

**Table 5-1. Fluorine Atom Concentration Measurements  
Performance Expectations**

Total diode laser power (laser analytics)	=	100 $\mu\text{w}$
Power in the single line at $404 \text{ cm}^{-1}$	=	20 $\mu\text{w}$
With losses through the monochromator (X 1/5)	=	4 $\mu\text{w}$
With losses through five KRS-5 elements (X 1/6)	=	0.67 $\mu\text{w}$
DC power incident on Cu/Ge detector	=	0.67 $\mu\text{w}$
Photolysis cell length	=	80 cm
Predicted lower limit in F-atom concentration	=	$3.1 \times 10^{15} \text{ cc}^{-1}$
F-atom absorption cross section at 50 torr		
Total pressure = $5.6 \times 10^{-19} \text{ cm}^2$		
Laser line attenuation	=	0.14
AC detector signal	=	0.092 $\mu\text{w}$
F-atom recombination time	=	2.0 sec
Detector responsivity ( $V_b = 150\text{v}$ , $R_l = 0.1 \text{ M}\Omega$ )	=	$5.35 \times 10^4 \text{ v/w}$
AC detector signal	=	4.92 mv
$D^* = 3.3 \times 10^{10}$	Area =	0.0707 $\text{cm}^2$
At 15 kHz: NEP	=	$9.9 \times 10^{-10} \text{ w}$
NEV	=	52.7 $\mu\text{v}$
$(S/N)_{AC}$	=	93

at intervals of 10 msec. The pressure broadened linewidth of atomic fluorine at 50 torr total pressure is approximately  $0.0033 \text{ cm}^{-1}$ . Therefore, if the lamp is flashed during the above periodic laser tuning, and if the tuning band contains the F-atom absorption line, photolytic production of F-atoms should be observed by a periodic attenuation of duration  $100 \mu\text{sec}$ . This requires a detector frequency response in excess of 10 kHz. The above scheme was chosen because it does not require precise knowledge of the absorption line position or of the diode laser wavelength.

Preliminary measurements of diode laser spectra indicated that the source did operate with adequate power over the wavelength range of interest. However, source performance was not repeatable from day to day. This may be due to the fact that the laser was cooled by a liquid helium dewar which warmed to room temperature daily. During testing, we learned that the laser did not tune to our sawtooth current input in the anticipated manner and to work with the observed response would have required substantial modifications in our detection system. These difficulties, coupled with the fact that we had no DC F-atom source for simple detection system shakedown, caused us to abandon this measurement scheme for the present photolysis studies. Instead, we chose to conduct absorption analysis on  $\text{C}_2\text{F}_3$  to measure its depletion by photolysis, as discussed later.

Early pulsed laser performance analysis by Chen, et al.<sup>(2)</sup> examined photolytic disassociation of molecular fluorine by the fast HF forming reaction,



The product, HF, is measured by absorption of an HF probe laser beam. This method of determination of F-atom concentration is not appropriate in laser mixtures, since it applies only in the absence of  $\text{H}_2$ . Furthermore, possible photolysis of  $\text{HC}_2\text{F}_3$ <sup>(17)</sup> and the possible occurrence of HF forming reactions must be examined carefully before this can be considered a reliable method of measuring photolytic production of F-atoms. Chen, et al.<sup>(2)</sup> also deduced the photolytic production of F-atoms in an HF laser gas mixture by observing the resultant rate of progress of

the chain reaction through the depletion of  $F_2$ . Depletion of  $F_2$  was determined by the time variation of attenuation of an  $N_2$  probe laser beam at 3370Å. McClure, et al.<sup>(1)</sup> also deduced the photolytic production of F-atoms in an HF laser from rate of depletion of  $F_2$  in the chain reaction. They examined  $F_2$  depletion by attenuation of a He Cd laser beam at 3250Å.

The deduction of initiation level (F-atom production) by chain reaction depletion of  $F_2$  in laser gas mixtures is complicated by the variations in  $F_2$  absorption cross section with temperature. Batovski and Gurev<sup>(20)</sup> have measured the variation in  $F_2$  absorption cross section with temperature in the wavelength range from 2400Å to 4000Å. Their results are shown here in Figure 18. The variation in absorption with temperature, shows a nearly null point at  $\lambda_0 = 3270\text{Å}$  and a temperature sensitivity near this point of the form.

$$\frac{1}{\sigma_0} \frac{d\sigma_{F_2}}{dT} \approx 1.66 \times 10^{-6} (\lambda - \lambda_0) (\text{sec}^{-1}) \quad , \quad (5-2)$$

where  $\sigma_0 = 1.3 \times 10^{-20} \text{ cm}^2$  and  $\lambda$  is in Angstroms. It is interesting to note the "false signal" associated with  $F_2$  attenuation measurements near this null point due to the variation in  $\sigma_{F_2}$  with T. With the neglect of this temperature sensitivity, a small variation in laser attenuation due to  $F_2$  depletion would be described by:

$$\frac{\Delta I}{I} = -\sigma_{F_2} \ell \Delta n_{F_2} = -\sigma_{F_2} \ell n_{F_2} \left( \frac{1}{n_{F_2}} \frac{dn_{F_2}}{dT} \right) \Delta T \quad , \quad (5-3)$$

where I is beam intensity at the output of an attenuation cell of length  $\ell$ . With the temperature dependence of  $\sigma_{F_2}$  included, the small laser beam attenuation change would be described by:

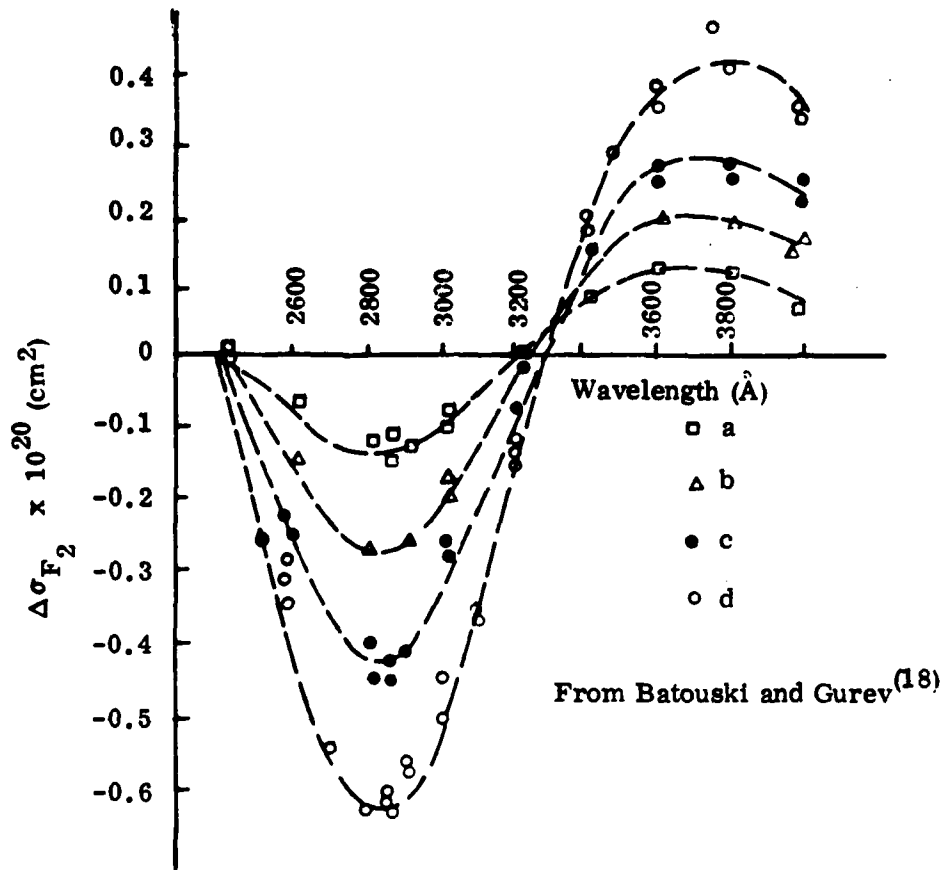


Figure 18. Absolute Variation in Absorption Cross Section of Molecular Fluorine With Temperature Increase Above 300°K by:  
 (a) 210°K; (b) 360°K; (c) 500°K; (d) 690°K

$$\begin{aligned} \frac{\Delta I}{I} &= -\sigma_{F_2} \ell \Delta n_{F_2} - \ell n_{F_2} \Delta \sigma_{F_2} \\ &= -\sigma_{F_2} \ell n_{F_2} \left( \frac{1}{n_{F_2}} \frac{dn_{F_2}}{dT} + \frac{1}{\sigma_{F_2}} \frac{d\sigma_{F_2}}{dT} \right) \Delta T \quad (5-4) \end{aligned}$$

As an example, consider an initial mixture of 85% He, 10% F<sub>2</sub>, and 5% H<sub>2</sub> at atmospheric pressure and room temperature. The variation of temperature with progress of the chain reaction is then,

$$\frac{1}{n_{F_2}} \frac{dn_{F_2}}{dT} = -2.47 \times 10^{-4} \text{ (sec}^{-1}\text{)} \quad (5-5)$$

Substitution of Eq. (5-2) and (5-5) into Eq. (5-4) yields,

$$\frac{\Delta I}{I} = \sigma_{F_2} \ell \Delta n_{F_2} \left[ 1 - 6.72 \times 10^{-3} (\lambda - \lambda_0) \right] \quad (5-6)$$

Equation (5-6) shows that if attenuation measurements were made with a He Cd laser at 3250Å, progress of the chain reaction  $\Delta n_{F_2}$  would be overestimated if temperature variation of  $\sigma_{F_2}$  were not considered, by the factor (1.13) or 13%. If an N<sub>2</sub> laser at 3370Å were used, the above interpretation could underestimate reaction progress by the factor (0.328) 67%. Clearly, the interpretation of such measurements is very sensitive to the details of studies shown in Figure 18, and considerable care must be taken in the determination of photolytic initiation level by this approach.

The above analysis serves to illustrate difficulties in the indirect determination of atomic fluorine production by photolysis. This is meant to stress the importance of a direct F-atom measurement technique. Work to this end is in progress by Crane,<sup>(19)</sup> in which the system is similar to that of Figure 17 with certain exceptions. His experiment uses a cryostat to cool the diode source and a steady state F-atom source would replace our photolysis cell.

## 6. FLASH LAMP SPECTRAL RADIATION MEASUREMENTS

Flash lamp design was based primarily on the requirements of  $C/F_3$  photolysis studies discussed in Section 7. For this purpose, substantial lamp radiation is required in the photolysis band of  $C/F_3$  (see Figure 1). Since lamp operating conditions appropriate to this end were not known, it was decided that the lamp design would allow adjustable gas fill pressure and simple maintenance and component replacement. Argon gas fill was used for convenience. The lamp consists of a stock Suprasil tube with 8.0 mm inside diameter and 2.0 mm wall thickness which is O-ring sealed at each end to a copper electrode with a gas fill (or exhaust) port. The tube and electrode and fittings are shown in Figure 19. The O-ring is positioned to provide a three-way seal to isolate the lamp volume, the photolysis cell, and the exterior. The photolysis cell end plug is shown in Figure 20 with the lamp end connector, the cell gas supply port, and an  $Mg F_2$  window for use in the attenuation studies of Section 7. Identical cell end plugs are held in position by tie-rods to provide a lamp arc length of 80 cm and a photolysis cell length of 77 cm.

The flash lamp was triggered by a 30 kv pulse through a wire wound along the tube outside wall. The discharge current was carried through the aluminum wall of photolysis cell to ground in order to minimize lamp circuit inductance. The lamp circuit contained six  $5 \mu f$  capacitors which were connected in parallel for a capacitance of  $30 \mu f$ . Each capacitor was rated at 25 kv with an internal inductance of less than  $0.040 \mu h$ .

UV detector channels are positioned in an array at 4.0 cm intervals to view the mid-portion of the flash lamp along its axis through Suprasil windows in the photolysis cell wall. A schematic of the UV detector array data train is shown in Figure 21. Each data channel contains a 1.0 mm aperture, a removable UV narrowband filter and a silicon diode/operational amplifier combination. Insertion of five different bandpass UV filters in the array provided a spectral analysis of the lamp radiation. Eight filters, which spanned the spectral region from  $1800\text{\AA}$  to  $3200\text{\AA}$ ,

**FLASH LAMP END CONNECTOR COMBINES:**

- (a) Through-the-wall vacuum seal
- (b) Removable, sealed electrode
- (c) Lamp gas fill and purge
- (d) Electrode insulator

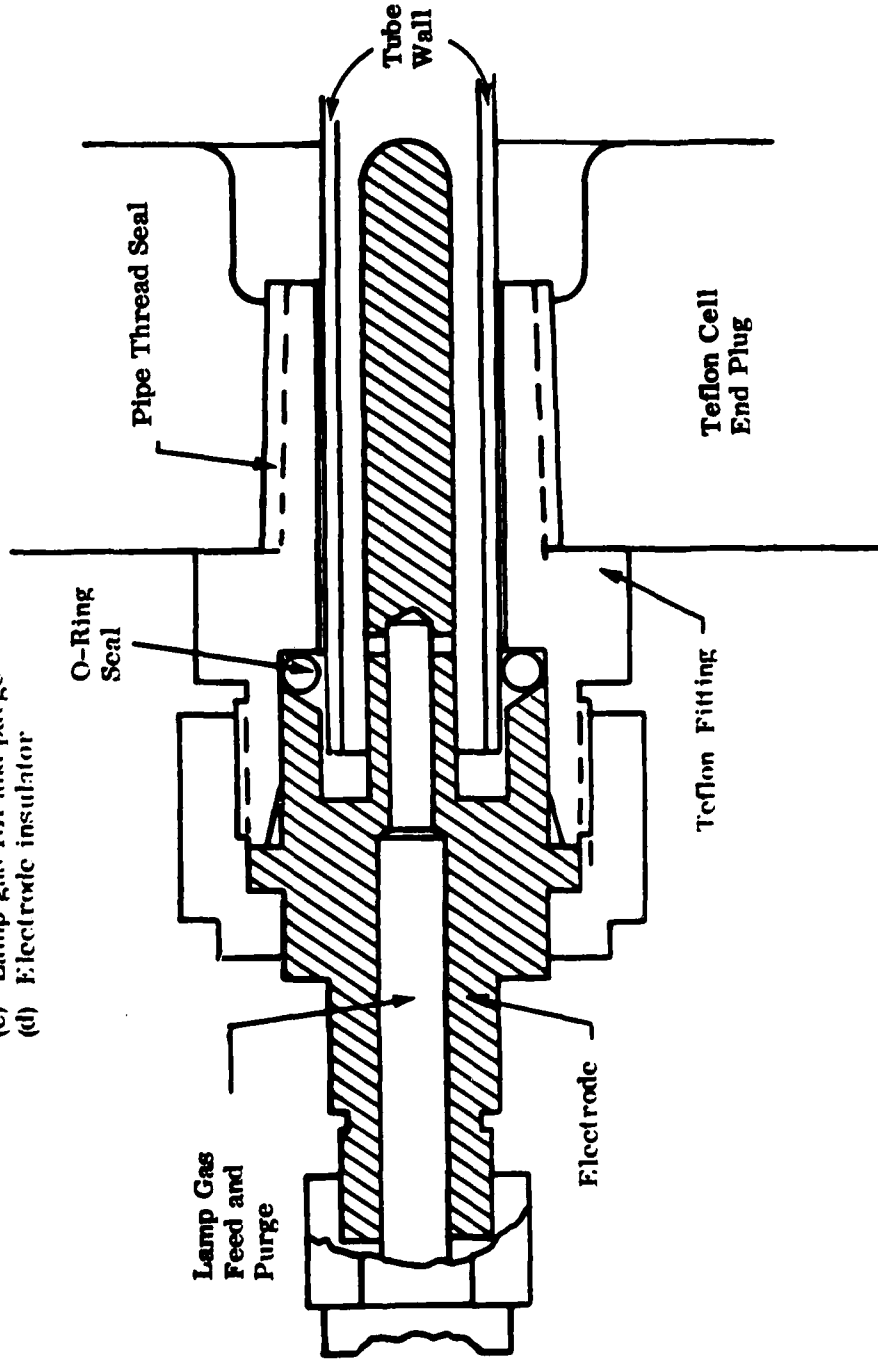


Figure 19. Lamp Electrode With Gas Supply and Wall Mounting Fittings

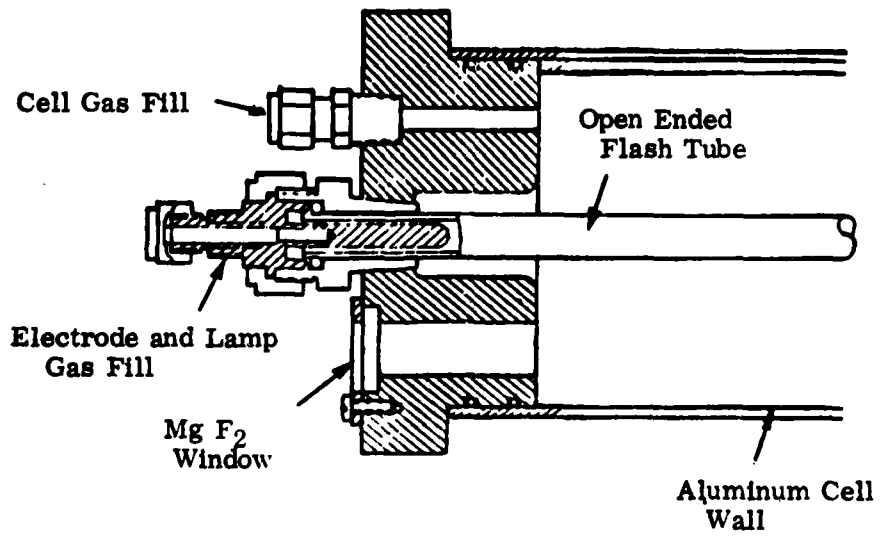


Figure 20. Photolysis Cell End Plugs With Fittings

Channels 1 thru 4 show time  
integrated power.  
Channel 5 shows power vs time  
or integrated power.

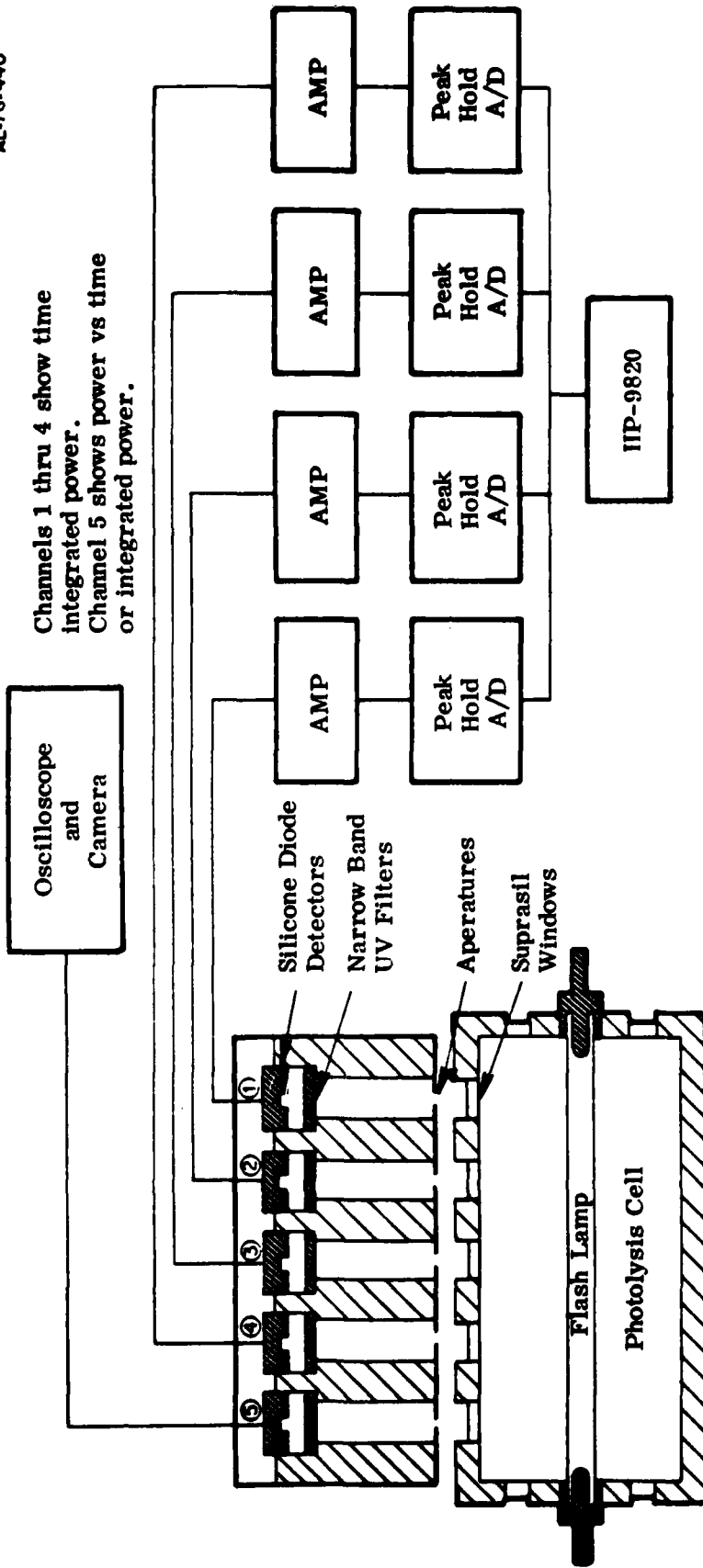


Figure 21. Lamp Spectral Energy Measurements Schematic

were used with this configuration. Four of the UV data channels were operated as time integrators to provide a measure of lamp spectral energy. An integrator decay time constant of 48 msec allowed amplified signal acquisition by peak and hold circuits and A/D converters. The stored signals were then transferred sequentially to an HP 9820 computer for storage and data reduction. The fifth channel was operated either as an integrator or as a fast response power detector. This channel was used to insure that spurious electrical signals did not significantly influence detector radiation measurements.

### 6.1 Calibration and Data Processing

Lamp spectral measurements were made using eight narrow band UV filters with measured transmission curves, shown in Figure 22. Four UV data channels were available for spectral energy measurements, thus, a complete spectral survey at eight wavelengths required a minimum of two lamp flashes. Each integrator data channel amplifier had a feedback resistor of  $22M\Omega \pm 5\%$  and a feedback capacitor of  $2200\text{ pf} \pm 2\%$ . A relative calibration of UV data channels was carried out by exposing each of the five channels with each of the eight UV filters to the same focused light from a DC arc lamp, which was mechanically chopped at 1.25 Hz. The total spread among these five detector signals with each UV filter is shown in Figure 23. This shows that the largest variation in detector responses at any wavelength considered is less than  $\pm 7\%$ . Consequently, in the data reduction, a single silicon diode spectral response curve was used. This response curve was obtained by absolute calibration of the diode/amplifier of UV data channel No. 1 by EG&G, Inc., and is shown in Figure 24. This calibration treats the operational amplifier as a unity gain current amplifier.

Lamp spectral energy measurements are viewed in terms of lamp spectral energy efficiency (lamp radiated energy per unit wavelength  $\div$  initial capacitor energy) by the following analysis. If the power radiated per unit wavelength,  $W_\lambda$ , from a lamp of diameter  $d$  and length  $l$  is assumed to have a diffuse spatial distribution, then the power transmitted through an aperture of diameter  $d_a$  and through

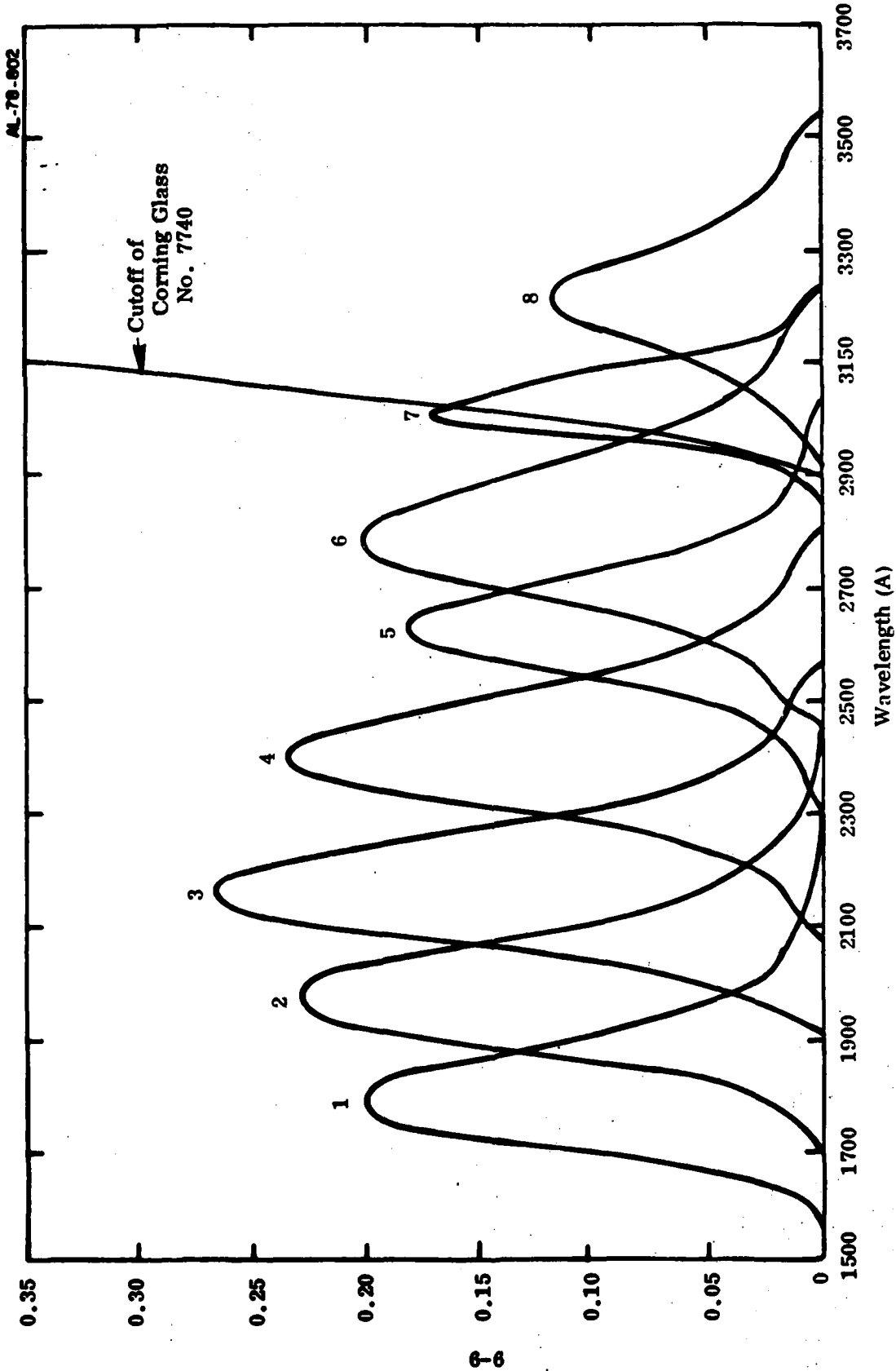


Figure 22. Transmission Spectra of Eight UV Filters, See Table 6-1 for Filter Specifications

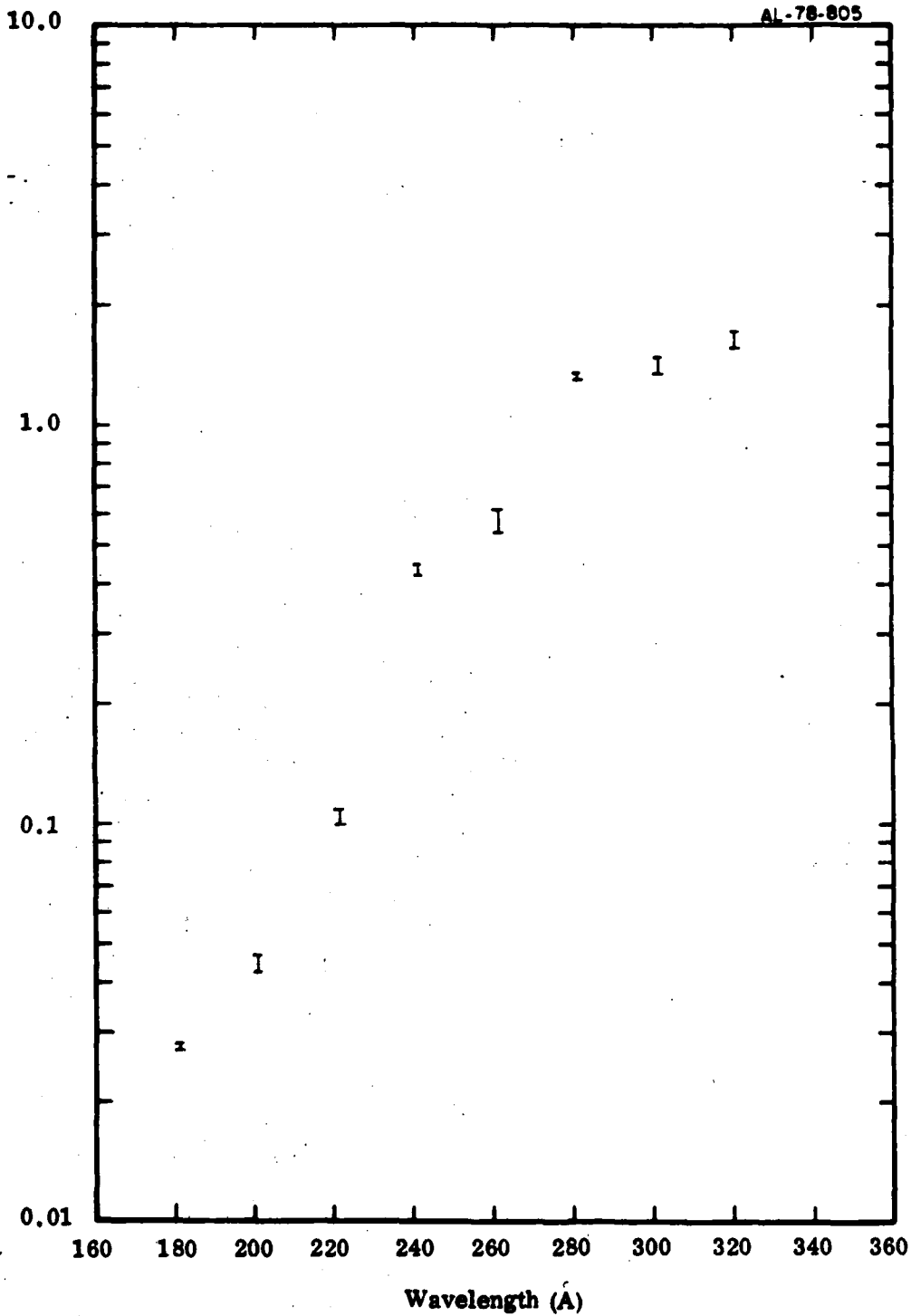


Figure 23. Total Spread In Response of Five UV Spectral Data Channels Using Each of Eight Narrow Band UV Filters

AL-78-062

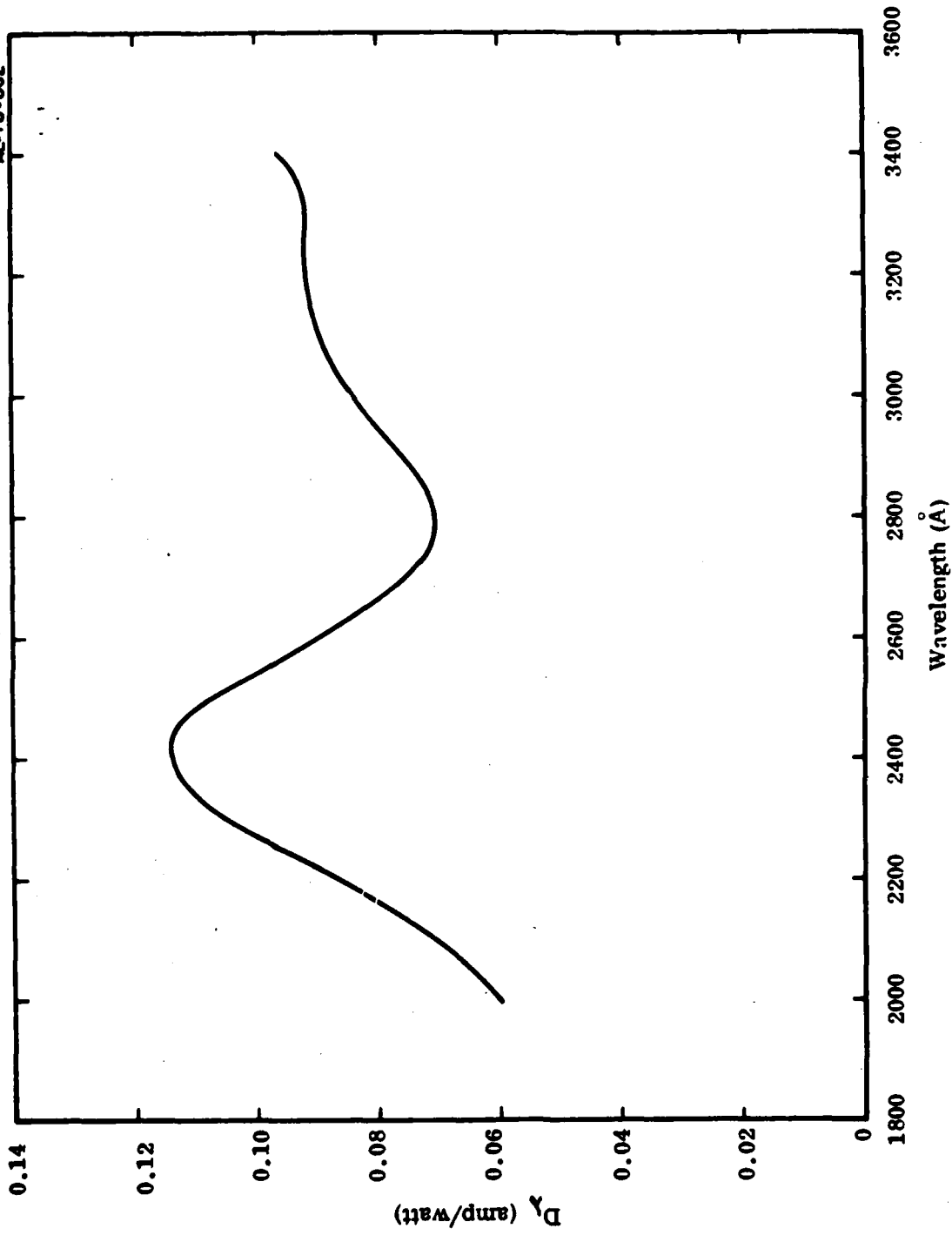


Figure 24. Spectral Response of Silicon Diode/Amplifier Elements in the Flash Lamp Spectral Energy Measurements Array

a filter of transmittance,  $\epsilon_\lambda$ , to a detector area,  $A_d$ , at a distance,  $\ell_d$ , from the aperture is:

$$P_{d\lambda} = \left( \frac{W_\lambda}{\pi d \ell} \right) \cdot \left( \frac{\pi}{4} d_a^2 \right) \epsilon_\lambda \cdot \frac{1}{\pi} \cdot \frac{A_d}{\ell_d^2} \quad (6-1)$$

If the silicon detector has a spectral responsivity of  $D_\lambda$  (amps/watt) and if the detector amplifier current goes to an integrating capacitor,  $C_d$ , then the peak integrator voltage resulting from the radiation over the entire filter bandpass is:

$$V_d = \frac{1}{C_d} \iint P_{d\lambda} D_\lambda d\lambda dt \quad (6-2)$$

If  $W_\lambda$  and  $D_\lambda$  are assumed to vary slowly with  $\lambda$  over the filter bandpass, substitution of Eq. (6-1) into Eq. (6-2) yields:

$$V_d \approx \frac{A_d D_\lambda}{4\pi d \ell C_d} \left( \frac{d_a}{\ell_d} \right)^2 \int \epsilon_\lambda d_\lambda \cdot \int W_\lambda dt \quad (6-3)$$

The second integral in Eq. (6-3) is the lamp spectral energy radiated per unit wavelength. Consequently, Eq. (6-3), after division by initial lamp capacitor energy  $E_i$ , may be inverted to yield:

$$E_\lambda/E_i = V_d \div \left[ \frac{A_d E_i D_\lambda}{4\pi d \ell C_d} \left( \frac{d_a}{\ell_d} \right)^2 I_n \right] \quad (6-4)$$

where

$$I_n = \int \epsilon_\lambda d_\lambda \quad (6-5)$$

which is evaluated for each of the eight narrow band filters of Figure 22 and results are given in Table 6-1. With substitution of the present circuit and geometrical parameters given in Table 6-1, Eq. (6-5) becomes:

$$E_{\lambda}/E_1 = 1.02 \times 10^{-4} V_d \div (D_{\lambda} I_n) \quad , \quad (6-6)$$

where  $V_d$  is in volts,  $D_{\lambda}$  is in amps/watt, and  $I_n$  is in Angstroms.

## 6.2 Spectral Measurements

Brief results of lamp spectral measurements are presented here, to assess the spectral energy content in the photolysis bands of  $C(F_3)$  and  $F_2$  for seasoned flash lamps. Lamp spectra were also obtained during photolysis studies which are reported in Section 7. All measurements reported here were conducted with a lamp circuit capacitance of 30  $\mu f$ , and a charging voltage of 15 kv using lamps of 8.0 mm inside diameter and 80 cm arc length.

The UV spectral data channels were electrically shielded so that Channel 5 (Figure 21) in the fast response mode ( $R_d = 470 \Omega$ ,  $C_d = 20$  pf) showed a spurious signal maximum with blocked aperture which was less than 13% of the open aperture radiation signal, using the 2400A filter and 380 torr Argon lamp fill. Under the same conditions, Channel 5, in an integrating mode ( $R_d = 22M\Omega$ ,  $C_d = 2200$  pf), showed signals with blocked apertures of less than 40 mv compared with open aperture radiation signals of the order of volts. The possibility of leakage of lamp visible radiation through the short wavelength filters No. 1 through 5 was examined by inserting a plate of Corning Glass No. 7740 between lamp and detector. The measured cutoff of this glass, as shown in Figure 22, should allow no detected radiation at those filter wavelengths. This study showed that each of the filters passed visible lamp radiation at a level less than 5% of that flash lamp radiation which is transmitted at its intended bandpass.

Lamp spectral energy efficiency is presented in Figure 25 for lamp operating conditions shown. Data Set A were taken after the lamp and photolysis cell had been exposed to  $C(F_3)$  at a partial pressure of 7.6 torr in 380 torr of  $N_2$  for a period

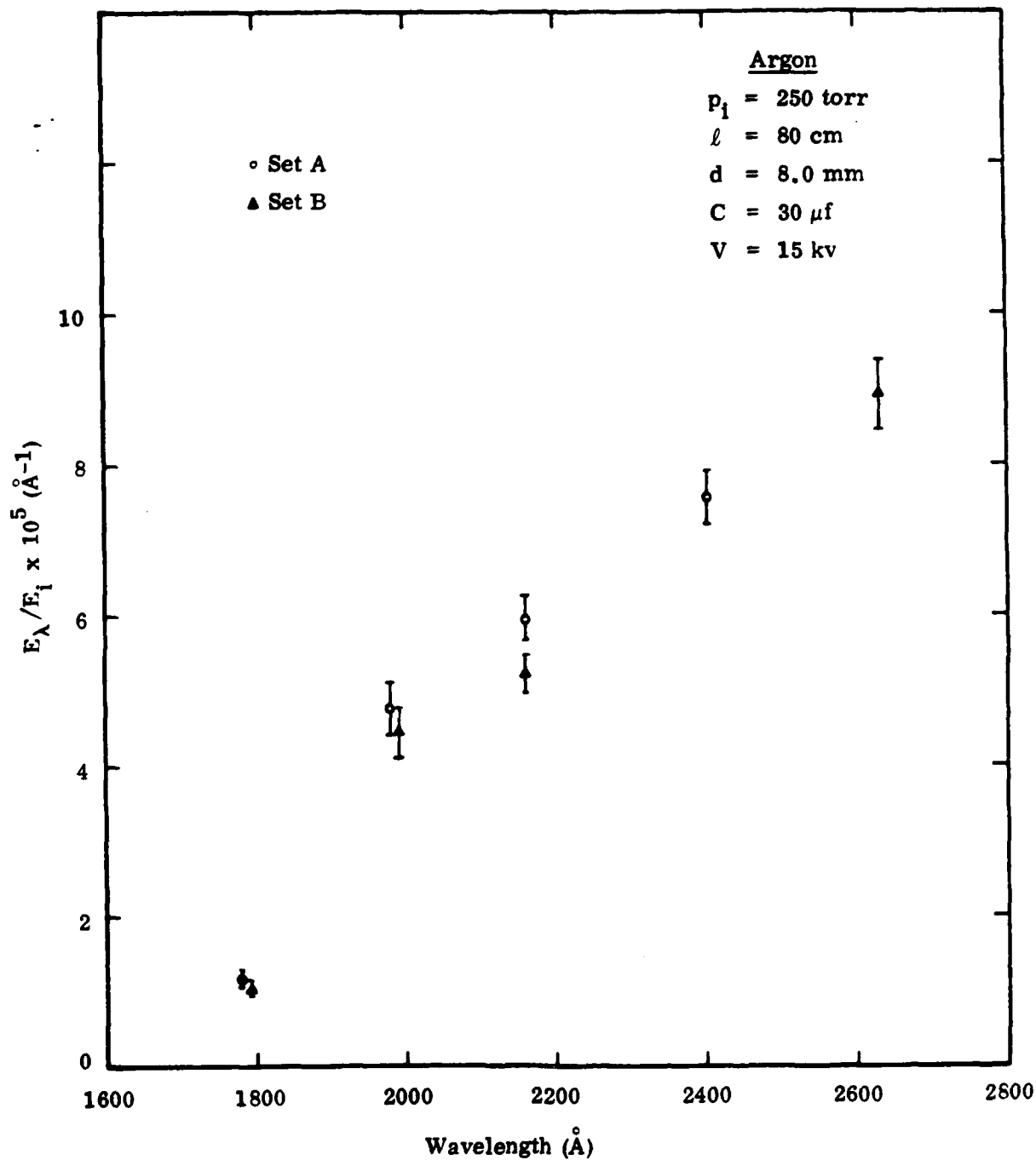


Figure 25. Comparison of Lamp Spectral Energy Efficiencies of a Flash Lamp at Two Periods in Its Lifetime

of 2.5 hours. The lamp had been flashed 35 times, 5 of which were in the presence of  $C\ell F_3$ . Data Set B were taken with the same lamp under identical operating conditions after additional exposure to  $F_2$  or  $C\ell F_3$  at partial pressures up to 25 torr in nitrogen for a combined duration of 8.0 hours. The lamp had been flashed 216 times, 16 of which had been in the presence of  $C\ell F_3$ . A comparison of these data sets shows little difference in radiation spectra even though visual observation of the flash lamp after Run Set B showed substantial clouding (etching) of the lamp exterior and slight electrode deposition near the ends of lamp interior.

A more extensive lamp data set (Set C) is shown in Figure 26, which was obtained from a second lamp after exposure to  $C\ell F_3$  at partial pressures below 7.6 torr in nitrogen for a period of 2.0 hours. The lamp had been flashed 19 times, 12 of which had been in the presence of  $C\ell F_3$ . Operating conditions were the same as those of Sets A and B, except that Argon fill pressure was 380 torr as compared with 250 torr in A and B. Comparison of Figures 25 and 26 shows little difference in spectral energy efficiency at these different lamp fill pressures over the spectral region studied. Figure 26 also contains the theoretical predictions of lamp spectral energy efficiency from both Figures 15d and 15e, i. e., without and with the transparency correction. Experimental results are seen to lie below or between two curves, but show an increase in spectral energy efficiency with increasing wavelength. In view of the approximations made in developing both the theoretical predictions, this degree of agreement is fair and lends support to the predictions of Section 3 concerning lamp radiation for short pulse lamps. Data in Figures 25 and 26 show an average of 3.5% of total lamp capacitor energy appears as radiation in the photolysis band of  $C\ell F_3$  (1750Å - 2400Å) and 13% appears as radiation in the photolysis band of  $F_2$  (2400Å - 3400Å) for the specified operating conditions.

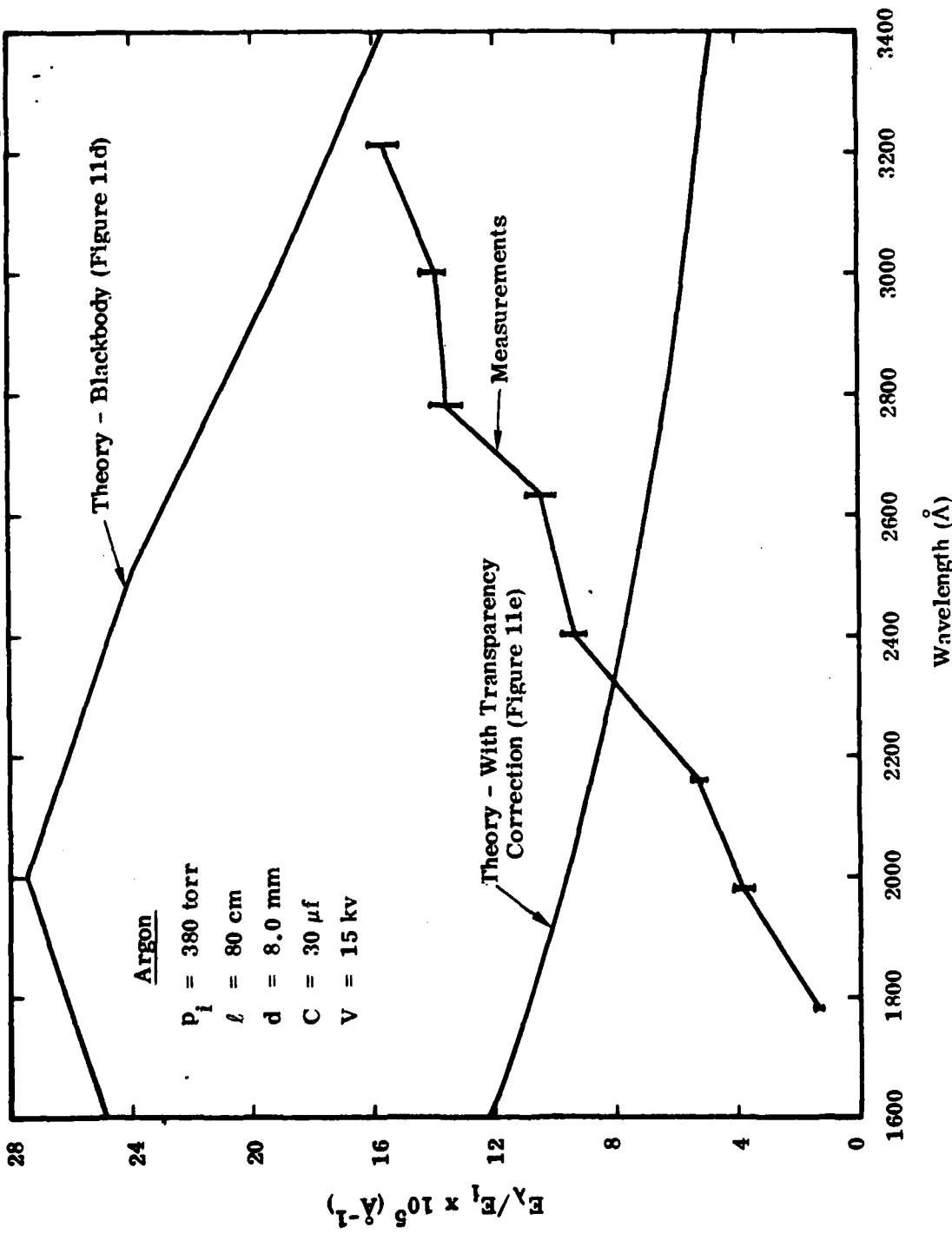


Figure 26. Comparison of Measured Lamp Spectral Energy Efficiencies With Theory

Table 6-1. Operating Parameters for Flash Lamp Spectral Analysis

Filter No.	Nominal Peak Transmission (Å)	Actual Peak Transmission (Å)	$I_n^*$ (Å)	$D_\lambda$ (amps/watt)**
1	1800	1780	44.9	0.06
2	2000	1980	55.1	0.06
3	2200	2160	64.3	0.086
4	2400	2400	59.0	0.114
5	2600	2630	40.1	0.089
6	2800	2780	58.4	0.071
7	3000	3000	22.9	0.084
8	3200	3210	27.9	0.092

$A_d = 0.051 \text{ cm}^2$        $E_i = 3375 \text{ j}$        $d = 0.8 \text{ cm}$        $l = 80 \text{ cm}$   
 $C_d = 2200 \text{ pf}$        $d_a = 0.1 \text{ cm}$        $l = 9.96 \text{ cm}$   
 \*Transmission integrals include 0.97 transmission through Suprasil windows.  
 \*\*Extrapolated

## 7. STUDIES OF PHOTOLYSIS OF $C\{F_3$

The purpose of this work is to demonstrate the dissociation of  $C\{F_3$  by flash lamp radiation in the absorption band shown in Figure 1, with the resultant production of F-atoms for application in the enhancement in initiation of pulsed chemical lasers. Results of Section 6 show that the present flash lamp design provides substantial radiation in the spectral region. Results of this Section show under what conditions of composition and pressure  $C\{F_3$  destruction can be demonstrated by UV radiation attenuation measurements, and conclusions are drawn concerning the applicability of these results to initiation enhancement in pulsed HF/DF lasers. Since a direct F-atom measurements technique was not available, F-atom production might instead be deduced from UV attenuation measurements before and after flash lamp photolysis of  $C\{F_3$  in the experimental arrangement shown in Figure 27. A permanent decrease in attenuation of radiation from an arc lamp over a narrow UV filter band at  $2400\text{\AA}$  as a result of lamp discharge would indicate destruction of  $C\{F_3$ , since the stage products  $C\{F$  and  $F_2$  are comparatively weak absorbers at this wavelength (see Figure 1). A temporary decrease in attenuation of radiation at this wavelength followed by recovery to the original attenuation level might indicate dissociation of  $C\{F_3$  followed by product recombination. Consider next attenuation measurements over a narrow UV filter band at  $3210\text{\AA}$  where, according to Figure 1,  $F_2$  and  $C\{F_3$  have comparable absorptions which are much stronger than that of  $C\{F$ . A temporary decrease in attenuation over this band followed by recovery to nearly the original level might indicate that dissociation of  $C\{F_3$  resulted in F-atom production; whereas no change in attenuation might indicate that photolysis of  $C\{F_3$  resulted in the products  $F_2$  plus  $C\{F$ . Temporal measurements, on the time scale for recombination of F-atoms, which are reported below are inconclusive since unknown photolysis products with large absorption cross sections obscure observations of the species of interest. Consequently, although photolytic dissociation of  $C\{F_3$  is demonstrated, the products are not identified.

A flash lamp with 8.0 mm inside diameter, 2.00 mm Suprasil wall thickness and 80 cm arc length was positioned along the centerline of an aluminum photolysis cell with teflon end plugs as shown schematically in Figure 27. The photolysis cell,

AL-76-059

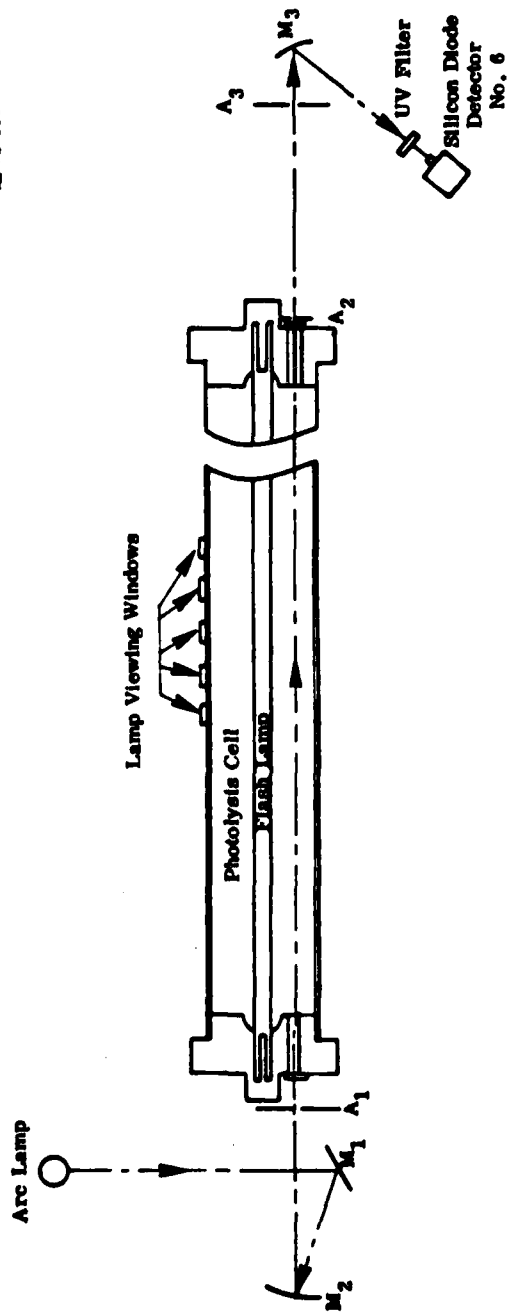
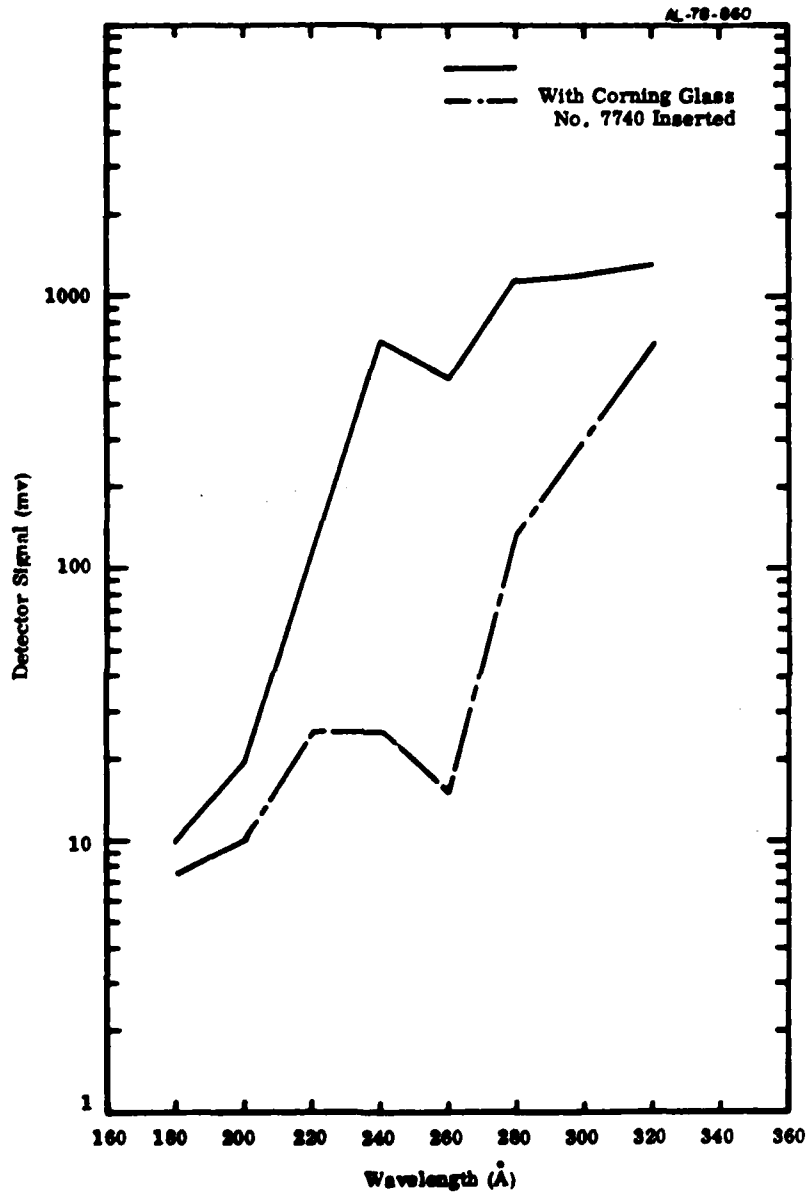


Figure 27. System Schematic for UV Attenuation Studies

with an inside diameter of 10.4 cm and a length of 77 cm, had  $MgF_2$  windows aligned in the end plugs with clear apertures of 1.50 cm, centered midway between cell center and cell inside wall. Radiation from a UV arc lamp was directed through the cell, parallel to its axis and onto a silicon diode detector as shown in Figure 27. Aperture of diameters 1.3, 0.18, and 0.32 cm were positioned along the lamp beam path at the cell inlet, the cell outlet, and 34 cm beyond the cell outlet, respectively. The arc lamp beam was focused at the 0.18 cm aperture. The latter two apertures excluded sufficient flash lamp radiation from the silicon detector (No. 6 Figure 27), such that, pickup did not influence attenuation measurement after 500  $\mu$ sec from flash lamp initiation. One of eight narrow band UV filters was placed before the detector as shown; all eight were used in DC attenuation studies; filter No. 4 (2400 $\text{\AA}$ ) and No. 8 (3210 $\text{\AA}$ ) were used in photolysis studies. Flash lamp spectra were recorded in photolysis studies by methods discussed in Section 6.

#### 7.1 System Operation and Analysis

Attenuation measurements used an arc lamp source and a silicon diode/operational amplifier detector with a feedback resistance of 2.2 M $\Omega$  and capacitance of 20 pf. The relative response of this source detector system, without gas attenuation, is shown in Figure 28 for each of eight UV filters of Figure 22. Detector response is also shown for each filter with a plate of Corning glass No. 7740 placed in the beam path. The glass cutoff in Figure 22 shows that visible lamp radiation leakage through filters No. 1 and 2 (1780 $\text{\AA}$  and 1980 $\text{\AA}$ ) is large compared to the very weak arc lamp radiation at those wavelengths. All reported UV attenuation measurements with filters No. 1 through 5 are based on signal differences between glass-out and glass-in. Attenuation measurements were made with the above system through  $F_2$  and  $ClF_3$  at known pressures. At pressures appropriate to maximum sensitivity, resulting absorption cross section using filters No. 5 through 8 (Figure 22) are in good agreement with previous measurements. The average absorption cross section for  $ClF_3$  over the band of filter No. 4 (2400 $\text{\AA}$ ) varied with pressure as is expected from the spectrum of Figure 1; examples are given in photolysis studies reported below. Arc lamp radiation was too weak (Figure 28) over the bands of filters 1 through 3 to provide good measurements of absorption cross sections.



**Figure 28. Attenuation Channel (6) Detector Signals Through Eight Narrow Band UV Filter With and Without Corning Glass No. 7740 Inserted**

Flash lamp spectral energy distributions were determined from measurements taken during photolysis studies using the array described in Section 6. These lamp spectral measurements were corrected for attenuation by cell gas between the lamp outer surface and the array viewing windows, with a separation distance of 4.7 cm. Photolysis studies were conducted for a matrix of gas compositions, shown in Table 7-1. Absorption cross sections of  $C\ell F_3$  at filter band centers were interpolated from measurements of Schmitz and Schumacher<sup>(20)</sup> and Axworth, et al.<sup>(7)</sup> and are also shown in Table 7-1. Attenuations for each of eight filters and each  $C\ell F_3$  concentration, are shown in Table 7-1 over the cell path for lamp spectral measurements, 4.7 cm. Attenuation at 2400Å and 3210Å are shown in Table 7-1 for each  $C\ell F_3$  concentration, over the cell path length for photolysis studies, 77 cm.

Flash lamp UV spectral energy distribution may be related to observations of photolytic dissociation of  $C\ell F_3$  in the present geometry only if cell wall spectral reflectivity is known. The UV detector array and photolysis cell, shown schematically in Figure 21, provides a convenient system for measuring the UV spectral variation in a reflectivity for diffuse reflectors. If the radiated energy per unit wavelength is  $E_\lambda$  for a lamp inside diameter,  $d$ , and length,  $\ell$ , then the spectral energy radiated from unit lamp area is:

$$L = E_\lambda (\pi d \ell)^{-1} \quad (7-1)$$

If an evacuated cylindrical cell has a length,  $\ell_c$ , which is large compared with its diameter,  $d_c$ , then over a central segment the spectral energy from unit wall area of reflectivity,  $r_w$ , after first reflection, is approximately:

$$L_{w1} = r_w E_\lambda (\pi d_c \ell)^{-1}$$

That reflected after the  $n^{\text{th}}$  reflection, with account taken of lamp blockage, is:

$$L_{wn} = r_w^n E_\lambda (\pi d_c \ell)^{-1} (1 - d/d_c)^{n-1}$$

**Table 7-1. Gas Compositions and Attenuation Calculations for Present  $ClF_3$  Photolysis Studies**

		$ClF_3$ Mole Fraction				
		4%	2%	1%	0.5%	0.1%
Cell Total Pressure $N_2 + ClF_3$ (atm)	1.0	30.4*	15.2	7.6	3.8	0.76
	0.5	15.2	7.6	3.8	1.9	
	0.25	7.6	3.8	1.9	0.95	

\*Partial pressure of  $ClF_3$  (torr).

			Attenuation $I_0/I_1$ Over a Path Length of 4.7 cm						
Filter	Band Center (Å)	$\sigma_{ClF_3}$	30.4*	15.2	7.6	3.8	1.9	0.95	0.76
1	1780	----	----	----	----	----	----	----	----
2	1980	1.35-18	0.002	0.045	0.211	0.460	0.678	0.823	0.856
3	2160	1.3 -18	0.003	0.050	0.224	0.473	0.689	0.829	0.861
4	2400	3.38-19	0.211	0.459	0.678	0.823	0.907	0.953	0.961
5	2630	4.51-20	0.812	0.901	0.949	0.974	0.987	0.994	0.995
6	2780	3.11-20	0.867	0.931	0.965	0.982	0.991	0.996	0.996
7	3000	2.52-20	0.890	0.935	0.971	0.986	0.993	0.996	0.997
8	3210	1.41-20	0.937	0.968	0.984	0.992	0.996	0.998	0.998

\*Partial pressure of  $ClF_3$  (torr)

			Attenuation $I_0/I_1$ Over a Path Length of 77 cm						
4	2400	3.38-19	0.000	0.000	0.003	0.055	0.235	0.485	0.560
8	3210	1.41-20	0.345	0.587	0.766	0.875	0.936	0.967	0.974

Consequently, the combined reflected spectral energy per unit wall area from all reflections is:

$$L_w = r_w E_\lambda (\pi d_c l)^{-1} \sum_0^{\infty} r_w^n (1 - d/d_c)^n = \frac{E_\lambda}{\pi d_c l} \left( \frac{r_w}{1 + d/d_c - r_w} \right) \quad (7-2)$$

If the detector array of Figure 21 were first positioned to view the lamp and then tipped to view the wall, under identical lamp discharge conditions, then the ratio of wall signal to lamp signal for each detector would be:

$$\frac{L_w}{L} = \frac{d}{d_c} r_w \left( 1 + \frac{d}{d_c} - r_w \right)^{-1} \quad (7-3)$$

Equation (7-3), when solved for  $r_w$ , yields,

$$r_w = \left( 1 + \frac{d_c}{d} \right) \left( \frac{d_c}{d} + \frac{L}{L_w} \right)^{-1} \quad (7-4)$$

Equation (7-4) shows a simple determination of wall reflectivity in terms of geometry and a ratio of detector signals. This is a relative measurement requiring no absolute detector or filter calibration and provides simultaneous wall reflectivity measurements in five narrow UV bands. For a lamp inside diameter of 0.8 cm and a cell inside diameter of 10.4 cm, Eq. (7-3) is plotted in Figure 29. This figure shows that measurements of low values of spectral reflectivity dictate stronger detector shielding requirements than lamp spectral studies.

Wall reflectivity studies were conducted with a cylindrical cell which was cut from the same stock as the above photolysis cell. It is an aluminum alloy of unknown composition. The cell interior was sand blasted and cleaned with acetone. Cell end construction, side viewing windows, and lamp spectral radiation instrumentation

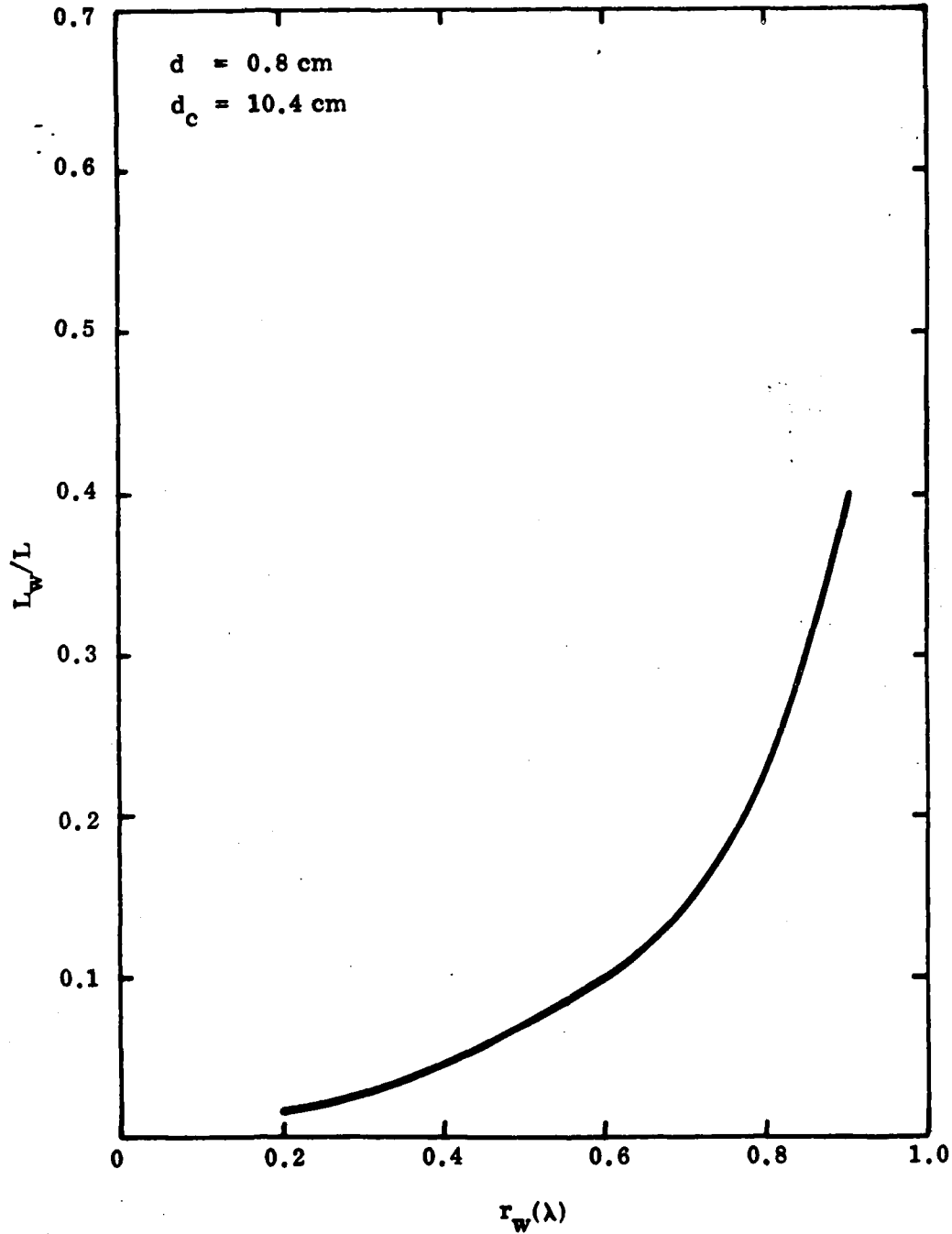


Figure 29. Ratio of Wall to Lamp Detector Signal Versus Spectral Reflectivity (Eq. (7-3))

were the same as that of the photolysis cell in Figures 21 and 27; however, the cell length and lamp arc length were 20 and 23 cm, respectively. Lamp spectral energy measurements were made with filters 1 thru 7 of Figure 22 and also with a narrow band filter centered at 3400Å. These measurements were made during ten lamp flashes with argon fill at 380 torr and a charging voltage of 5.0 kv on 30 μf capacitance. Wall reflected spectral energy measurements were made during ten lamp flashes, also at the above operating conditions. Resulting averaged ratios of wall to lamp signal at each wavelength are shown in Figure 30, where error bars indicate the extremes in detector signal variations at each wavelength. Wall reflectivity is calculated from Eq. (7-4) ( $d_c/d = 13.0$ ) at each wavelength and these results are also shown in Figure 30. Wall reflectivity is seen to be reasonably uniform over the spectral region considered, except at the shortest wavelength where it is very low.

Cavity illumination and resultant  $CfF_3$  photolytic dissociation may now be predicted in the geometry of Figure 27 if one assumes diffuse lamp radiation and diffusely reflecting walls. Radiation attenuation is assumed to be small over a distance of one cell radius. Cell end absorption and lamp blockage of wall reflected radiation are not considered. Spectral illumination energy from the flash lamp on a gas element of unit cross sectional area in the cell at a radial position,  $r$ , off the cell axis is:

$$\mathcal{L}_f = 2dL(\pi r)^{-1} \quad (7-5)$$

The added contribution from wall reflections is simply  $4L_w$ , thus, the combined illumination,  $\mathcal{L}$  is:

$$\mathcal{L} = \mathcal{L}_f + \mathcal{L}_w = 2dL(\pi r)^{-1} + 4L_w \quad (7-6)$$

Equation (7-3) relates  $L_w$  to  $L$ ; thus, after substitution of Eqs. (7-1) and (7-3) with lamp blockage neglected, one obtains,

$$\mathcal{L} = \frac{2E_\lambda}{\pi^2 \ell} \left( \frac{1}{r} + \frac{2\pi}{d_c} \frac{r_w}{(1-r_w)} \right) \quad (7-7)$$

The absorption of the radiated energy per unit volume by  $C\ell F_3$  is:

$$\frac{d\mathcal{L}}{dv} = \sigma_{C\ell F_3} n_{C\ell F_3} \mathcal{L} \quad (7-8)$$

If photon absorption at radiation frequency,  $\nu$ , is assumed to result in  $C\ell F_3$  dissociation, the dissociation per unit volume per unit wavelength is then:

$$\frac{d}{d\lambda} (\Delta n_{C\ell F_3}) = \sigma_{C\ell F_3} n_{C\ell F_3} \mathcal{L} (h\nu)^{-1} \quad (7-9)$$

The average change in  $n_{C\ell F_3}$  per unit wavelength throughout the cell volume is then:

$$\frac{d}{d\lambda} (\Delta n_{C\ell F_3}) = \frac{4E_\lambda}{\pi v} \sigma_{C\ell F_3} n_{C\ell F_3} (h\nu)^{-1} \cdot \left[ \frac{1}{2} (d_c^2 - d_o^2) + \frac{\pi}{4d_c} \frac{r_w}{(1-r_w)} (d_c^2 - d_o^2) \right] \quad (7-10)$$

where  $v$  is photolysis cell volume and  $d_o$  is lamp outside diameter. Finally, the average fractional change in  $C\ell F_3$  concentration by photolysis is obtained by integrating Eq. (7-10) over the absorption band of  $C\ell F_3$ .

$$\frac{n_{ClF_3}}{n_{ClF_3}} = \frac{4E_1}{\pi v} \int \frac{\sigma_{ClF_3}}{h\nu} \left( \frac{E_\lambda}{E_1} \right) \cdot \left[ \frac{1}{2} (d_c - d_o) + \frac{\pi}{4d_c} \frac{r_w}{(1-r_w)} (d_c^2 - d_o^2) \right] d\lambda \quad (7-11)$$

If  $\sigma_{ClF_3}$  is taken from Table 7-1,  $(E_\lambda/E_1)$  from Figure 26, and  $r_w$  from Figure 30, then for  $E_1 = 3375$  j (15 kv, 30  $\mu$ f) Eq. (7-11) yields the predicted average dissociation level, for weak absorption,

$$\Delta n_{ClF_3} / n_{ClF_3} = 0.285 \quad (7-12)$$

The local level of dissociation along the centerline of the arc lamp beam in Figure 27 was also calculated by integrating Eq. (7-9) over wavelength. The resulting value is very nearly equal to that of Eq. (7-12). This predicted dissociation is compared with measurements in the following section.

The above analysis assumes small radiation attenuation, hence, a small fraction of lamp spectral energy is given up to the gas. This fraction of lamp spectral energy given to the gas is obtained by multiplying Eq. (7-10) by  $(h\nu) v/E$ .

$$\frac{\Delta E_\lambda}{E_\lambda} = \frac{4}{\pi} \sigma_{ClF_3} n_{ClF_3} \cdot \left[ \frac{1}{2} (d_c - d_o) + \frac{\pi}{4d_c} \frac{r_w}{(1-r_w)} (d_c^2 - d_o^2) \right] \quad (7-13)$$

This expression was evaluated for present experimental conditions and results are given in Table 7-2 for  $ClF_3$  cell partial pressures of Table 7-1 at filter wavelengths within the  $ClF_3$  absorption band. Clearly, Table 7-2 shows that only for the

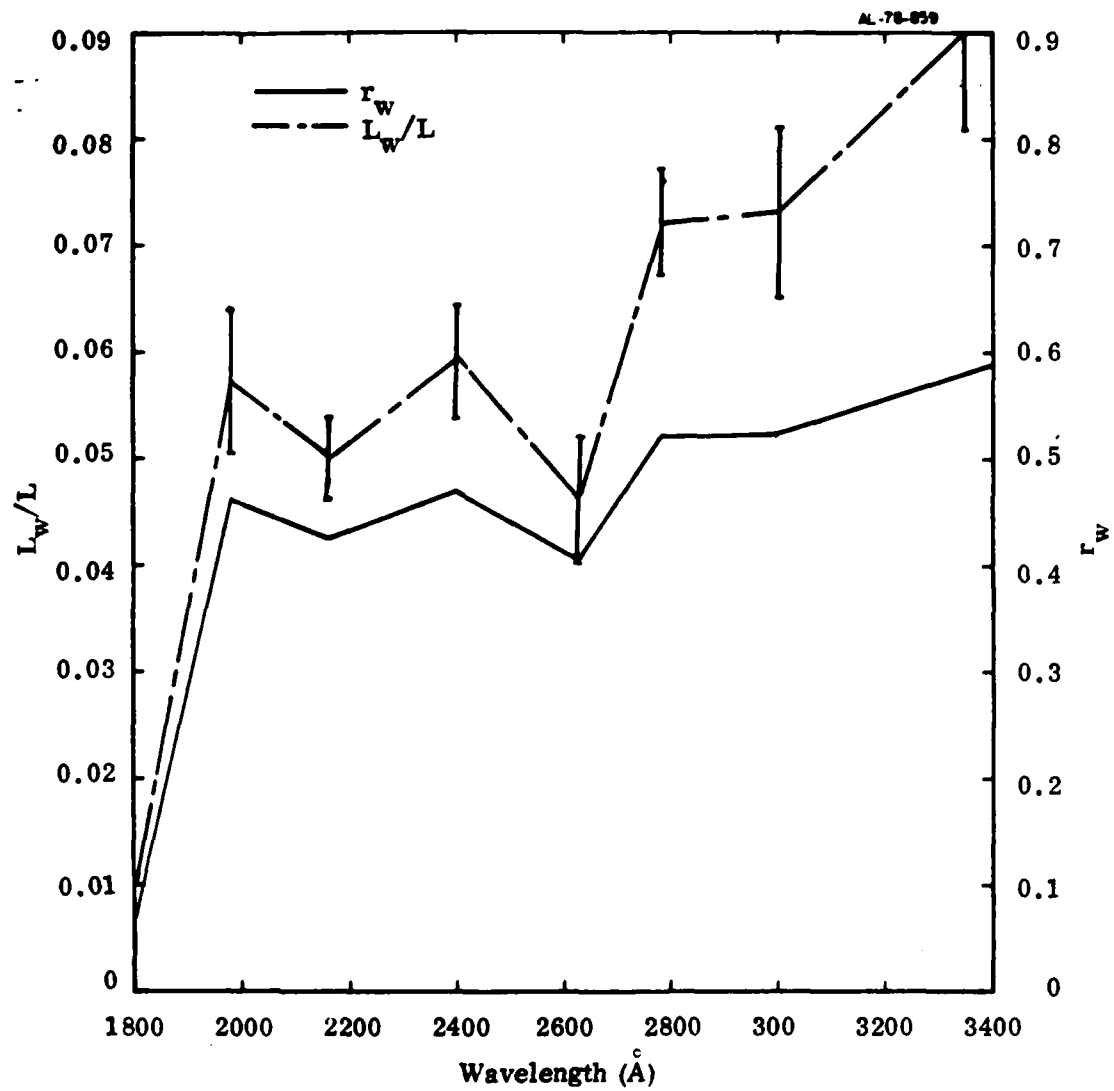


Figure 30. Measured Ratios of Wall to Lamp Detector Signals  $L_w/L$ , and Calculated Wall Spectral Reflectivities  $r_w$

Table 7-2. Predicted UV Attenuation Change Due to Photolysis of  $C\ell F_3$ .  
Based on Unity Photon Dissociation Efficiency

Filter	$\Delta E_\lambda / E_\lambda$ From Eq. (7-13)						
	30.4*	15.2	7.6	3.8	1.9	0.95	0.76
1 - 1780	7.20	3.60	1.80	0.90	0.45	0.23	0.18
2 - 1980	19.4	9.68	4.84	2.42	1.21	0.61	0.48
3 - 2160	17.2	8.60	4.30	2.15	1.08	0.54	0.43
4 - 2400	4.96	2.48	1.24	0.62	0.31	0.16	0.12
5 - 2630	0.56	0.28	0.14	0.07	0.04	0.02	0.01
*Partial pressure of $C\ell F_3$ (torr).							
$\Delta n_{C\ell F_3} / n_{C\ell F_3}$	0.015	0.030	0.059	0.118	0.236	0.285	0.285
$(I_{of} - I_{oi}) / I_{oi}$ :							
4 - 2400	0.466	0.466	0.466	0.466	0.466	0.255	0.199
8 - 3210	0.016	0.016	0.016	0.016	0.016	0.010	0.008
$(I_{of} - I_{oi}) / I_i$ :							
4 - 2400	0.000	0.000	0.001	0.019	0.095	0.115	0.105
8 - 3210	0.006	0.009	0.012	0.014	0.015	0.010	0.008

two lowest  $C\ell F_3$  partial pressure in our test matrix is the weak gas absorption assumption valid; even then, the average cell illumination is reduced by cell gas absorption. Absorbed radiation fractions, in excess of unity in Table 7-2, are clearly valid. A simple correction to the calculation of  $C\ell F_3$  dissociation applied to the five highest  $C\ell F_3$  partial pressures in Table 7-2 by assuming that all the lamp energy in the absorption band of  $C\ell F_3$  is absorbed by the gas. In this case, Eq. (7-11) is replaced by:

$$\Delta n_{C\ell F_3} / n_{C\ell F_3} = E_1 (n_{C\ell F_3} v)^{-1} \int (E_\lambda / E_1) (h\nu)^{-1} d\lambda \quad (7-14)$$

If  $E_1 = 3375$ , then with Figure 26 this becomes,

$$\Delta n_{C\ell F_3} / n_{C\ell F_3} = 5.78 \times 10^{16} / n_{C\ell F_3} \quad (7-15)$$

Values from Eq. (7-15) are given in Table 7-2 for the five highest  $C\ell F_3$  partial pressures and from Eq. (7-12) for the remaining two cases.

Attenuation of the arc lamp beam in the configuration of Figure 27 may now be interpreted in terms of efficiency of dissociation by photon absorption for  $C\ell F_3$ . Measurements in the following section may be compared to present predictions which are based on the assumption that every absorbed photon dissociates  $C\ell F_3$ . Ratios of measured to predicted signals will provide an efficiency measure. If  $I_1$  is the measured arc lamp beam intensity in the absence of gas absorption, and if  $I_{oi}$  is the intensity with  $C\ell F_3$  absorption, but prior to flash lamp discharge, then the signal  $I_{of}$  after photolytic depletion  $\Delta n_{C\ell F_3}$  is related to these reference intensities as,

$$\Delta I_o / I_{oi} = (I_{of} - I_{oi}) / I_{oi} = (e^{-\sigma_\lambda l_c \Delta n} - 1) \quad (7-16)$$

and

$$\Delta I_o / I_1 = e^{-\sigma_\lambda n l_c} (e^{-\sigma_\lambda l_c \Delta n} - 1) \quad (7-17)$$

where  $\sigma_\lambda$ ,  $n$ , and  $\Delta$  refer to  $C\ell F_3$  and it is assumed that  $\Delta n/n \ll 1$ . Equations (7-16) and (7-17) are evaluated for two filters, 2400Å and 3210Å, at each  $C\ell F_3$  partial pressure, using the predicted values of  $\Delta n_{C\ell F_3}$  based on unity photon dissociation efficiency. Results listed at the bottom of Table 7.2 show that attenuation measurements at 2400Å are sensitive to photolysis effects only at the lowest four  $C\ell F_3$  partial pressures of the experimental matrix. Attenuation measurements at 3210Å, although much less sensitive than those at 2400Å, are of comparable sensitivity over the entire test matrix.

## 7.2 Measurements of Photolysis of $C\ell F_3$

Attenuation measurements were made with data channel 6, shown in Figure 27, with two narrow band filters No. 4 (2400Å) and No. 8 (3210Å) with transmission curves shown in Figure 22. Changes in attenuation were sought as a result of dissociation of  $C\ell F_3$  by flash photolysis. A decrease in attenuation at 2400Å would demonstrate  $C\ell F_3$  dissociation. A decrease in attenuation at 3210Å in a time frame of order of the recombination time for F-atom might demonstrate the dissociation of  $C\ell F_3$  into  $C\ell F + 2F$ , followed by recombination of F-atoms to form  $F_2$  or  $C\ell F_3$ . The rationale for this study has been discussed previously, and is based on the relative absorption spectra of  $C\ell F_3$ ,  $C\ell F$ , and  $F_2$  in Figure 1. The recombination rate coefficient for  $F_2$  formation by atomic fluorine with  $N_2$  as chaperon, is reported by Ganguli and Kaufman<sup>(21)</sup> as  $8.0 \times 10^{-34}$  cm<sup>6</sup>/sec. If this rate is applied to the test matrix of Table 7-1 with predicted  $C\ell F_3$  dissociation levels of Table 7-2, recombination times would range from 3.5 to 23 msec. Events in this time frame may be observed without disturbances from the flash lamp in the attenuation data channel 6. It was observed, however, at both filter wavelength and under all operating conditions, that a strong increase in beam attenuation followed flash lamp discharge and recovery times from this phenomenon extended beyond the expected F-atom recombination times. Consequently, no convincing demonstration of the production of F-atoms by  $C\ell F_3$  dissociation was obtained from attenuation measurements at 3210Å. However, data obtained with the 2400Å filter show permanent decreases in attenuation as a result of flash photolysis. Furthermore, the attenuated probe beam signal from the arc lamp also increased with time when viewed through the 2400Å filter without flash lamp discharge when the cell was continuously exposed. These observations, reported below, demonstrate the photolytic dissociation of  $C\ell F_3$ . This section is concluded by a comparison between observed  $C\ell F_3$  photolytic dissociation levels and predictions of the previous section to determine photon efficiency of dissociation.

Oscilloscope traces of probe beam attenuation after flash lamp discharge as viewed through the 3210Å filter by data channel 6, are shown in Figure 31 for four combinations of  $C\ell F_3$  partial pressure and total cell pressure with  $N_2$  diluent. If

Fig. 31-a

Date: 8/24/78 Run 6  
Lamp: Argon 0.5 atm 30  $\mu$ f 15 kv  
Cell: 4.0% C/F<sub>3</sub> in N<sub>2</sub>, 1.0 atm Total Press.

Lamp Spectral  
Data Channels: 1980Å 2160Å 2630Å 2780Å

Signal Corrected  
For Cell Attenuation: Low Low 3.20 6.55  
Attenuation Measurements: Ch 6 Filter = 3210Å

Prerun:  $I_{of}/I_i$  (2400Å) = Low  
Prerun:  $I_{of}/I_i$  (3210Å) = 0.336  $\rightarrow$  31.2 torr C/F<sub>3</sub>

$$(I_{of} - I_{oi})/I_{oi} \quad (I_{of} - I_{oi})/I_i$$

Photograph: \_\_\_\_\_  
Short Time: 0.01 0.00  
Long Time: 0.01 0.00

Comments: No Attenuation Decrease

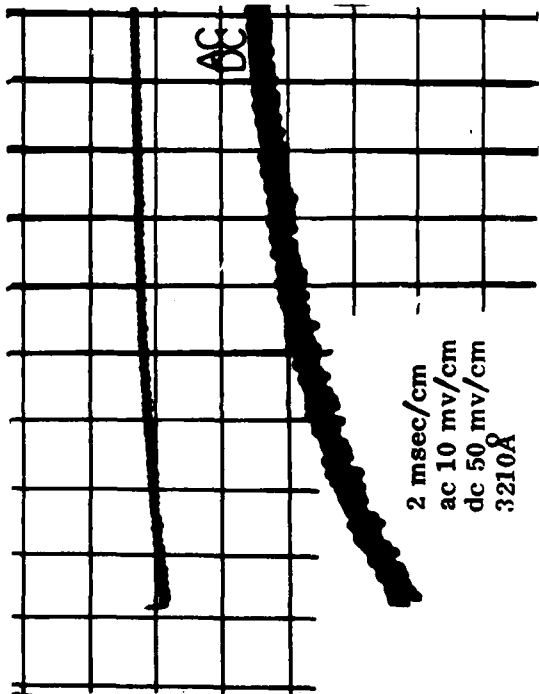


Fig. 31-b

Date: 8/24/78 Run 9  
Lamp: Argon 0.5 atm 30  $\mu$ f 15 kv  
Cell: 4.0% C/F<sub>3</sub> in N<sub>2</sub>, 0.5 atm Total Press.

Lamp Spectral  
Data Channels: 1980Å 2160Å 2630Å 2780Å

Signal Corrected  
For Cell Attenuation: Apertures Blocked  
Attenuation Measurements: Ch 6 Filter = 3210Å

Prerun:  $I_{of}/I_i$  (2400Å) = Low  
Prerun:  $I_{of}/I_i$  (3210Å) = 0.592  $\rightarrow$  14.9 torr C/F<sub>3</sub>

$$(I_{of} - I_{oi})/I_{oi} \quad (I_{of} - I_{oi})/I_i$$

Photograph: \_\_\_\_\_  
Short Time: 0.00 0.00  
Long Time: 0.01 0.00

Comments: No Attenuation Decrease

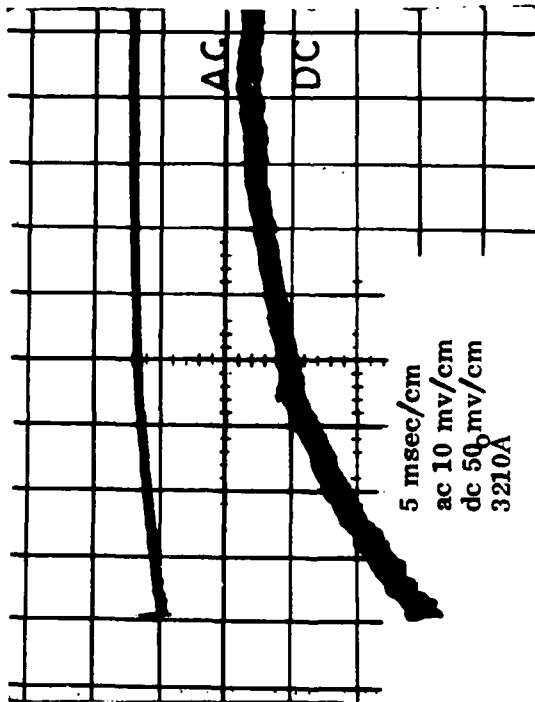


Figure 31. Attenuation at 3210Å by C/F<sub>3</sub> at Partial Pressures of 30.4, 15.2, and 7.6 torr with Flash Photolysis

Fig. 31-c  
 Date: 8/25/78 Run 12

Lamp: Argon 0.5 atm 30  $\mu$ f 15 kv

Cell: 2.0% C/F<sub>3</sub> in N<sub>2</sub>, 1.0 atm Total Press.

Lamp Spectral  
 Data Channels: 1980Å 2160Å 2630Å 2780Å

Signal Corrected  
 For Cell Attenuation: Low Low 3.25 6.53

Attenuation Measurements: Ch 6 Filter = 3210Å

Prerun:  $I_{of}/I_i$  (2400Å) = Low

Prerun:  $I_{of}/I_i$  (3210Å) = 0.571  $\rightarrow$  15.9 torr C/F<sub>3</sub>

$$(I_{of} - I_{oi})/I_{oi} \quad (I_{of} - I_{oi})/I_i$$

Photograph: \_\_\_\_\_  
 Short Time: 0.01 0.00  
 Long Time: 0.01 0.00  
 Comments: No Attenuation Decrease

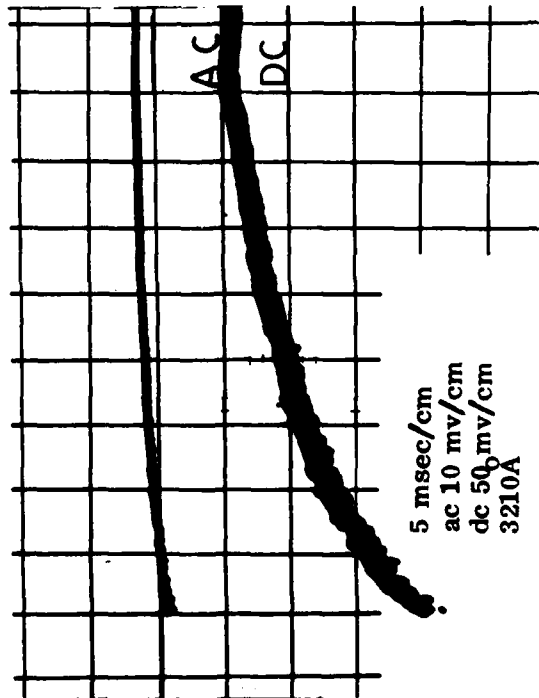


Fig. 31-d  
 Date: 8/25/78 Run 24

Lamp: Argon 0.5 atm 30  $\mu$ f 15 kv

Cell: 2.0% C/F<sub>3</sub> in N<sub>2</sub>, 0.5 atm Total Press.

Lamp Spectral  
 Data Channels: 1980Å 2160Å 2630Å 2780Å

Signal Corrected  
 For Cell Attenuation: Low Low 3.25 6.84

Attenuation Measurements: Ch 6 Filter = 3210Å

Prerun:  $I_{of}/I_i$  (2400Å) = Low

Prerun:  $I_{of}/I_i$  (3210Å) = 0.799  $\rightarrow$  6.41 torr C/F<sub>3</sub>

$$(I_{of} - I_{oi})/I_{oi} \quad (I_{of} - I_{oi})/I_i$$

Photograph: \_\_\_\_\_  
 Short Time: 0.01 0.00  
 Long Time: 0.01 0.00  
 Comments: No Attenuation Decrease

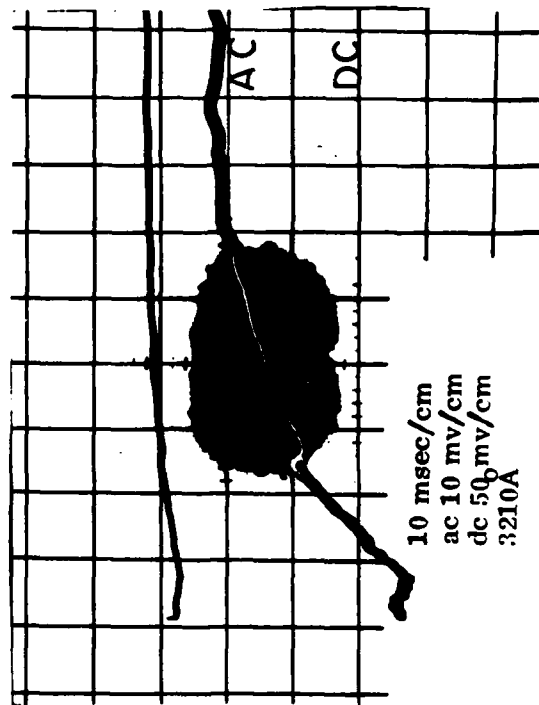


Figure 31. Attenuation at 3210Å by C/F<sub>3</sub> at Partial Pressures of 30.4, 15.2, and 7.6 torr with Flash Photolysis (Cont.)

$\text{ClF}_3$  photolysis results in the products  $\text{ClF} + 2\text{F}$  and is followed by recombination either to  $\text{F}_2 + \text{ClF}$  or to  $\text{ClF}_3$ , then one might look for an initial decrease in attenuation at 3210Å followed by recovery to the initial level over the recombination time. Recombination time for  $\text{F}_2$  formation at operating conditions of Figure 31 is expected to be between 3.5 and 7.0 msec. All four cases show that attenuation recovers from a strong increase by photolysis in a time frame that would mask the above phenomenon. This phenomenon was present in all studies at 3210Å, consequently, no identification of the initial products of  $\text{ClF}_3$  photolysis was achieved. The four cases shown, indicate that the strongly absorbing product of photolysis has a creation level that is independent of total pressure or  $\text{ClF}_3$  partial pressure, and the time constant for signal recovery varies as  $\text{ClF}_3$  partial pressure, but not with total pressure. These cases all correspond to nearly complete absorption of lamp radiation in the absorption level of  $\text{ClF}_3$  as shown in Table 7-2. Figures 31a - d show lamp and cell operating conditions and lamp spectral data when obtained which is corrected for cell gas absorption. In all cases, the gas attenuation in the 1980Å and 2160Å spectral data channels was too large to allow meaningful interpretation. Lamp spectra, with an  $\text{N}_2$  filled cell, was obtained at intervals during the studies and lamp spectra were found to be reproducible and consistent with measurements reported in Section 6. Partial pressures of  $\text{ClF}_3$  may also be calculated from preflash attenuation studies. These were done at both 2400Å and 3210Å. Signals at 2400Å were too low to be meaningful, however, attenuation at 3210Å is shown to be in reasonable agreement with the specified gas fill pressure. Attenuation signal variations at the specified wavelength (3210Å) after flash lamp discharge are referenced to the attenuated pre-shot detector signal  $I_{01}$  and to the unattenuated detector signal  $I_1$ . Errors in the latter ratio  $\Delta I_0/I_1$  are approximately  $\pm 0.01$  at both 2400Å and at 3210Å for all operating conditions. Data channel 6 traces are shown with both DC and AC scope coupling; scales and zero levels are shown in the figures.

Attenuation traces are shown in Figure 32 with the 2400Å filter in Channel 6. Lamp and cell conditions in Figure 32a are the same as those of Figure 31d. Although the signal at 2400Å is weak, the attenuation increase from photolysis appears to be less dramatic here and of shorter duration than observed at 3210Å. Still, the

Fig. 32-a

Date: 8/25/78 Run 23  
 Lamp: Argon 0.5 atm 30  $\mu$ f 15 kv  
 Cell: 2.0% C/F<sub>3</sub> in N<sub>2</sub>, 0.5 atm Total Press.

Lamp Spectral  
 Data Channels: 1980Å 2160Å 2630Å 2780Å

Signal Corrected  
 For Cell Attenuation: Low Low 3.00 6.27  
 Attenuation Measurements: Ch 6 Filter = 2400Å

Prerun:  $I_{of}/I_i$  (2400Å) = Low  
 Prerun:  $I_{of}/I_i$  (3210Å) = 0.818  $\rightarrow$  5.74 torr C/F<sub>3</sub>  
 $(I_{of} - I_{oi})/I_{oi}$   $(I_{of} - I_{oi})/I_i$

Photograph: —  
 Short Time: 0.03 0.00  
 Long Time: No Data No Data

Comments:

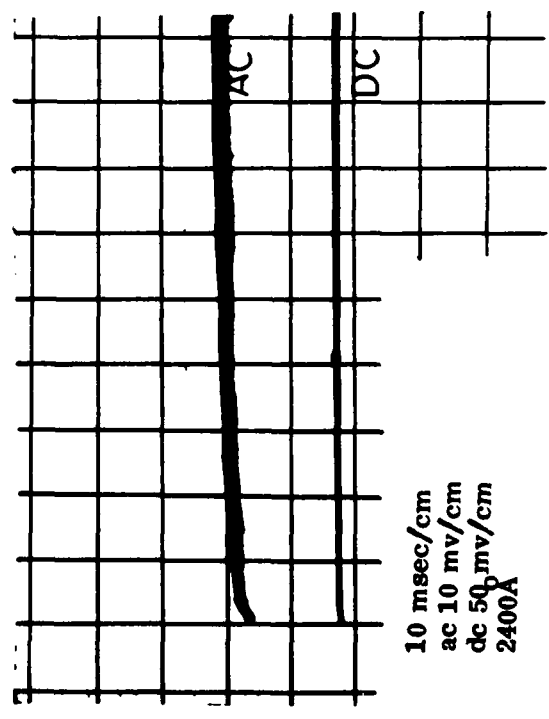


Fig. 32-b

Date: 8/25/78 Run 26  
 Lamp: Argon 0.5 atm. 30  $\mu$ f 15 kv  
 Cell: 2.0% C/F<sub>3</sub> in N<sub>2</sub>, 0.25 atm Total Press.

Lamp Spectral  
 Data Channels: 1980Å 2160Å 2630Å 2780Å

Signal Corrected  
 For Cell Attenuation: Low Low 3.16 6.82  
 Attenuation Measurements: Ch 6 Filter = 2400Å

Prerun:  $I_{of}/I_i$  (2400Å) = Low  
 Prerun:  $I_{of}/I_i$  (3210Å) = 0.890  $\rightarrow$  3.33 torr C/F<sub>3</sub>  
 $(I_{of} - I_{oi})/I_{oi}$   $(I_{of} - I_{oi})/I_i$

Photograph: 0.03 0.00  
 Short Time: 0.04 0.01  
 Long Time: 0.05 0.01

Comments:

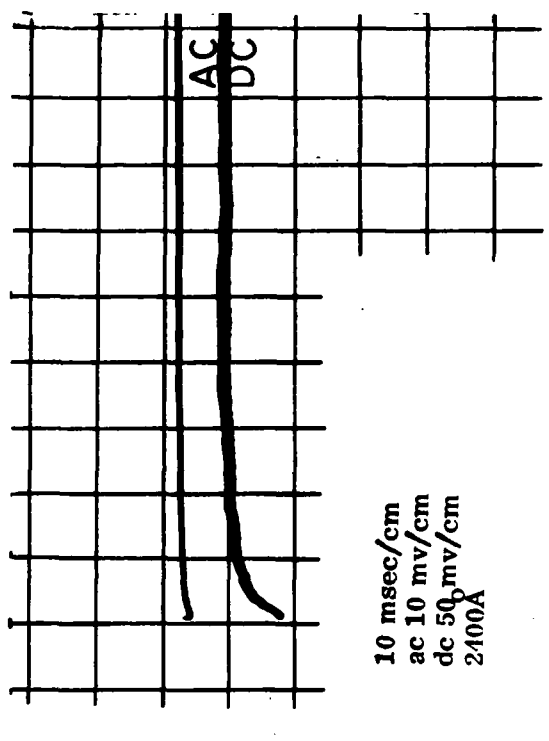


Figure 32. Attenuation at 2400Å by C/F<sub>3</sub> at Partial Pressures of 7.6 and 3.8 torr with Flash Photolysis

attenuation would mask transient  $C\ell F_3$  depletion on the time scale of F-atom recombination. Consequently, the investigation is limited to observations of attenuation decrease at  $2400\text{\AA}$  as a result of  $C\ell F_3$  depletion in a time frame of the order of 50 to 100 msec. Thus, these measurements apply to the final or permanent depletion of  $C\ell F_3$  and inferred levels of dissociation production of F-atoms may ignore a portion which goes to the recombination of  $C\ell F_3$ . The details of the attenuation increase at  $2400\text{\AA}$  from photolysis is shown more clearly in Figure 32b. Recover from this phenomenon is sufficiently fast to show a decrease in attenuation in the scope trace. Based upon this signal increase of  $\approx 1.2$  mv. A value of  $\Delta I_o/I_{oi}$  is given in Figure 32b of 0.03. A second value of  $I_o/I_{oi}$  at  $2400\text{\AA}$  was obtained from DC attenuation measurements within one minute before and after lamp flash; this is identified in the figure as short time. A third value of  $\Delta I_o/I_{oi}$  was obtained from DC attenuation measurements before and approximately five minutes after lamp flash; the long time measurement allowed sufficient time to reach uniformity in cell gas composition by diffusion. Positive signal changes at these three times are also referenced to the unattenuated detector signal as  $\Delta I_o/I_i$  and are also shown in the figures. The time constant for AC scope coupling is 220 msec; consequently, signal roll-off should and does occur in scope traces in time of order 100 msec. In view of this, a good correlation has been observed between positive signal variations in photographs and in short times. Thus, these positive changes in photographs at  $2400\text{\AA}$  are representative of permanent depletion of  $C\ell F_3$ .

At low  $C\ell F_3$  partial pressures, the arc lamp probe beam of data channel 6 was itself effective at  $C\ell F_3$  depletion without flash lamp discharge. At an initial mole fraction of  $C\ell F_3$  of 0.1% in one atmosphere of nitrogen, attenuation signal variations with time are shown in Figure 33 at both  $2400\text{\AA}$  and  $3210\text{\AA}$ ; unattenuated signal levels, before and after the test, are also shown. The initial attenuated signal levels are used to calculate  $C\ell F_3$  partial pressures of 0.58 and 0.66 torr at  $2400\text{\AA}$  and  $3210\text{\AA}$ , respectively, which compare with the measured pressure of 0.76 torr. The  $2400\text{\AA}$  signal at  $t = 107$  minutes corresponds to a  $C\ell F_3$  pressure of 0.025 torr or nearly complete destruction of  $C\ell F_3$ . If all the depleted  $C\ell F_3$  is assumed to form  $C\ell F + F_2$ , then the ratio of final to initial

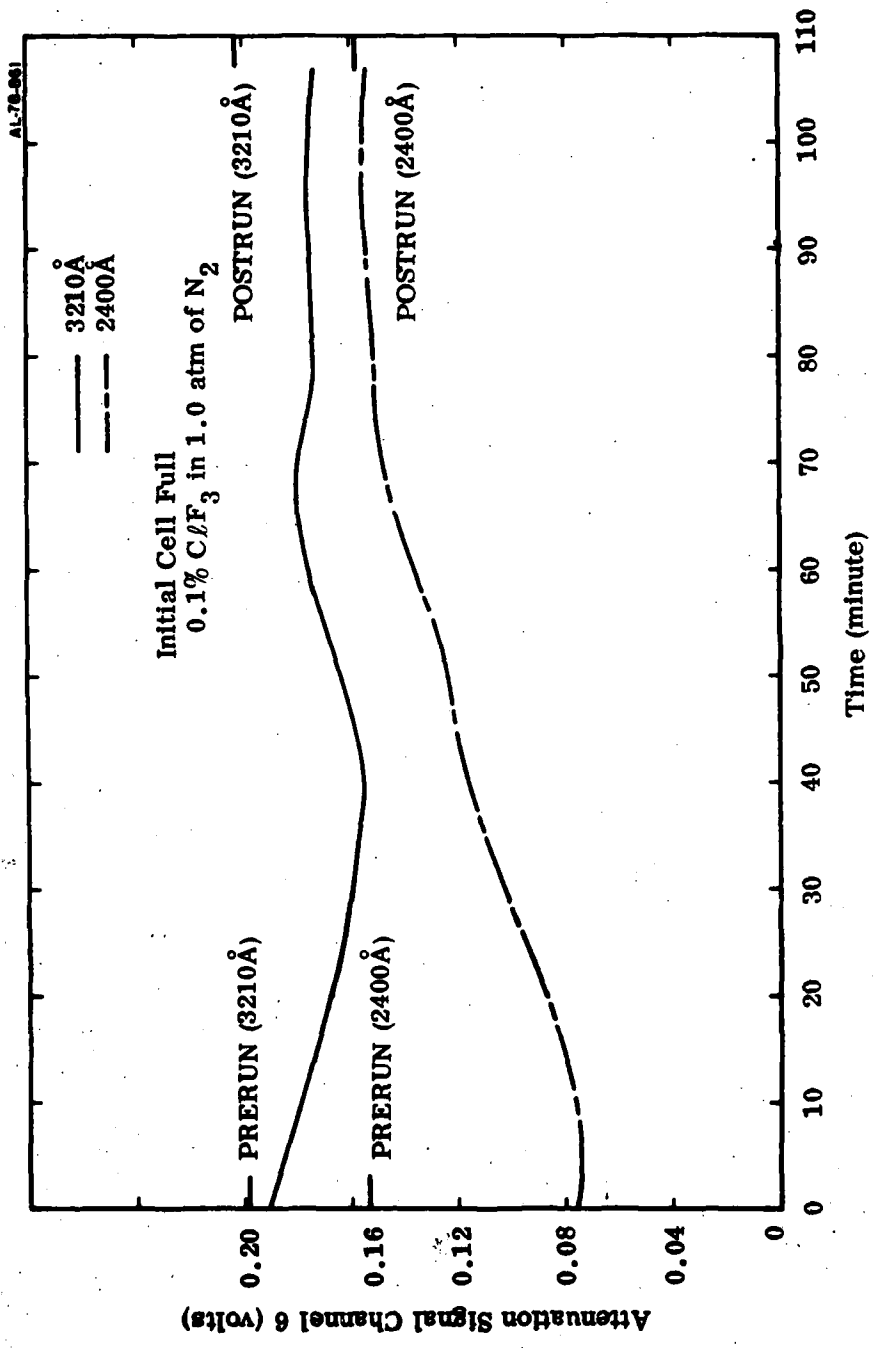


Figure 33. Histories of C/F<sub>3</sub> Attenuations at 2400 Å and 3210 Å During Exposure to the Arc Lamp Attenuation Probe Beam

3210Å attenuation signal should be approximately in the ratio of absorption cross sections of  $C\ell F_3$  and  $F_2$ ,  $1.41 \times 10^{-20} \text{ cm}^2$  and  $1.55 \times 10^{-20} \text{ cm}^2$ , respectively. This attenuation signal ratio, in Figure 33, is 0.912 as compared with the above cross section ratio of 0.909. This is persuasive evidence of the product species of continuous photolysis of  $C\ell F_3$ , however, different products may result from flash photolysis. Attenuation measurements were made over a time period comparable with the above study and at the same cell gas composition while the cell was blocked from the arc lamp. No changes in attenuation were detectable at either 2400Å or at 3210Å. In flash lamp photolysis studies of  $C\ell F_3$  depletion, discussed here, the cell was exposed to the arc lamp only at brief intervals when attenuation measurements were made.

Results are presented in Figure 34 for flash photolysis studies at low partial pressures of  $C\ell F_3$ . Lamp spectral measurements are shown as spectral energy efficiencies,  $E_\lambda/E_1$ , which may be compared with results in Figure 26 at identical lamp operating conditions. Partial pressures of  $C\ell F_3$  are inferred from pre-flash attenuation signals at both 2400Å and 3210Å and results are in fair agreement with measure pressures of 0.76 and 0.95 torr in Figures 34a and 34b, respectively. Oscilloscope traces were obtained from the attenuation data channel 6 at 2400Å. Three values of positive attenuation signal changes at 2400Å are reported, which were obtained by comparing trace photograph signals and DC attenuation shortly after and approximately five minutes after lamp discharge with the value just prior to discharge. These differences are normalized by pre-flash attenuation signal

$$\Delta I_o/I_{oi} = (I_{of} - I_{oi})/I_{oi} \quad ,$$

and by unattenuated detect or signal,

$$\Delta I_o/I_i = (I_{of} - I_{oi})/I_i \quad .$$

Fig. 34-a

Date: 8/30/78 Run 3  
 Lamp: Argon 0.5 atm 30  $\mu$ f 15 kv  
 Cell: 0.1% C/F<sub>3</sub> in N<sub>2</sub>, 1.0 atm Total Press.  
 Lamp Spectral  
 Data Channels: 1980Å 2160Å 2630Å 2780Å

Signals Corrected  
 For Cell Attenuation: 1.13 2.40 3.18 6.55  
 $E_{\lambda}/E_1(\text{Å}^{-1}) \times 10^5$  3.26 4.14 8.50 15.1

Attenuation Measurements: Ch 6 Filter = 2400Å  
 Prerun:  $I_{oi}/I_1(2400\text{Å}) = 0.530 \rightarrow 0.70$  torr C/F<sub>3</sub>  
 Prerun:  $I_{oi}/I_1(3210\text{Å}) = 0.972 \rightarrow 0.81$  torr C/F<sub>3</sub>

	$(I_{of} - I_{oi})/I_{oi}$	$(I_{of} - I_{oi})/I_1$
Photograph:	0.08	0.04
Short Time:	0.11	0.05
Long Time:	0.23	0.11

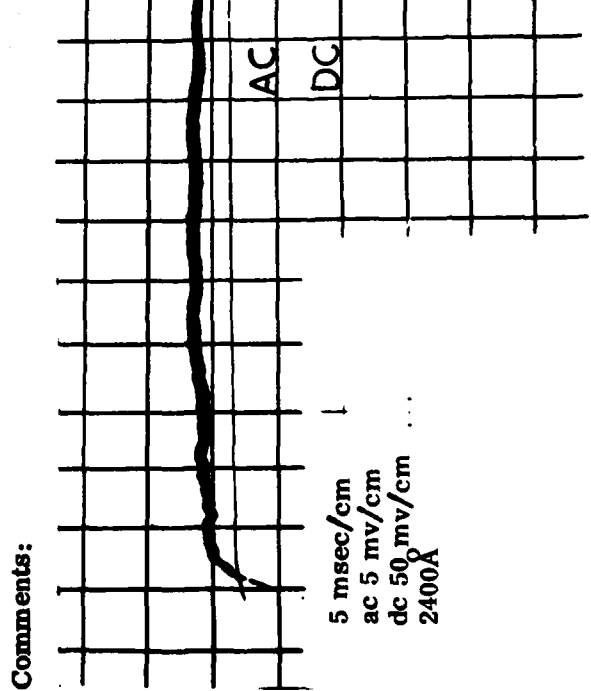


Fig. 34-b

Date: 9/1/78 Run 7  
 Lamp: Argon 0.5 atm 30  $\mu$ f 15 kv  
 Cell: 0.5% C/F<sub>3</sub> in N<sub>2</sub>, 0.25 atm Total Press.  
 Lamp Spectral  
 Data Channels: 1980Å 2160Å 2630Å 2780Å

Signals Corrected  
 For Cell Attenuation: 0.93 2.56 3.37 5.84  
 $E_{\lambda}/E_1(\text{Å}^{-1}) \times 10^5$  2.69 4.42 9.01 13.4

Attenuation Measurements: Ch 6 Filter = 2400Å  
 Prerun:  $I_{oi}/I_1(2400\text{Å}) = 0.517 \rightarrow 0.87$  torr C/F<sub>3</sub>  
 Prerun:  $I_{oi}/I_1(3210\text{Å}) = 0.965 \rightarrow 1.01$  torr C/F<sub>3</sub>

	$(I_{of} - I_{oi})/I_{oi}$	$(I_{of} - I_{oi})/I_1$
Photograph:	0.03	0.02
Short Time:	0.06	0.03
Long Time:	0.17	0.09

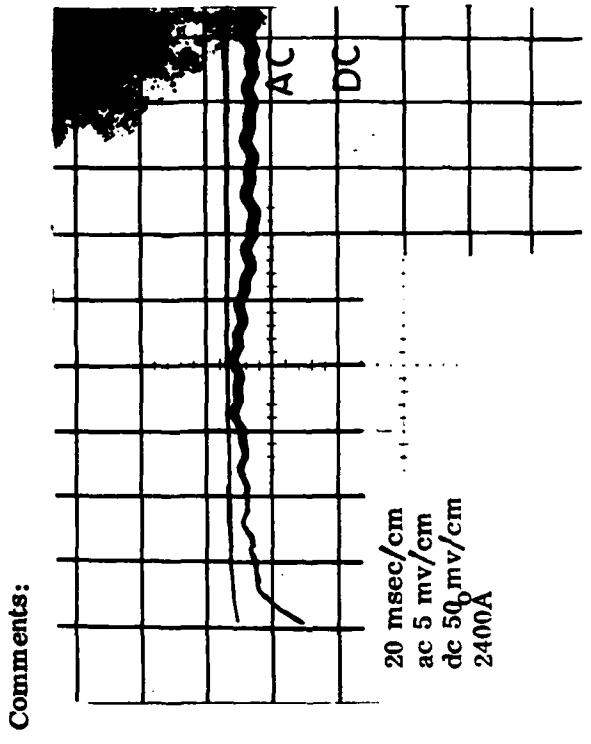


Figure 34. Attenuation at 2400Å by C/F<sub>3</sub> at Partial Pressures of 0.76 and 0.95 torr with Flash Photolysis

In this form, these results may be compared with predictions in Table 7-2 to assess the photon efficiency for  $\text{ClF}_3$  dissociation. Differing values for attenuation change between trace photographs and short time measurements are due to roll-off in AC scope coupling. Differences between short and long time measurements may be due to diffusion caused by photolytically produced gradients in  $\text{ClF}_3$  concentration. The pattern of variation in  $\Delta I_0$  with time, shown in Figure 34, was common to all tests where significant positive signal change occurred. Detectable positive attenuation change at  $2400\text{\AA}$  was obtained in scope traces ( $\Delta I_0/I_1 \geq 0.01$ ) for only the lowest two  $\text{ClF}_3$  partial pressures in Tables 7-1 and 7-2. Weak post-flash steady state attenuation decreases at  $2400\text{\AA}$  were observed also at partial pressures of 3.8 and 1.9 torr; (see Figure 32b). This is reasonably consistent with the prediction in Table 7-2 of rapid decrease in  $2400\text{\AA}$  detectivity,  $\Delta I_0/I_1$ , at  $\text{ClF}_3$  pressures above 1.9 torr.

Short time and steady state (long time) signals of Figure 34 at  $2400\text{\AA}$  are now compared with prediction of Subsection 7.1 to assess the photon efficiency for  $\text{ClF}_3$  dissociation.

	$P_{\text{ClF}_3} = 0.76 \text{ torr}$	$P_{\text{ClF}_3} = 0.95 \text{ torr}$
Observed $\Delta I_0/I_{01}$ (short time)	$0.11 \pm 0.02$	$0.06 \pm 0.02$
Associated $\Delta n_{\text{ClF}_3}/n_{\text{ClF}_3}$	$0.18 \pm 0.03$	$0.08 \pm 0.03$
Observed $\Delta I_0/I_{01}$ (steady state)	$0.23 \pm 0.02$	$0.17 \pm 0.02$
Associated $\Delta n_{\text{ClF}_3}/n_{\text{ClF}_3}$	$0.41 \pm 0.04$	0.23
Predicted $\Delta I_0/I_{01}$ - Table 7-2	0.199	0.255
Associated $\Delta n_{\text{ClF}_3}/n_{\text{ClF}_3}$	0.285	0.285
Photon Dissociation Efficiency:		
Based on Short Time	63%	60%
Based on Steady State	144%	81%

One sees that at 0.76 torr of  $C\ell F_3$ , the steady state prediction of photon efficiency exceeds unity. This is not alarming in view of the elaborate analysis which led to the predictions in Table 7-2.

From the above measurements, it is concluded that both DC arc lamp and flash lamp radiation will permanently dissociate  $C\ell F_3$ . It appears that the photon efficiency for dissociation in the absorption band of  $C\ell F_3$  is of the order of unity.

## 8. SUMMARY

It has been proposed that trace addition of  $C\ell F_3$  to conventional gas mixtures in photo-initiated HF/DF pulsed lasers might substantially improve chain reaction initiation and consequently, system electrical efficiency. The UV absorption band for  $C\ell F_3$  has a peak cross section near  $2000\text{\AA}$  which is approximately 50 times the peak value for  $F_2$ . If laser flash lamps have substantial energy in the  $C\ell F_3$  band and if  $C\ell F_3$  photolysis results in F-atom formation, then addition of  $C\ell F_3$  at a concentration of a few percent of that of  $F_2$  could effectively broaden the UV band for F-atom production by approximately 66%. This increase in initiation level, and thus laser chemical efficiency, could allow a direct tradeoff in the form of reduced lamp electrical energy requirements.

It has further been proposed that steady flow of a spatially tailored trace addition of  $C\ell F_3$  might improve uniformity of initiation and, hence, cavity homogeneity in repetitively pulsed devices by providing enhanced initiation (F-atom production) in regions of diminished lamp illumination.

The present study has addressed the questions: Can a flash lamp operate reliably with substantial radiation in the absorption bands of both  $F_2$  and  $C\ell F_3$ ? May this be achieved for short pulse lamps appropriate to pulsed chemical lasers? Does  $C\ell F_3$  absorption result in dissociation and F-atom production? What degree of spatial uniformity of initiation in repetitively pulsed devices may be expected with uniform gas mixture? What degree of gain in initiation uniformity might be expected with steady, spatially tailored trace addition of  $C\ell F_3$ ? These questions are not answered completely, however, the potential of trace addition of  $C\ell F_3$  is indicated for gains in electrical efficiency, cavity optical homogeneity, and gas mass utilization.

An argon filled flash lamp with observed pulse duration (FWHM) of approximately 40  $\mu\text{sec}$  radiated 3.5% of its initial electrical energy in the absorption band of  $C\ell F_3$  ( $1750\text{\AA}$  to  $2400\text{\AA}$ ) and 13% of its energy in the absorption band of  $F_2$  ( $2400\text{\AA}$  to  $3400\text{\AA}$ ).

This was determined by spectral radiation measurements through narrow band filters with peak transmissions spaced at 200Å intervals from 1800Å to 3200Å. Theoretical modeling of flash lamp radiation indicates that short lamp pulses appropriate to pulsed chemical lasers would show equal or better radiation distribution of lamp electrical energy in these absorption bands.

The above flash lamp was used in photolysis studies which show that absorption of radiation by  $\text{ClF}_3$  results in dissociation with efficiency of order unit. Photolytic production of F-atoms could not be determined in the present UV attenuation studies due to the occurrence of a strongly absorbing unidentified photolysis product or products. Difficulties in this indirect study of F-atom production points to the importance of the development of a direct measurement of F-atoms as proposed by Schlossberg.

Cavity illumination modeling of repetitively pulsed chemical lasers points to severe penalties in electrical efficiency and gas mass utilization if spatial uniformity of photolytic initiation is to be better than  $\pm 5\%$ . One might eliminate the penalties if *spatial tailoring of trace addition of  $\text{ClF}_3$  to laser gas mixtures* were used to enhance F-atom production in regions of diminished illumination. For example, with the above measured distribution of lamp radiated energy in the absorption bands of  $\text{ClF}_3$  and  $\text{F}_2$ , a local addition of 11%  $\text{ClF}_3$  in relation to  $\text{F}_2$  may double the local production of F-atoms at fixed illumination.

## 9. REFERENCES

1. D. McClure, M. Weisbach, B. Thayer, V. Buonadonna, B. Shepherd, B. Sherman, J. Artura of Boeing Aerospace Co., R. Taylor, and P. Lewis, Physical Sciences, Inc., "High Power Pulsed Chemical Lasers," presented at the Tri Services Chemical Laser Conference, White Oak, Maryland (3-5 May 1978).
2. Hao-Lin Chen, Raymond L. Taylor, Jack Wilson, Paul Lewis, and Walter Fyfe, "Atmospheric Pressure Pulsed HF Chemical Laser," Journal of Chemical Physics, 61, 1, (1 July 1974).
3. Boeing Aerospace Co., Seattle, Washington, "Development and Performance Evaluation of a Large Pulse Photoinitiated Chemical Laser (PHOCL)," Interim Report, Contract N00173-76-C-0190 (30 September 1976).
4. R.L. Taylor, P. Lewis, J. Cronis, and R. Root, Interim Report, Physical Sciences, Inc., TR-79 (31 January 1977).
5. Howard Schlossberg, "Fluorine-atom Probe Techniques for Chemical Lasers," Journal of Applied Physics, 47, 5 (May 1976).
6. W. Dallas Adams, Emily B. Turner, and J.F. Hold, Information Processing Division, Engineering Science Operations, D.G. Sutton and Harold Mirels, Aerophysics Laboratory, "The RESALE Chemical Laser Computer Program," Air Force Weapons Laboratory, Kirkland Air Force Base, N. Mexico, Interim Report, SAMSO-TR-75-60 (20 February 1975).
7. Arthur E. Axworthy, R.D. Wilson, and K.H. Mueller, "Photochemistry of Interhalogen Compounds of Interest as Rocket Propellants," Rockwell International Corporation, Report No. AD-771-537 (September 1973).
8. Paul A. Lovoi, "Flashlamp Technology for Pulsed Lasers," Proceedings of the Society of Photo-Optical Instrumentation Engineers, 138, (March 28-29, 1978)
9. EG&E, Electro-Optics Division, "Linear Xenon Flashtubes Quartz Envelope," Data Sheet F1002C-2.
10. M. Mitchner and Charles H. Kruger, Jr., "Partially Ionized Gases," Department of Mechanical Engineering, Stanford, University, published by John Wiley & Sons.

References (Cont.)

11. W.A. Menard, T.E. Horton, "Shock-Tube Thermochemistry Tables for High-Temperature Gases - Helium, Neon, and Argon," National Aeronautics and Space Administration, Technical Report 32-1408, III (January 1, 1970).
12. Ya. B. Zel'dovich and Yu. P. Raizer, "Physics of Shock Waves and High-Temperature Hydrodynamic Phenomena," Academic Press, Vol. I (1966).
13. Robert Siegel and John R. Howell, "Thermal Radiation Heat Transfer," McGraw-Hill Book Company (1972).
14. N. Cohen and J.F. Bott, "A Review of Rate Coefficients in the  $H_2 - F_2$  Chemical Laser System, Air Force Weapons Laboratory, Interim Report, SAMSO-TR-76-83 (15 April 1976).
15. J.F. Bott and N. Cohen, "Relaxation of HF ( $v = 1$ ) By Various Polyatomic Molecule," J. Chem. Phys., 61, 681 (1974).
16. J.K. Hancock and N.H. Grun, "Vibrational Deactivation Rates of HF ( $v = 1$ ) by  $CH_4$ ,  $C_2$ ,  $H_2$ ,  $C_3H_3$ ,  $C_4H_{10}$ ,  $C_3H_6$ , and  $ClF_3$ ," J. Chem. Phys., 59, 6350 (1973).
17. J.G. Calvert and J.N. Pitts, Jr., "Photochemistry," Published by John Wiley & Sons (January 1967).
18. O.M. Batovskii and V.I. Gurev, "Temperature Dependence of the Continuous Ultraviolet Absorption Spectrum of Molecular Fluorine," Opt. Spectrosc., 41, 2 (August 1976).
19. Capt. B. Crane, "AFWL F-atom Experiment," Tri Services Chemical Laser Conference, White Oak, Maryland (3-5 May 1978).
20. Heinz Schmitz and Hans Joachim Schumacher, "Das Absorptionsspektrum des  $ClF_3$ ," Z. Naturforschg. 2a 363 (1947): eingeg. am 2. (April 1947).
21. P.S. Ganguli and M. Kaufman, "The Rate of Homogeneous Recombination of Fluorine Atoms," Chemical Physics Letters, 25, 2 (March 15, 1974).